UNIVERSITÀ DEGLI STUDI DI TRIESTE

XXXII CICLO DEL DOTTORATO DI RICERCA IN

BIOMEDICINA MOLECOLARE

PhD Thesis

STEROL REGULATORY ELEMENT BINDING PROTEIN COUPLES MECHANICAL CUES TO LIPID METABOLISM

Settore scientifico-disciplinare: BIO/11

DOTTORANDO / A
REBECCA BERTOLIO

COORDINATORE
PROF. GERMANA MERONI

SUPERVISORE DI TESI
PROF. GIANNINO DEL SAL

ANNO ACCADEMICO 2018/2019

UNIVERSITÀ DEGLI STUDI DI TRIESTE

XXXII CICLO DEL DOTTORATO DI RICERCA IN

BIOMEDICINA MOLECOLARE

STEROL REGULATORY ELEMENT BINDING PROTEIN COUPLES MECHANICAL CUES TO LIPID METABOLISM

Settore scientifico-disciplinare: BIO/11

DOTTORANDO / A
REBECCA BERTOLIO

COORDINATORE
PROF. GERMANA MERONI

SUPERVISORE DI TESI
PROF. GIANNINO DEL SAL

ANNO ACCADEMICO 2018/2019

To the little one of our family and to you,
Love of our infinite lives.

“Don’t be scared, it’s all a show!”
A. Watts

Index

Abstract

Sterol regulatory element binding proteins (SREBPs) are a family of transcription factors that regulate lipid biosynthesis and adipogenesis by controlling the expression of several enzymes required for endogenous cholesterol, fatty acid, triacylglycerol, and phospholipid synthesis. In vertebrates, SREBPs activation is mainly controlled by a complex and well-characterized feedback mechanism mediated by cholesterol, a crucial bio-product of the SREBP-activated mevalonate pathway.

In this work, we identified the acto-myosin contractility and mechanical forces imposed by the extracellular matrix (ECM) as SREBP1 regulators. The control of SREBP1 by mechanical cues depends on geranylgeranyl pyrophosphate, another key bio-product of the mevalonate pathway, and impacts on stem cell fate in mouse and on fat storage in *Drosophila melanogaster*.

Mechanistically, we show that activation of AMP-activated protein kinase (AMPK) by ECM stiffening and geranylgeranylated RhoA-dependent acto-myosin contraction inhibits SREBP1 maturation and functional activation. Our results unveil an unpredicted and evolutionary conserved role of SREBP1 in rewiring cell metabolism in response to mechanical cues.

Introduction

1. Lipid metabolism

Lipids are hydrophobic biological molecules that play several and important role at the cellular and organismal levels. Most adult mammalian cells take up lipids from the bloodstream either as free fatty acids or complexed with proteins as low-density lipoprotein (LDL). These lipids are obtained from dietary sources or are synthesized in the liver or in the adipose tissue, where they can also be stored in lipid droplets[1].

Based on their structures and properties, lipids can be divided into different groups, including cholesterol, fatty acids (FA), triacylglycerols, phospholipids and isoprenoids. They have a structural role as major components of biological membranes and are used in energy metabolism and storage, they are necessary also for post-translation modifications (PTMs) of proteins and act as signaling molecules[2,3].

Fatty acids hydrophobic tails are modified to form phospholipids and glycolipids, which provide important structural molecules for biological membranes[2]. Moreover, membrane lipids can give rise to intermediates such as diacylglycerol (DAG), phosphatidylinositol (3,4,5)-trisphosphate (PIP3), phosphatidic acid (PA), lysophosphatidic acid (LPA) and sphingosine-1-phosphate (S1P) that function as second messengers involved in signal transduction pathways, crucial in some aspects of cell-cell communication; in fact, they can be released in the extracellular compartment and can control different biological processes as cell proliferation, migration and invasion[4,5].

Triacylglycerides are a common, simple type of lipid consisting of three long-chain fatty acids esterified to glycerol, which provide a reservoir of fatty acids that can be utilized for energy production. Apart from being the most reliable energy reserves of the human body, triacylglycerols take part in metabolic processes that determine the rate of fatty acid oxidation, the plasma levels of free fatty acids, the biosynthesis of other lipid molecules and the metabolic fate of lipoproteins[6].

Long-chain fatty acid are the major energy source for most cells. Most tissues, except for liver and adipose tissue, have little capacity for *de novo* FA synthesis and depend on FA uptake for their needs. Free-fatty acids (FFA) are internalized via CD36 fatty acid translocase or via the fatty acid transport proteins (FATPs of the SLC27 solute carrier

family)[7,8]. FA uptake is also aided by the action of lipid chaperons, known as fatty acid-binding proteins (FABPs), that facilitate the transport of lipids to specific compartments, among which the mitochondria for oxidation[9]. FA with 12-carbon chain can enter the mitochondria without any transporter. However, 14-carbon or more FA chain need to be modified before entering into the mitochondria: they are coupled to coenzyme-A (CoA) and the acyl chain is transferred to carnitine by carnitine acyltransferase (CPT1) into the mitochondrial matrix[10]. Once in the mitochondria, acyl chains are reattached to CoA and degraded by repeated rounds of oxidation and hydration. This process is known as β-oxidation and produces NADH, FADH2 as well as acetyl-CoA, which can enter the TCA cycle to be oxidized. The mode of regulation of β-oxidation ensures that lipid synthesis and degradation are mutually exclusive: indeed, when malonyl-CoA, the first intermediate of fatty acid biosynthesis pathway, is present in large amount, it inhibits the activity of carnitine palmitoyltransferases (CPTs), leading to the activation of the biosynthetic route [4,11].

As previously reported, oxidation of fatty acids produces acetyl-CoA which can be utilized in different ways. Among others, one of them is to be employed as epigenetic mark, leading to the acetylation of histones, and therefore regulating gene expression[12]. Indeed, it has been demonstrated that, in immortalized hepatocytes, lipid-derived carbons are deposited onto histone lysines, suggesting that lipids are a source of carbon for histone acetylation. This occurs through a lipid oxidation reprogram, leading to the production of lipid-derived acetyl-CoA [13]. Moreover, since acetyl-CoA derived from β-oxidation cannot cross the mitochondrial membrane, it is converted to citrate and, in this way, it diffuses to the nucleus. Once in the nucleus, the nuclear isoform of the ATP-citrate lyase (ACLY) cleaves citrate to generate acetyl-CoA molecules to be utilized for histone acetylation [14].
Additionally, while some short-chain fatty acids, such as butyric acid and valproic acid function as histone deacetylases inhibitors, promoting histone acetylation[15], on the opposite hand, several long-chain free fatty acids such as myristic, oleic and linoleic acids have been found to bind to the SIRT6 histone deacetylase, inducing its activity toward H3K9Ac[16]. In addition, also histone methylation is regulated by lipid metabolism. Indeed, cells that lack phosphatidylethanolamine (PE) methyltransferases disrupt SAM homeostasis, leading to hypermethylation of histones (as H3K4me3, H3K36me3, and H3K79me3) and consequent deregulation of gene expression[17].

1.1 De novo fatty acid biosynthesis

Many lipids are synthesized from fatty acids (FA), molecules consisting of hydrocarbon chains of different lengths and degree of saturation. FAs are synthesized in the cytosol and the first step is the production of a two-carbon unit, the acetyl-Coenzyme A (acetyl-CoA), which is generated from citrate by the enzyme ACLY, as shown in Fig.1 [18].

The committed step of fatty-acid biosynthesis requires the activation of acetyl-CoA to malonyl-CoA, which is catalyzed by the enzyme acetyl-CoA carboxylases (ACC1); then, acetyl and malonyl groups are coupled to the acyl-carrier domain of a multifunctional enzyme protein complex, the fatty-acid synthase (FASN) (Fig.1)[1,19]. Repeated condensation of acetyl groups generates a basic 16-carbon saturated fatty acid, the palmitic acid. Further elongation and desaturation take place on the cytoplasmic side of the endoplasmic reticulum (ER) membrane by two enzymes: elongation of very-long-chain fatty-acid proteins (ELOVL1-7), which adds two carbon units at the end of the chain in each cycle of the reaction, and stearoyl-CoA desaturase (SCD), which introduces a double bond in cis-Δ9 position of palmitic and stearic acids to produce mono-unsaturated fatty acids (MUFA) (Fig.1). The desaturation of FA significantly alters the physical properties of long-chain FA and is a fundamental determinant of membrane fluidity [20].

Fatty acids are the building blocks for phospholipids and are also used as energy stores as triacylglycerols (TAGs) in lipid droplets (LDs), intracellular organelles that are formed from the endoplasmic reticulum through a budding process [21]. LDs consist of a core of neutral lipids surrounded by a phospholipid monolayer that is characterized by integral and peripheral proteins and they fulfill different functions, from lipid storage sites to protection of the cell from some forms of stress [21,22].

Moreover, intermediates of the *de novo* fatty acid biosynthesis pathway can be converted into different phosphoglycerides, including phosphatidylcholine (PC), phosphatidylethanolamine (PE), phosphatidylglycerol (PG) and phosphatidylserine (PS), which constitute the major structural components of biological membranes (Fig.1)[19,23].

Other lipids generated from FAs are the sphingolipids, phosphoinositides and eicosanoids. Sphingolipids are bioactive lipids, which means that levels of this type of lipid respond to the action of specific stimuli, thus regulating specific downstream effectors and targets [24,25]. They contain acyl chains bound to serine and polar head groups derived from ethanolamine, serine or choline, among which sphingosine, sphingosine-1-phosphate (S1P) and ceramide are the most studied [25]. They cover a plethora of functions that can touch almost all the aspects of cell biology, including cell growth, cell cycle, cell death, cell senescence,

inflammation, immune response, cell adhesion and migration, metabolism, nutrient uptake, intracellular trafficking, responses to stress stimuli and autophagy[26].

Eicosanoids are produced from arachidonic acid, a polyunsaturated 20-carbon FA, which can be converted into prostaglandin H2 (PGH2) by prostaglandin H2 synthases, also known as cyclooxygenases (COX1 and COX2), or into leukotrienes by leukotriene synthases. PGH2 can be converted into additional prostaglandins, including prostaglandin E2 (PGE2), prostacyclin and thromboxanes[27]. They are key inter- and intracellular signalling molecules, which are primarily involved in mediating inflammatory responses [28,29].

Phosphoinositides, which are present in cell membranes, contain two acyl chains coupled to an inositide head group and are important second-messenger molecules[30,31]. Furthermore, sphingolipids, such as ceramide or sphingosine-1-phosphate, eicosanoids (e.g. PGE2) and phosphoinositides have important signaling functions in cells and tissues[27,32].

1.2 The mevalonate pathway

Another important biosynthetic process within the lipid metabolism is the mevalonate (MVA) pathway, which leads to the production of cholesterol and other useful intermediates for the cell[33]. The MVA pathway, indeed, provides isoprenoid building blocks for distinct classes of end products. These include, steroids, bile acids, vitamin D, dolichols, haem A, ubiquinone, isopentenyl adenine and cholesterol (Fig.2)[34]. Cholesterol can either be derived by receptor-mediated uptake of low density lipoproteins (LDL) from blood plasma or be synthesized *de novo* from acetyl-coenzyme A (CoA)[35]. Acetyl-CoA is first converted into acetoacetyl-CoA by thiolase (also known as ACAT2); this fusion molecule is then converted into 3-hydroxy-3-methylglutaryl Coenzyme A (HMG-CoA) by the HMG-CoA synthase which, in turn, is converted into mevalonate by the HMG-CoA reductase, the rate-limiting step of the pathway which is tightly regulated (Fig. 2)[36]. Through three enzymatic reaction, mevalonic acid is then converted in isopentenyl pyrophosphate (IPP), which represents the isoprenoids precursor molecule. Consequent reactions result in the production of farnesyl-pyrophosphate (FPP) and geranylgeranyl-pyrophosphate (GGPP), used as intermediates for post-translational modifications, such as prenylation of small GTPases, including the farnesylation of Ras and the geranylgeranylation of Rho proteins[19]. Lastly, sterols, end products as cholesterol, also have an important role in development, as they supply the structural backbone for hormone synthesis[1]. In the cholesterol/steroid biosynthesis branch,

squalene synthase can convert FPP in squalene, in turn converted in lanosterol and then in cholesterol (Fig.2) [36]. Despite being essential in membrane compositions, cholesterol results important also in regulating signal-transduction pathways, for example the subcellular regulation of Hedgehog, important regulator in cell development [37,38]. Moreover, cholesterol is one key component of lipid rafts, in addition to sphingolipids, important for maintaining membrane structure, which also act as signaling hubs for the cell[39].

1.3 Post-translational modifications – Lipidation

In addition, lipids are also important for post-translational modifications (PTMs), since they control the expression, localization and the proper function of a various number of proteins. This process is named *lipidation* and includes different kind of modification (Fig.3): *a)* saturated and unsaturated fatty acids can be bound to cysteine, serine or lysine residues of proteins, through a process named fatty acylation [40,41]; *b)* the myristate molecules can be attached to the N-terminal glycine residue as a stable and irreversible co-translational modification, which potentiate protein-membrane interaction and is required for the proper localization and function of the target proteins [42]; *c)* S-Palmitoylation (or S-acylation) is another major form of fatty acylation, in which palmitate (or stearic acid) is attached to cysteine residues of proteins (i.e. Wnt, TEAD) [43–46]. It is a reversible modification, due to the presence of a thioester group that leads to cycles of acylation and deacylation in response to diverse upstream signals; *d)* glycosylphosphatidylinositol (GPI) anchor is a complex glycolipid that is attached to the C-terminus of proteins[47]. GPIs are synthesized in the ER by sequentially adding monosaccharides, acyl groups, and phosphoethanolamine residues to phosphatidylinositol[48]. In addition to its role in targeting protein to the membrane, GPI anchor has many other biological functions, such as mediating immune response and inflammation, depending on the GPI structure [49]; *e)* covalent modification of proteins by cholesterols is uncommon, but, however, Hedgehog proteins form an ester bond at the C-terminal glycine of the cleaved signaling peptide with cholesterol, therefore regulating cell polarity, development and proliferation[50,51]; *f)* modification of proteins by isoprenoids is known as prenylation. Most prenylated proteins contain a CAAX motif at their C terminus, in which the consensus Cys residue is modified by farnesyl (15-carbon) or geranylgeranyl (20-carbon) groups by farnesyltransferase or geranylgeranyltransferase I, respectively. Prenylation is

generally considered as an irreversible modification, which alters the membrane affinity of proteins[52].

2. Sterol Regulatory Element Binding Proteins – SREBPs

Lipid homeostasis in mammalian cells is tightly regulated. The synthesis of cholesterol and fatty acids is controlled by a family of transcription factors that are homologous of basic helix-loop-helix-leucine zipper (bHLH-Zip) transcription factors, called sterol regulatory element binding proteins (SREBPs)(Fig.4)[53]. In the mammalian genome, three isoforms are present, two encoded by the *SREBF1* gene, located in chromosome 17, SREBP-1a and SREBP-1c, resulting from alternative transcription start sites usage[54]. Additional splice variants have also been reported, although it is likely that represent only minor forms. The *SREBF2* gene, located on chromosome 22, encodes for the SREBP2 protein. All the three isoforms share a common domain structure: N-terminal transactivation domain, a DNA-binding domain, two transmembrane domains and a large C-terminal regulatory domain (Fig.4).

SREBPs differ from other bHLH transcription factors for a tyrosine in place of arginine in the DNA binding domain, that allows the dual binding specificity to both E-box inverted repeats (5'-CANNTG-3') and to the sterol regulatory element sequence (SRE; 5'-ATCACCCCAC-3'), first identified in the LDLR gene promoter[55]. The specificity of the SREBPs isoforms for different target genes is partially explained by the unique binding kinetics to their *cis*-elements. The transcriptional activity of the three SREBPSs isoforms is potentiated by the binding of transcriptional co-factors, such as SP1 and NFY on both cholesterogenic and lipogenic genes[56]. SREBP1a and SREBP2 are able also to bind to CBP and p300, which in turn recruit the Mediator complex to mediate the transcription of lipid genes[57].
Although the SREBP isoforms have been shown to share many common target genes, they have also been found to regulate distinct transcriptional profiles *in vivo.* SREBP1c is principally responsible for the transcription of fatty acid-related genes (i.e. *Fatty Acid Synthase, FASN; Stearoyl-CoA Δ-9 Reductase 1, SCD1)*, SREBP2 induces the transcription of genes involved in cholesterol biosynthesis (i.e. *3-hydroxy-3-methyl-glutaryl-CoA reductase, HMGCR; Low-Density Lipoprotein Receptor, LDLR)*, while SREBP1a seems to regulate genes in both the biosynthetic pathways. It has also been shown that SREBP1a is mostly expressed in cultured cells, rather than SREBP1c, probably because of its ability to

stimulate both the lipogenic and cholesterogenic enzymes and is thus required to provide lipid components to build up cell membranes[56].

Over the last few years, genome-wide studies have identified novel SREBP target genes involved in FA and cholesterol synthesis, as well as genes involved in other biological processes other than lipid metabolism. It has been shown that SREBP1a is able to directly induce the expression of cyclin-dependent kinase inhibitor p21 (CDKN1A)[58] in transgenic mouse livers; in HepG2 cells it induces genes involved in the insulin signaling pathway and genes related to cell cycle control, after treatment with insulin and glucose[59].

In addition, it has been shown that SREBPs has CASP2 and CASP7 as direct targets, which have both been shown to contain SRE binding sequence within in their promoters [60].

2.1 Regulation of SREBP activity

2.1.1 Regulated intramembrane proteolysis (RIP)

SREBPs are synthesized as 125 kDa proteins as an inactive form that reside in the ER membrane. Here, SREBPs form a complex with another ER transmembrane protein, SREBP cleavage activating protein (SCAP). The C-terminal domain of SCAP projects in the cytoplasm and, through the WD40 domain, interacts with the C-terminal domain of SREBP1 and of SREBP2. In addition, SCAP interacts with other two ER membrane proteins, the insulin-induced gene 1 and 2 proteins, INSIG1 and INSIG2, causing the retention of the complex SCAP-SREBPs on the ER (Fig.5)[61]. It is worth noting that INSIG proteins, in addition to hinder the SCAP-SREBP complex in the ER, simultaneously accelerate the degradation of HMGCR, thereby reducing cholesterol production [62].

SCAP is essential for SREBPs transport from the ER to the Golgi; indeed, when cholesterol levels are low, it acts as an escort protein that allows SREBPs to enter the COPII transport vesicles. At a molecular level, SCAP contains a specific binding motif for the COPII vesicle, known as the MELADL motif, that allows the loading of the complex into the COPII vesicles. Moreover, SCAP has two large ER luminal loops, loop 1 and 7 that bind to each other, which allow SCAP to bind to the COPII proteins SEC23 and SEC24 (Fig.5)[63].

Once embedded in the vesicles, SREBPs are transported to the Golgi, where they undergo two sequential steps of proteolytic processing: the first cleavage occurs within the N-terminal luminal loop of SREBPs by site-1-protease (S1P) at the amino acid in position 530, which initially remain tethered to the Golgi membrane[64]. Then, the second cleavage is performed by the site-2-protease (S2P) at the amino acid in position 420 and it results in the release of

the N-terminal active transcription factor, named mature SREBP[65]. Following cleavage by S1P and S2P, the active form is released, it dimerizes with another mature form of SREBP, and via its bHLH domain interact with the nuclear protein importin-β, enters the nucleus as homodimer and binds to the promoter of its target genes (Fig.5)[66,67].

It should be noted that activation of SREBP2 is regulated by cholesterol and oxysterols through SCAP and INSIGs, whereas activation of SREBP1 remains incompletely understood. Indeed, long-chain unsaturated fatty acids and some polyunsaturated fatty acids (PUFAs) are reported to hinder SREBP1 activation, while having little effect on SREBP2 protein. This inhibitory effect is likely due to the activity of the ubiquitin regulatory X domain-containing protein 8 (UBXD8), a protein sensor for long-chain unsaturated fatty acids (FAs)[68,69]. Moreover, in addition to intracellular fatty acids and sterols, some extracellular stimuli also regulate SREBP activity. For example, it has been shown that the transforming growth factor-b-activated kinase 1 (TAK1), which is a signaling molecule activated by inflammatory cytokines, is able to stop the proteolytic maturation of SREBPs by directly interacting with the full-length form[70]. Similarly, the LATS2 tumor suppressor, a kinase that has a central role in the Hippo pathway in controlling organogenesis, prevents SREBP processing and activation via the interaction with the precursor form of the protein[71].

2.1.2 Transcriptional activity and regulation

The transcriptional activity of SREBPs is also regulated at the transcriptional level through several mechanisms. Once in the nucleus, the homodimers of mature SREBPs are able to bind the promoter of their target genes alone or by directly interacting with other transcriptional co-activators or transcription factors. The genes encoding for SREBP1 and SREBP2 contain Sterol Responsive Elements (SRE) motives within their own promoters that mediate feed-forward transcriptional regulation, which also leads to the expression of two micro-RNAs, miR-33a and miR-33b, that are encoded within introns of the human SREBP2 and SREBP1 genes, respectively. The main target of these two miRNAs is the mRNA of the ATP-binding cassette transporter 1 (ABCA1), that mediates the cholesterol efflux. Thus, feed-forward transcription increases not only the precursor form of SREBPs, but also reduces the efflux of newly synthesized cholesterol from cells[72,73].

Early studies of promoters of cholesterogenic and lipogenic genes indicate that, in proximity of the SRE motif, there are binding sites for the general transcription factors SP1 and/or NFY, indicating that these interactions coordinate the transcription of many SREBPs target genes[74,75].

In response to extracellular stimuli, SREBPs are able to interact with other transcription factors. For instance, lipophilic ligands are able to activate some nuclear receptors such as hepatocytes nuclear factor 4 (HNF4) and the liver X receptor (LXR), that regulate SREBP activity by a direct binding. The transcriptional activity of HNF4 is enhanced by the presence of the peroxisome proliferator-activated receptor γ co-activator 1α (PGC1α). Mechanistic analyses revealed that SREBPs compete with PGC1α for direct interaction with HNF4, inhibiting functions related to HNF4 target genes expression[76,77]. SREBPs also inhibit PGC1α co-activation of other transcription factors such as the androgen receptor, the pregnane X receptor and the farnesoid X receptor. On the other hand, the interaction of HNF4 and SREBPs increases the transcription of SREBPs target genes, potentiating its transcriptional program[78]. Moreover, SREBP1a mRNA is expressed at high levels in cells of the immune system by the activity of NFκB in macrophages, as part of the proinflammatory phase of the innate immune response [79].

Another layer of regulation is represented by the tumor suppressor p53 and by its mutant forms. The wild-type form of p53 can inhibit SREBPs transcriptional activity [80,81]. On the contrary, it has been demonstrated that gain of function (GOF) mutant p53s interact with SREBPs, playing a role in the disruption of morphology of mammary epithelial cells grown in 3D[82].

The transcription of SREBP-1 is activated by liver X receptors (LXRs) [83]. LXR has two isoforms, LXRα and LXRβ, which are nuclear receptors that regulate cholesterol and bile acids metabolism [84]. It has been demonstrated that LXR can activate SREBP at the transcription level, mainly because there are two LXR-responsive elements within the SREBP1c promoter, which activates SREBP-1c transcription in response of cholesterol overloading, possibly to increase the unsaturated fatty acids needed for cholesterol esterification and storage[53,85,86]. LXR has been established as an oxysterol receptor and plays a key role in managing an excess amount of free cholesterol in the cells by enhancing cholesterol efflux or bile acid synthesis. Since SREBP1c can activate fatty acids synthesis, activation of SREBP1c by the oxysterol receptor could be another cellular adaptation for

excess cholesterol by enhancing formation of cholesterol esters, suggesting a new link between cholesterol and fatty acids metabolism[87].

2.1.3 Post-translational modifications

Beyond sterols, SREBPs are regulated by growth factors, by the energy status of the cell, and in response to nutrient levels. In addition to the proteolytic regulation, SREBPs activity is tightly modulated by different transcriptional programs, associated to various signaling pathway.

Nuclear SREBPs are rapidly degraded by the ubiquitin and the proteasomal system, suggesting that the transcription of the target genes is tightly controlled by the stability of the mature form of SREBPs. Moreover, not only the nuclear form is subjected to the degradation via the ubiquitin-proteasomal pathways, but also the precursor form of SREBPs. Indeed, it is first phosphorylated by glycogen synthase kinase-3-β (GSK3β) at three residues in the mature protein (T426/S430/T434), that then recruits the SCF^{Fbw7} ubiquitin ligase and the subsequent degradation of the protein by the proteasome pathway occurs[88,89]. On the contrary, nuclear SREBP is stabilized by acetylation of the ubiquitylated Lys residue in the DNA-binding domain. The interaction with transcriptional co-activators, such as p300 and CBP, that have an intrinsic histone acetyltransferase activity, boosts SREBP transcriptional activity [90].

In addition to GSK3β, other kinases have been reported to phosphorylate SREBPs: it is the case of Cdk1/cyclin B complex. Indeed, hyperphosphorylation of mSREBP1a and mSREBP1c leads to the increased stability of the proteins during mitotic division [91].

The insulin-stimulated SREBP-1c activation is PI3K/Akt dependent, leading to the activation of mTOR complex 1. Many works demonstrated that mTORC1 stimulates SREBP1c activity. For example, Düvel and colleagues showed that SREBP1 is activated in Tsc1/2 null mouse embryonic fibroblasts (MEFs) and activation of SREBP1 is inhibited upon rapamycin treatment, indicating that activation of mTORC1 is sufficient to stimulate SREBP1 activity and similarly, the inactivation of mTORC1 is sufficient to shut down SREBP1 and lipogenesis[92]. mTOR activity is required for the nuclear accumulation of SREBP1 in response to Akt activation. mTORC1 also regulates the expression of SREBP1 and is required for the stimulation of lipogenesis in the liver[1]. Consequently, hyper-activation of

mTORC1 boosts the deregulation of *de novo* lipid synthesis necessary for sustained membrane production and cell proliferation[93]. Strikingly, in a recent work, the expression of oncogenic PI3K or K-Ras induces de novo lipogenesis via mTOR and SREBP1 in several breast cancer cell lines[94]. Moreover, mTORC1 phosphorylates and throws out from the nucleus the phosphatidic acid phosphatase lipin-1, which leads to activation of nuclear SREBP1; however, the specific molecular mechanism by which lipin-1 causes nuclear remodeling through its activity on the nuclear lamina, and thus regulates nuclear transport of SREBP1, is still unknown [95].

Under condition of energy stress, SREBPs and the anabolic pathways such as lipogenesis are usually turned off and inhibited by factors sensitive to energy depletion. The AMP-activated protein kinase (AMPK) is the sensor of cellular energy homeostasis and antagonizes pathways stimulated by insulin[96]. Recently, it was reported that AMPKα subunit strongly associates with and is able to phosphorylate serine residues in the bHLH domain of SREBP1c and SREBP2 in diabetic rat livers. These phosphorylation events prevent cleavage and subsequent nuclear translocation of the transcription factors in response to polyphenols and metformin treatment[97]. AMPK may also influence lipid biosynthesis through the regulation of acetyl-CoA carboxylases ACC1 and ACC2, which catalyzes the rate-limiting step of fatty acid biosynthesis and of HMG-CoA reductase, inhibiting the cholesterol synthesis[98,99].

As previously mentioned, upon cellular sterols depletion, cholesterol dissociates from the sterol-sensing domain of SCAP, releasing Insig and allowing the SCAP-SREBP complex to exit the ER through COPII vesicles transport. Moreover, it is known that the ER is the principal site for folding and maturation of transmembrane, secretory and ER-resident proteins and that it contains many chaperon proteins, such as GRP78/94 and calreticulin, all involved in the correct folding of newly synthetized proteins and in preventing the accumulation of misfolded proteins[100]. Disruption of the ER primary functions that interferes with proper folding and maturation of proteins causes ER stress and initiates the unfolded protein response (UPR)[101]. Conditions that cause ER stress or apoptosis induce SREBPs activation, independent of the intracellular cholesterol content. Previous studies revealed also that caspase-3 and caspase-7 cleave the SREBPs following apoptotic stimuli in a sterol-independent manner, suggesting that caspase cleavage site is located in the N-terminal cytoplasmic side of SREBP at a site other than S1P/S2P[102]. Later, Colgan and

colleagues demonstrated that ER-stress induced SREBP-2 activation and downstream cholesterol accumulation does not require caspase activation and can be inhibited by disrupting the conventional proteolytic pathway[101].

In conclusion, the transcriptional activity of SREBPs is regulated by a plethora of inputs downstream of signaling pathways, oncogenes, metabolites feedback and upon many different metabolic stimuli.

2.1.4 SREBPs in model organisms

SREBPs translocation and proteolytic maturation mechanisms are widely conserved, but the auto-regulatory systems show differences among animal species. For example, SREBP activity is primarily sensitive to phospholipids in *Drosophila melanogaster* and *Caenorhabditis elegans,* which are cholesterol auxotrophs, because they lack several enzymes involved in cholesterol biosynthesis pathway[103].

In *Drosophila melanogaster*, the genome encodes for a single form of SREBP, for SCAP, S1P and S2P, but no Insig proteins. Seegmiller et al. found out that *Drosophila* SREBP (herein named dSREBP) mediates the fatty acid biosynthesis by transcriptional regulation, showing that dSREBP increases the transcription of genes whose protein products are required for fatty-acid synthesis, such as fatty-acid synthase (FAS). Moreover, in *Drosophila* S2 cells, it was shown that dSREBP proteolytic cleavage occurs in the same manner as in mammalian cells, involving dSCAP and the dS1P and dS2P[104]. However, despite the high similarities of the proteolytic processing among species, in *Drosophila* dSREBP activation cannot be suppressed by sterols, nor by unsaturated fatty acids as seen in mammalian cells. Instead, dSREBP cleavage is suppressed by the saturated fatty acid palmitate[105].

Palmitate has many fates, but in particular it is utilized for the formation of sphingolipids; detailed studies revealed that dSREBP is activated in response to levels of phosphoethanolamine (PE): in conditions of low PE levels, dSREBP upregulates enzymes involved in the biosynthesis of phospholipids, such as phosphocholine cytidylyltransferase, in addition to enzymes of the fatty-acid biosynthetic pathway[106]. Moreover, studies of dSREBP in whole animal suggest that dSREBP is necessary for larval development. Indeed, flies lacking dSREBP are fatty acids auxotroph and have developmental defects[107].

In *Caenorhabditis elegans*, the SREBP ortholog SBP-1/LPD-1 is required for fat accumulation [108,109]. Worms lacking SBP-1 have impaired fat storage in the intestine, and gene expression analyses indicates that SBP-1 is required for expression of lipogenic genes[57]. Moreover, SBP-1 is also required for the biosynthesis of the branched-chain fatty

acid (BCFA), which are important for post-embryonic development and growth control, through regulation of the expression of two long-chain fatty acid elongases, *elo-5* and *elo-6*, and the very-long-chain acyl CoA synthetase *acs-1*[110,111].

2.2 SREBP sustains protein prenylation

The post-translational modification of proteins by the addition of isoprenoids has been recognized as a key physiological process in facilitating cellular protein-protein interactions and membrane-associated protein trafficking. Protein prenylation occurs by the covalent addition of two types of isoprenoids, farnesyl pyrophosphate (FPP) or geranylgeranyl pyrophosphate (GGPP), produced exclusively by the mevalonate pathway. All the isoprenoid molecules derive from a common five-carbon (C5) building unit, the isopentenyl diphosphate (IPP) and its isomer dimethylallyl diphosphate (DMAPP)[112].
The isoprenoids farnesyl pyrophosphate (C15) and geranylgeranyl pyrophosphate (C20) are key products of this pathway, and farnesyl transferase (FTase) and geranylgeranyl transferase (GGTase I and II), that are under the control of SREBP transcriptional program, catalyze protein prenylation. FTase and GGTase are both heterodimers sharing the alpha subunit and recognize proteins with a specific C-terminal CAAX, CXC or CC motifs, essential to determine which of the two enzymes act on the protein. If X is a Ser, Met, Ala or Gln, the protein is processed by FTase, while if it is a Leu residue, GGTase directs the protein modification[113,114]. These isoprenoid groups can be covalently attached to proteins to facilitate membrane associations and protein-protein interactions[19].

After the attachment of the two lipid molecules, a post-prenylation process occurs. First, the CAAX proteins are further modified by Ras converting enzyme 1 (RCE1), an endoprotease that cuts off the -AAX tripeptide from the CAAX box. The final step of the enzymatic processing is the carboxyl methylation of the isoprenylcysteine residue, by the isoprenylcysteine-carboxyl-methyltransferase (ICMT). This conclusive step, together with prenylation, makes the carboxyl-terminal end of the protein hydrophobic and prone to associate with membranes[114]. Overall, prenylation enhances lipophilicity and favors lipid-lipid interactions of small GTPases with cellular membranes. This enzymatic transfer is fundamental for the proper localization in the cell of several proteins involved in many aspects of cell biology, including cell division, migration, death, intracellular trafficking, protein stability and cytoskeleton organization[115]. Deregulation of isoprenoid levels and

protein prenylation is involved in many pathological conditions such as neurodegeneration, cardiovascular diseases and cancer[116–118].

Among the prenylated proteins, a large group that undergoes this post-translational modification is the one of the small GTPases, that includes the Ras, Rho, Ran and Sar/Arf1 families. Prenylation of these proteins allows their proper localization and function within the cell.

Exemplifying, the subfamily of Ras has been the most extensively studied due to its well-known role in carcinogenesis. In fact, Ras is known to be mutated in around 30% of human cancers. All these mutations stabilize Ras in a constitutively active GTP-bound conformation that contribute to its oncogenic function [119].

The Rho family included Cdc42, Rac and RhoA, which are important in many biological processes, such as regulation of cytoskeleton, in cell polarity, proliferation, apoptosis, actin filament formation, adhesion and motility. In particular, RhoA is involved in the regulation of stress fiber formation, cell contraction and mechanotransduction process[120].

Rho family has also been linked to tumorigenesis, affecting gene expression, cell proliferation and survival their deregulated activation can also drive transformation by altering tumor metabolism[35].

Overall, all the functions related to these class of proteins are strictly dependent on their prenylation status, suggesting a central role of FPP and GGPP in the biology of the cell.

3. Mechanotransduction: transmission of physical inputs from the outside to the inside of the cell

It is well known that cells receive information from their surrounding by chemical signals, such as hormones, chemokines and secreted signaling factors. However, multiple studies suggest that cells can also receive information from the physical properties and forces of their microenvironment. All the cells of an organism are subjected to a plethora of forces, including compressive, tensile, fluid shear stress and hydrostatic pressure, each playing important roles in determining the shape, the development and the maintenance of the tissue. For example, during early embryonic development, cell movements at the gastrulation stage are the key to locate the developing tissues in their correct spatial organization; during organogenesis, mechanical forces are crucial for the formation of many, if not all, the organs, such as lungs, blood vessels, mammary gland, brain, kidneys, muscles,

heart, bones as well as the hematopoietic system; later on, tensional forces and ECM mechanics are fundamental to maintain the differentiated status of epithelial cells during the mammary gland development, while the complete loss of ECM structure lead to the regression of the tissue and the involution of capillary blood vessels [121,122].

It is important to note how cells interact with the forces they are subjected to and how they respond to them, and it is strictly dictated by the physical properties of the cells themselves, their neighboring cells and the surrounding environment, defined as extracellular matrix (ECM), which is the major components of the extracellular space of all the tissues and organs. To sustain all these interactions, cells exhibit viscoelastic properties, meaning that they can deform in a time-dependent manner upon the force is applied, and then they can return in their original physical state after the removal of the applied forces [123].
Moreover, during the last decade, a series of studies led to the concept that mechanical forces are fundamental for cells to perceive their position within space, to dictate and maintain the architecture of the tissue, to determine the fate of stem cells and in general, to define the physiology of the cell and the tissue homeostasis. Conversely, perturbations of physiological forces and changes in ECM composition can result in the development of several diseases, such as atherosclerosis, arthritis, developmental disorders, tissue fibrosis, neurodegeneration and cancer [122,124,125].
Thus, it is important to understand the mechanotransduction mechanism, defined as how cells translate extracellular mechanical and physical inputs into biochemical signals, enabling the cell to respond in the proper way. It generated a series of studies that took the scientific world to better understand the role of forces in cell biology.
The so-called “mechanotransduction” can then be divided into three key steps: mechanosensing, mechanotransmission and mechanoresponse.

3.1 Mechanosensing – perception of the mechanical signal at the cell-ECM interface

Several reports indicate that forces initiate complex signal transduction cascades leading to gene transcription and functional responses via interaction of integrins with extracellular matrix proteins, or by stimulation of G protein coupled receptors, tyrosine kinase receptors or ion channels.
One of the main sources of environmental signals is the rigidity of the ECM. Over the past years, it has been demonstrated that rigidity sensing often involves the periodic formation

and disruption of sensory modules that, after the perception of extracellular signals, is able to transduce this signal from the outside to the inside of the cell. This sensing process is indeed mediated by the integrins, transmembrane proteins that form the interaction between the ECM at the extracellular side and the actin cytoskeleton, via adapter proteins, at the intracellular side [126–128]. In particular, they have been shown to bind to collagen, fibronectin, tenascin, in complex with glycosaminoglycans and proteoglycans which are key components of the ECM. These interactions between the cell and the ECM are referred to as “Focal Adhesions” which can span up to several microns in area, indicating their importance in anchoring the cell to the ECM (Fig.6) [129,130].

The structure of focal adhesions has been demonstrated and consists of the aggregation of several players. It is composed by the cytosolic tail of the integrins, which act as docking site of other components, such as the focal adhesion kinase (FAK), and paxillin assembled with a stratum containing talin and vinculin, and an uppermost actin-regulatory sheet consisting of zyxin, VASP (vasodilator Stimulating phosphoprotein) and alfa-actinin, which tethers the FA to the actomyosin cytoskeleton[131]. The adhesions alter their size, strength and dynamics in response to the applied force and to resistance of the matrix, resulting in larger adhesion on rigid matrices (Fig.6).

3.2 Transmission of mechanical cues through the cytoskeleton

The main player of the propagation of extracellular signals and cell-generated forces is the cytoskeleton. It provides mechanical support and control motility, shape and tension homeostasis of the cell. It is a highly dynamic structure that is composed by actin fibers (F-actin), microtubules (MTs) and intermediate filaments (IFs), whose structure determine the intracellular organelle integrity and maintenance. Among these elements, the actin cytoskeleton is thought to play a prominent role in force development, while microtubules can be considered as force-resisting modules [122]. Cytoskeleton contractility is ensured by F-actin sliding on the motor protein myosin II, which are bond by crosslinking proteins, such as a-actinin, fascin and filamin, to form complex structures called stress fibers (Fig.6).

F-actin filaments are anchored to the focal adhesion and connect the ECM to the nucleus. Hence, when the FAs sense the external forces (inside-out signaling), they transmit the input to the cytoskeleton that, in turn, induces its own contraction and enable the cell to change its shape or to migrate. By this same system, cells can also measure extracellular forces and their variations. It is currently thought that a tensional equilibrium exists between cells

and the ECM: when cells are subjected to external forces from the ECM, they immediately generate opposite internal forces through the actomyosin cytoskeleton (outside-in signaling).

One way that cells have to propagate external signals by stress fibers occurs through the activation of the Rho/ROCK signaling pathway. Upon mechanical stimulation, the small GTPase RhoA is recruited at the focal adhesion site and triggers a signaling cascade that leads to the acto-myosin contraction. It activates its kinase ROCK that, in turn, induces myosin II activation by the direct phosphorylation of myosin regulatory light chain (MLC) in Ser19 residue or by inhibition of MLC phosphatase (MLCP), leading to the activation of myosin II ATPase, generating contractile forces. This then leads to the activation of mechanosensory proteins, such as YAP/TAZ or SRF, that alter the biological response of the cell, in relation to the stimuli they are subjected to [132,133]. At the same time, ROCK has a role in cytoskeletal stabilization. The RhoA/ROCK pathway activates also the formin Diaphanous (mDia), which directly and through the Arp2/3 complex promotes F-actin polymerization (Fig.6,7)[134].

Overall, the actin cytoskeleton acts as a mechanosensor by rapidly altering its composition, organization and function to enable cells to sense and adapt to their immediate environment.

3.3 Cellular signaling in response to mechanical stimuli

Cells change their shape and drive cytoskeleton rearrangements in response to different mechanical cues. It has also been shown that mechanical stimuli modulate cellular phenotypes according to the nature of the stimuli, such as growth, proliferation, differentiation and apoptosis [122]. Changes in the ECM physical properties, perturbations of the actin cytoskeleton tension, culturing cells in defined geometry are all inputs that cause a rearrangement of the cell. Indeed, culturing cells on stiff matrices enables cells to spread on the surface and to generate large focal adhesion sites and internal forces, while on soft matrices remain rounded with lower internal forces. One example of how mechanical cues regulate cell phenotypes is the demonstration that substrate stiffness modifies the direct differentiation of mesenchymal stem cells (MSCs). MSCs were cultured on synthetic substrates that were crosslinked to varying degrees to modify the elastic modulus of the surface: when cultured on stiff substrates (> 25 kPa), MSCs differentiate in the osteogenic lineage, cultured on soft substrates (< 1kPa) in adipogenic phenotype and on medium stiffness substrate (8-17 kPa) in myogenic phenotype [135].

From this and other important studies emerged the idea that ECM rigidity and cytoskeleton tension are able to modulate some transcriptional program to let the cell to adapt to its own environment. Indeed, several biochemical pathways associated to the mechanotransduction process have been identified so far. A stiff ECM environment leads to the formation of focal adhesions that, as mentioned before, recruit signaling proteins that in turn activate many signaling pathways, such as FAK and Src-associated kinases that activates the Mitogen-Activated Protein Kinases (MAPKs), enhancing activation of ERK1/2 (Fig.7)[136,137]. In addition, other players are involved into the transmission of extracellular stimuli to the inside of the cell and, among the growing list of mechanosensitive proteins, we can find the c-jun N-terminal kinase (JNK), nuclear factor kappa-light-chain-enhancer of activated B-cells (NFκB), β-catenin, SNAIL1, TWIST, Notch and KLF2a[138–144].

As said before, cytoskeletal remodeling involves the activation of the Rho/ROCK signaling pathway: indeed, it can be recruited to the focal adhesion sites upon stiff ECM rigidity and promote actin fibers generation. The shift from the monomeric (G-actin) to the filamentous-polymerized status of actin (F-actin) leads to the activation of mechanosensitive molecules, the myocardin-related transcriptional factors MAL/MRTF. Once MAL/MRTF is free in the cytosol, it is able to translocate to the nucleus and, together with the Serum Response Factor (SRF), modulate a specific transcriptional program involved in cell motility and fate regulation (Fig.7)[145,146].
Moreover, actin remodeling activates other mechanosensitive transcriptional co-factors, involved in organ growth, tissue homeostasis and stem cell maintenance, known as Yes-associated protein 1 (YAP1) and PDZ-binding motif (WWTR or TAZ). In response to a number of mechanical stimuli, YAP/TAZ translocate to the nucleus, interact with different transcription factors and activate a given genetic program [147]. Increasing evidence suggests that YAP/TAZ are relays for ECM mechanics given their extreme sensitivity to substrate stiffness, cell-cell interaction and cell spreading (Fig.7) [148–150].

Emerging evidence indicates that external mechanical forces trigger changes in nuclear envelope structure and composition, chromatin organization and gene expression [151]. Forces generated from the outside are transmitted to the nucleus through the cytoskeleton. The cytoskeleton networks bridge the cell membrane and the nucleus through the linker of nucleoskeleton and cytoskeleton (LINC) complex, thereby allowing the direct transmission of mechanical signals (Fig.7)[152,153]. The LINC complex span over the inner nuclear

membrane, binding then to the web of nuclear lamina, giving rise to the nuclear cytoskeleton. Then, the LINC complex mediates force transmission from focal adhesions to the nuclear envelope, resulting in nuclear deformation and possibly to alterations of chromatin structure and organization, impinging on the activation of given transcriptional program upon defined stimuli.

Aim of the thesis

SREBPs are transcription factors which function as master regulators of genes that control cellular lipid homoeostasis to meet organismal requirements. Its activity is sensitive not only to sterols, but also to polyunsaturated fatty acids (PUFAs), independently of cholesterol.
In addition to sterols, the SREBP-induced mevalonate pathway produces key isoprenoid metabolites, farnesyl pyrophosphate (FPP) and geranylgeranyl pyrophosphate (GGPP), which serve as lipid donors for regulatory PTMs of target proteins (prenylation).
Inhibition of SREBPs, by reducing the levels of isoprenoids, impacts on a plethora of biological processes, including cell division, migration, death, intracellular trafficking, protein stability and cytoskeleton organization. Deregulation of isoprenoid levels and protein prenylation is involved in many pathological conditions such as neurodegeneration, cardiovascular diseases and cancer.

Despite their crucial activity as pathophysiological effectors of SREBPs, the role of isoprenoids in the regulation of SREBP activation has been poorly investigated so far.
While a number of studies have demonstrated the control of SREBPs by sterols, the effect of the isoprenoids on SREBPs transcriptional activity remains mainly un-investigated.
Thus, the aim of this thesis is to investigate the role of the isoprenoid geranylgeranyl pyrophosphate in the regulation of SREBPs nuclear activity and, consequently, to dissect the biological process linked to GGPP that might regulate SREBPs activation.

Results

Protein geranylgeranylation controls SREBP1 transcriptional activity.

To investigate whether isoprenoids play a role in the activation of SREBPs, human epithelial breast cell lines were transfected with two reporter plasmids, low density lipoprotein promoter-luciferase (LDLR-Luc)[154] and Steaoryl-CoA desaturase promoter-luciferase (SCD1-Luc), as readouts of SREBP activation and were maintained in conditions of reduced intracellular cholesterol in order to activate SREBPs. Specifically, cells were treated with cerivastatin, or grown in serum-free or lipid-depleted media. All these conditions induced a robust activation of SREBPs, as demonstrated by increased luciferase activity after 24 hours, using either LDLR-Luc (Fig. 8a) or SCD1-Luc (Fig. 13a). As expected, supplementing the medium with cholesterol prevented SREBP activation (Fig. 8a and Fig. 13a). Interestingly, addition of GGPP to the medium, but not of FPP, inhibited SREBP activation to an extent comparable to cholesterol addition (Fig. 8a and Fig. 13a). These results were confirmed by analysing the expression in serum-starved cells of four endogenous SREBP target genes, *LDLR*, *SCD1*, *Acetyl-CoA Carboxylase 1 (ACC1)* and *Fatty Acid Synthase (FASN)* at the mRNA levels (Fig. 8b), and of SCD1 protein level (Fig. 8c).

The processing of SREBP1 was strongly prevented by GGPP in serum-starved cells after 24 hours of treatment, while under the same conditions SREBP2 processing remained unaltered (Fig. 8c). To completely deprive cells of cholesterol, both exogenously uptaken and endogenously synthetized, cells were maintained in lipid-depleted medium and treated with statin. In these conditions, GGPP addition prevented activation of LDLR-Luc (Fig. 8d) and SCD1-Luc (Fig. 13b), upregulation of *LDLR*, *SCD1*, *ACC1* and *FASN* mRNA (Fig. 13c), of SCD1 protein (Fig. 13d), and processing of SREBP1 (Fig. 13d). This result clearly demonstrates that the effect of GGPP was independent of cholesterol.

The effect of GGPP on SREBP1 processing was further confirmed in a panel of cell lines from different tissues, as breast (MDA-MB 231), lung (H1299) and liver (Mahlavu and Immortalized Human Hepatocytes, namely IHH) (Fig. 13e, f). In line with these results, GGPP treatment prevented SREBP1 nuclear translocation induced by serum starvation (Fig. 13g). Altogether, these results establish GGPP, a key intermediate of the mevalonate pathway, as an endogenous modulator of SREBP1 maturation and function.

Upon binding to geranylgeranyl-transferase 1 (GGTI, hereafter referred to as GGTase1), GGPP modifies a considerable number of target proteins (Fig. 8e) mainly involved in signal transduction, structural organization and trafficking, controlling their localization and function [155]. To test whether protein geranylgeranylation was involved in SREBP1 activation, we inhibited the transfer of the geranylgeranyl moiety to target proteins by using GGTI-298, a specific inhibitor of GGTase1[118]. This treatment induced a strong activation of SREBP1 transcriptional activity, as assessed using the LDLR-Luc (Fig. 8f and Fig. 13h) and SCD1-Luc (Fig. 13i) reporters. This effect was specific, since a mutation of a single nucleotide within the sterol responsive element (SRE) of the LDLR-Luc reporter construct completely prevented the luciferase signal (Fig. 8f). GGTI-298 treatment also caused a robust and time-dependent increase of SREBP1 maturation (Fig. 8g and Fig. 13k), with a consequent induction of SREBP1 target genes, as monitored by upregulation of *SCD1* mRNA (Fig. 8h and Fig. 14l) and protein (Fig. 8g and Fig. 13k) levels, and upregulation of *LDLR*, *ACC1*, *FASN*, and *3-hydroxy-3-methylglutaryl-CoA reductase* (*HMGCR*) mRNA levels (Fig. 8h, Fig. 13j and Fig. 14l). This effect was prevented by SREBP1 knock-down (Fig. 8i and Fig. 13l). SREBP1 activation upon GGTI-298 treatment also increased the intracellular content of lipids, with a consequent accumulation of lipid droplets within the cytoplasm (Fig. 8j). Under these conditions, adding back GGPP did not reverse SREBP1 activation (Fig. 13m), suggesting that protein prenylation, instead of the GGPP intracellular levels, is required for SREBP1 regulation.

Taken together, these data demonstrate that SREBP1 is controlled by protein geranylgeranylation and suggest that one or more GGTase1 target proteins are involved in SREBP1 activation and lipid biosynthesis.

SREBP inhibition is mediated by RhoA and acto-myosin contraction.

In humans, a total of 124 proteins (including isoforms), corresponding to 75 genes[156,157], are predicted to be geranylgeranylated by GGTase1. To identify geranylgeranylated proteins involved in SREBP1 regulation, we assembled a custom library of siRNAs targeting all but one (PALM3) of the mRNAs coding for proteins predicted to be GGTase1 targets. Next, we screened this library in MDA-MB-231 cells, in condition of basal SREBP activity (medium supplemented with 10% Fetal Bovine Serum, FBS), using a LDLR-Luc-based SREBP1 activation assay. As shown in Figure 9a, the majority of transfected siRNAs led to SREBP

activation. Of note, many of the targeted proteins, whose downregulation by siRNA was able to activate SREBP1, were involved in actin cytoskeleton dynamics (Fig. 14a).

Among these proteins, RhoA, a small GTPase known to control acto-myosin dynamics, scored as second best hit in the screening (Fig. 9a and Table 3) and the first one after validation of the top five hits using independent siRNAs and LDLR-Luc or SCD1-Luc reporter (Fig. 14b-d)[158]. This evidence led us to hypothesise that RhoA could act as a negative regulator of SREBP1 and lipid biosynthesis. We next evaluated the level of RhoA prenylation in cells in which statin treatment inhibited mevalonate pathway, leading to SREBP1 activation. In these conditions, a reduction of RhoA prenylation correlated with the activation of SREBP1 (Fig. 9c), while addition of GGPP to the medium efficiently rescued RhoA prenylation (Fig. 9c). This suggested that RhoA activation might play a role on SREBP1 regulation. Confirming this hypothesis, silencing of RhoA by two independent siRNAs (Fig. 14b) caused SREBP1 maturation and functional activation, as assessed by SCD1 protein accumulation (Fig. 9b) and either LDLR-Luc or SCD1-Luc reporter activity (Fig. 14c, d). Conversely overexpression of a constitutively active form of RhoA, RhoA G14V (Fig. 14g), caused a reduction of LDLR-Luc (Fig. 9d and Fig. 14h) signal and SCD1-Luc (Fig. 14i), while overexpression of the dominant negative RhoA T19N (Fig. 14g) caused LDLR-Luc (Fig. 9d and Fig. 14h) and SCD1-Luc activation (Fig. 14i). Accordingly, RhoA inhibition by C3 toxin caused LDLR-Luc (Fig. 9e and Fig. 14j) and SCD1-Luc activation (Fig. 14k) and induction of *LDLR*, *SCD1* and *HMGCR* mRNA expression (Fig. 14l).

Upon geranylgeranylation, RhoA localizes at the plasma membrane and triggers actin polymerisation and acto-myosin contraction, via activation of its downstream effector Rho-kinase (ROCK)[159], which phosphorylates the myosin light chain 2 (MLC2). To test whether the regulation of SREBP1 by RhoA requires the canonical ROCK pathway, we treated human epithelial breast cells with either the ROCK inhibitor Y-27632 or the myosin inhibitor Blebbistatin and monitored SREBP1 transcriptional activity. Both treatments activated SREBP1, as shown by induction of either LDLR-Luc (Fig. 9f and Fig. 14j) or SCD1-Luc reporter activity (Fig. 14k), and by *LDLR*, *SCD1, ACC1, FASN* and *HMGCR* mRNA expression (Fig. 14l). Moreover, the effect of RhoA overexpression on SREBP1 activation was abolished by inhibition of actin polymerisation with Latrunculin A treatment (Fig. 9d and Fig. 14h, i), thus demonstrating that actin polymerisation acts downstream of RhoA/ROCK signalling to control SREBP1 activation. Furthermore, inhibition of either RhoA or ROCK induced a massive accumulation of lipid droplets in liver cells (Fig. 9g). Taken together,

these experiments show that RhoA/ROCK signalling and acto-myosin dynamics impact on SREBP1 activation and lipid biosynthesis in human cells.

Evolutionarily conserved SREBP inactivation via RhoA/acto-myosin axis

We further investigated the impact of the ROCK/acto-myosin axis on SREBP activity, by using *Drosophila melanogaster* as a model organism, taking advantage that it expresses a single SREBP homolog (dSREBP)[104] whose activity is controlled independently of cholesterol[106,160]. dSREBP turned out to be activated in *Drosophila* S2 cells maintained for 24 hours in serum-free medium. This effect was prevented by supplementing the medium with GGPP (Fig. 15a). Moreover, inhibition of either actin polymerisation or acto-myosin contraction, with Latrunculin A or the ROCK inhibitor Y-27632 respectively, caused activation of dSREBP to an extent similar to maintaining cells in lipid-depleted medium [160] (Fig. 15b), thus demonstrating that the ROCK/acto-myosin axis controls SREBP maturation in *Drosophila* cells.

We next validated these findings *in vivo*, by monitoring dSREBP activation and lipid accumulation in the larval adipose tissue (fat body)[161], upon either tissue-specific knockdown of *Drosophila* RhoA (dRhoA), or inhibition of ROCK by Y-27632 [162,163]. dRhoA knockdown and ROCK inhibition impaired acto-myosin contractility in adipocytes, as demonstrated by reduced staining of phosphorylated MLC2 (pMLC2) (Fig. 9h, i). Strikingly, both conditions promoted dSREBP maturation (Fig. 15c, d), nuclear translocation (Fig. 9h, i) and transcriptional activity in these cells, as shown by upregulation of mRNA levels of the dSREBP target *Fatty Acid Synthase* (*FAS*) (Fig. 15e), and expansion of LDs (Fig. 9h,i and Fig. 15f,g). Treatment with fatostatin, a potent SREBP1 inhibitor[164], suppressed both phenotypes induced by dRhoA knockdown, *i.e*. *FAS* upregulation (Fig. 15e) and lipid accumulation (Fig. 9h) , demonstrating that these effects were the result of dSREBP activity. Altogether, these experiments demonstrate that modulation of acto-myosin dynamics impacts on dSREBP activation and lipid biosynthesis and accumulation in a living organism.

ECM stiffening inhibits SREBP-dependent lipid biosynthesis.

Acto-myosin contractility has a key role in intracellular sensing and transduction of mechanical forces generated by the architecture and rigidity of the ECM. The physical properties of the ECM influence the growth and shape of virtually all tissues and organs [165], and impact on a plethora of processes ranging from tissue morphogenesis to cancer development.

Physical cues are promptly sensed by acto-myosin through RhoA[165]. Therefore, we hypothesized that the physical features of the ECM could impact on SREBP1 activation via RhoA. We tested this hypothesis by growing human epithelial breast cells on fibronectin-coated hydrogels characterized by progressively reduced elastic moduli (e.g. 50, 4 and 0.5 kPa; Fig. 10a). In these conditions, ECM softening led to a marked impairment of mechano-signaling pathways, as demonstrated by reduction of phosphorylated MLC2 (pMLC2) and Focal Adhesion Kinase (pFAK), as well as of the protein levels of the mechano-transducer TAZ (Fig. 10b, e), and triggered a progressive induction of SREBP1 protein maturation (Fig. 10b, e) and transcriptional activity (Fig. 10c, d and Fig 16a, b). Furthermore, cells grown in soft ECM showed a marked SREBP1-dependent lipid droplets accumulation (Fig. 10f).

In line with these data, unbiased gene set enrichment analysis showed that the genes involved in lipid metabolism were enriched in MDA-MB-231 cells grown on soft as compared to cells grown on stiff hydrogels (Fig. 16c)[166]. Using the same culturing conditions, the impact of mechanical stimuli on SREBP1 cleavage and activity was further confirmed in primary cells from mouse mammary and liver epithelia, and in cell lines from different human tissue origin (i.e. liver, colon, breast, pancreas and others). Indeed, along with reduced pMLC2 and TAZ protein levels, all the cells grown on soft conditions exhibited an increased maturation of SREBP1 and, an enhancement of its transcriptional activity, as demonstrated by increased SCD1 protein levels (Fig. 16d).

Taken together, these results demonstrate that SREBP1 activity is under control of mechanical cues and that increase of ECM stiffness may inhibit its biological function.

To validate our observations in human samples, we generated a signature specific for SREBP1 [167] (Table 4), as a proxy of SREBP1 activation, to interrogate two public datasets of human transcriptional profiles from different physiological and pathological conditions: i) normal breast tissue with high v_s low mammographic density[168], a parameter that directly correlates with tissue stiffness[169]; ii) lung tissue from patients affected by Idiopathic Pulmonary Fibrosis, a condition linked to pulmonary tissue stiffness[170], v_s healthy

controls[171]. Of note, activation of SREBP1 inversely correlated with mammographic density and lung tissue fibrosis, suggesting that in these physio-pathological conditions SREBP1 might respond to mechanical cues (Fig 10g).

AMPK suppresses SREBP1 activation downstream of mechanical inputs.

We next investigated how mechanical stimuli and acto-myosin dynamics control SREBP1 activation. SREBP1 maturation, stability, nuclear accumulation and transcriptional activity are controlled by a complex repertoire of PTMs [88,172–174]. Among them, phosphorylation by AMP-activated protein kinase (AMPK), a key sensor of the cellular energy status, inhibits SREBP1 proteolytic maturation[172].

AMPK has been recently found to be activated by E-cadherin-dependent actin polymerisation [175] and by mechanosensitive Ca^{2+} influx at focal adhesions [176]. Therefore, we reasoned that, in response to an increase in ECM stiffness, acto-myosin contraction leads to AMPK activation and consequent SREBP1 inhibition, as a mechanism to prevent anabolic processes and increase ATP availability. Consistently, in human breast epithelial cells, inhibition of RhoA/ROCK by either siRNA, treatment with different drugs (C3 and Y-27632), or soft ECM culture conditions, suppressed AMPK activation, as demonstrated by reduced phosphorylation of its activation loop (pThr172) and its target protein Acetyl-CoA Carboxylase (ACC1, Fig. 11a-c). Importantly, in human epithelial breast cells either treated with Y-27632 or grown on soft ECM, reactivation of AMPK by AICAR, an AMP analogue known to activate AMPK, inhibited SREBP1 maturation, SCD1 transcriptional induction and lipid droplet accumulation (Fig. 11d-f), indicating that AMPK mediates the effects of mechanical forces on SREBP1.

These data demonstrate that AMPK coordinates SREBP1 activation and lipid biosynthesis downstream of environmental mechanical cues.

SREBP1 drives mechano-dependent mesenchymal stem cells (MSC) adipogenic commitment.

Based on our evidence, it is conceivable that, through this mechanism, soft substrates could promote adipogenesis by unleashing SREBP1 activity upon inhibition of actomyosin contraction [177,178]. This could be the case of MSCs. Indeed, adult MSCs are known to spontaneously differentiate into adipocytes or osteoblasts when cultured on a soft or stiff matrix, respectively [135,179].

However, the mechanisms by which a soft microenvironment instructs MSCs to undergo adipogenesis are largely unknown. To test our hypothesis, we cultured mMSCs on either stiff or soft fibronectin-coated hydrogels, or we treated mMSCs cultured in stiff matrix with Y-27632. In these conditions, we monitored adipogenesis by evaluating mRNA levels of the adipogenesis markers *Pparg, AdipoQ, Fabp4* and *Cebpa* (Fig. 12a, d) and by Oil-Red-O staining (Fig. 12b, e). As expected, adipogenesis was significantly induced by ECM softening (Fig. 12a, b) or by ROCK inhibition in stiff substrates (Fig. 12d, e), thus confirming a key role of ECM rigidity in MSC fate determination. Importantly, in mMSCs grown on soft ECM or treated with the ROCK inhibitor, AMPK activity was reduced and SREBP1 was strongly activated (Fig. 12c, f), while SREBP1 pharmacological inhibition by fatostatin (Fig. 12c, f) prevented MSC differentiation into adipocytes (Fig. 12a, b and 12d, e). These results demonstrate that SREBP1 in response to mechanical cues drives adipogenic specification of MSCs.

Discussion

Lipid homeostasis exerts an important role throughout the whole organism. Indeed, cellular lipids are involved in the formation of plasma membranes, in membranes of organelles, post translational modifications, energy production and storage and in signalling pathways that direct cell function. In order to meet their needs, uptake, synthesis, metabolism, and disposal of lipids by all cells are tightly regulated. Intracellular lipid synthesis can be regulated by a plethora of factors that activate the master regulators of lipid homeostasis, the sterol regulatory element binding proteins (SREBPs).

SREBPs are leucine zipper transcription factors that localize in the ER membrane, bound in a complex with SCAP. When sterol levels are low, SREBPs move from the ER to the Golgi, assembled with SCAP. Here, SREBPs undergoes two proteolytic cleavages that allow their translocation to the nucleus, where they can start the transcription of all the enzymes of the mevalonate pathway and fatty acids synthesis, in order to maintain cellular lipids homeostasis.
Sustained activation of these transcription factors leads to increased cholesterol and fatty acid synthesis and accumulation, and high triglyceride and cholesterol contents. When the intracellular lipid content increases, SREBP transcription is suppressed, which aim at restoring lipid levels to normal. It undergoes a well-defined regulation by negative feedback mechanisms that allow their activation or inhibition[53]. Moreover, to avoid products accumulation, SREBPs undergoes a negative feedback inhibition by cholesterol, the final bioproduct of the mevalonate pathway[56].
Given the fact that the mevalonate pathway produces not only cholesterol but also isoprenoids, as farnesyl pyrophosphate (FPP) and geranylgeranyl pyrophosphate (GGPP), we hypothesized that isoprenoids, beyond cholesterol, might regulate SREBPs transcriptional activity.

In this work, we first highlighted a cholesterol-independent feedback mechanism of SREBP1 regulation, mediated by geranylgeranyl pyrophosphate (GGPP) (Fig 8a). Our results show that GGPP has a key role in controlling the SREBP-mediated activation under conditions of nutrient stress. Mechanistically, we found that, in condition of sterol deprivation, GGPP prevented the SREBP1 proteolytic processing thus reducing its nuclear accumulation (Fig 8c). Moreover, to better dissect the role of GGPP on SREBP regulation, we employed

Drosophila melanogaster animal model that lack for the enzymes involved in cholesterol biosynthesis, and we observed that this layer of regulation is conserved among the species (Fig. 15a).

Geranylgeranyl pyrophosphate is a mevalonate-derived metabolite exerting crucial functions in regulating several cellular processes, such as membrane trafficking, cell division, migration and cytoskeleton dynamics, mainly through protein geranylgeranylation [114]. Deregulation of this process is known to cause the onset of different diseases, as cardiovascular, neurodegenerative diseases and cancer [116,118,180,181].
We showed that by inhibiting the geranylgeranyl transferase (GGT-I) with a specific inhibitor (GGTI-298), we observed a strong induction of SREBPs transcriptional activity (Fig. 8f-h) and the addition of GGPP did not reverse SREBP1 activation (Fig. 13m), suggesting that protein prenylation, instead of the GGPP intracellular levels, is required for SREBP1 regulation. Our results demonstrate that SREBP1 is controlled by protein geranylgeranylation and suggest that one or more GGTase1 target proteins are involved in SREBP1 activation and lipid biosynthesis.

We provided evidence that RhoA and other proteins involved in the cytoskeleton remodelling (RhoB, LmnA, Rac2) are able to inhibit SREBP activity. Geranylgeranylation of Rho-GTPases is required to coordinate acto-myosin dynamics in response to chemical and physical stimuli [113]. We demonstrated that prenylation of RhoA strongly inhibits SREBP1 activity, thus establishing a crucial role of SREBP1 as a transducer of environmental mechanical cues and unveiling a link between the physical properties of the ECM and lipid metabolism (Fig 9).

Moreover, this regulation of SREBP1 inhibition exerted by RhoA turned out to be conserved from invertebrates to humans. In addition to *Drosophila*, we found out that impairment of cytoskeleton dynamics, in terms of culturing cells on stiff (50 kPa) or soft (0.5 kPa) matrices, is conserved in mice, as demonstrated by experiments of mammary epithelial cells and primary hepatocytes (Fig. 10) and among tissue, since this regulation occurs also in cell lines derived from different origins (bone, lung, liver, breast, colon), supporting the idea that this regulatory mechanisms is widely occurring (Fig. 16).

The fact that we observed a GGPP and RhoA-dependent SREBP in both *Drosophila* and human cells suggests that this is an evolutionary conserved mechanism of lipid homeostasis. Indeed, mechanotransduction may represent an ancient and fundamental mechanisms of SREBP regulation, predating sterol-dependent regulation.
Moreover, given that remodelling of the ECM and transmission of mechanical inputs are fundamental for animal development, it is tempting to speculate that SREBP may convey force-imposed regulation of lipid production during development. Indeed, studies of SREBP function in *Drosophila* prove that dSREBP is required for larval development, providing fatty acids in the fat bodies and in the gut [107,182].
Furthermore, in worms, SBP-1 is responsible of BCFA synthesis, which are essential for post-embryonic development and growth control.

The physical properties of the ECM and thus mechanotransduction are known to regulate different physiological processes either at the organismal or at cellular levels. For example, skeletal and cardiac muscles can respond to an increased load (as resistance exercises), with a hypertrophic growth [183183]. In addition, it is well known that the morphology and physiology of the heart and the vasculature are influenced by pressure and shear stress [184]. Another example that describes the role of mechanotransduction in controlling tissue homeostasis is the bone: indeed, compressive forces, generated for example during locomotion, allow small deformation of the poro-elastic bone, resulting in pressure gradients that drive interstitial fluid flow through the lacunae-canalicular network. This fluid flow is then thought to stimulate bone remodelling in a localized space [185]. At the same time, chondrocytes can adapt to a plethora of stresses by the secretion of a glycosaminoglycan-rich ECM that confers the proper mechanical features to the cartilage.

Likewise, also other organ physiology responds to diverse mechanical stimuli from development through maturation, such as the lungs, which their state is continuously defined by the cyclic distension and contraction, and as the kidney, whose morphogenesis is regulated by the sensing of the urine flow in the kidney tubules [186,187]. Moreover, an increased number of studies are showing that mechanotransduction also has a crucial role in directing tissue development. Indeed, stem cells can be directed to a specific fate during differentiation on the basis of the geometry and stiffness of the substrate on which they grow, and intercellular physical interaction as tension and adhesion are important in embryonic development as concentration gradients of morphogenic factors [182,188]. At the cellular level,

mechanotransduction can modulate several functions such as protein synthesis, secretion, adhesion, migration, viability, proliferation and apoptosis.

As shown by our results, the control of SREBP1 by acto-myosin dynamics may represent a fundamental mechanism to regulate cell behaviour. Indeed, it has been demonstrated that mechanical cues are instrumental for stem cell to differentiate into osteocytes (stiff environment) or adipocytes (soft environment) [189]. Furthermore, SREBP1 has been shown to promote adipocyte differentiation, by enhancing the transcription of typical adipocytes markers as LPL, FAS and PPARγ[190]. To support this notion, we showed, for the first time, that it is in response to altered mechanical cues that SREBP1 activation determines the fate into adipocytes of MSCs (Fig. 12).

Acto-myosin dynamics has been estimated to drain an important fraction of cellular energy, yet it is unknown how the cell derives the vast amount of energy it needs to support these processes. It has been demonstrated that as well as to foster glycolysis via the release of aldolase A from actin fibres [191,192].
Moreover, Bays et al have demonstrated that LKB1-mediated activation of AMPK is a key player in a junctional contractility pathway that increases glucose uptake and ATP synthesis and that by mechanosensitive Ca2+ influx at focal adhesions [175,176]. Our finding that SREBP1-dependent lipid anabolism is prevented by cytoskeleton contraction via activation of AMPK suggests that this mechanism could be important to integrate environmental mechanical signals with intracellular requirements, allowing a cell to maintain an optimal energy status (Fig. 11 and Fig.12).

As said before, we found that acto-myosin contractility regulates *Drosophila* fat storage via SREBP-dependent lipid biosynthesis and accumulation, supporting that coordination between mechanical and metabolic pathways may have implications at the organismal level, such as in human physio-pathologic conditions, which is shown by our results (Fig. 10g). Indeed, we found that in breast and lung tissues with altered ECM deposition and stiffening of the surrounding environment, in terms of mammographic density and IPF, SREBP1 signature is downregulated, supporting the finding that an increased mechanotransduction is altering somehow the correct physiological regulation of metabolic processes.

In other diseases, for example in cancer, this homeostatic interplay might be overcome at multiple levels. It has been established by several papers that tumours rely on an altered increased ECM stiffening to sustain their aggressiveness, growth and the malignant phenotype [193]. This characteristic is known to affect biological pathways, included the metabolic ones. Moreover, tumours alter their metabolic program to maintain cell-autonomous proliferation, even in the nutrient-poor conditions of the tumour microenvironment [194]. Indeed, in a recent work, Bertero and colleagues showed that ECM stiffening activates glycolysis and glutamine metabolism, in a mechano-dependent manner, and thus coordinates nonessential amino acid flux within the tumour niche. They found a metabolic crosstalk between cancer-associated fibroblasts (CAFs) and cancer cells in which CAF-derived aspartate sustains cancer cell proliferation, while cancer cell-derived glutamate balances the redox state of CAFs to promote ECM remodelling, linking mechanical stimuli to dysregulated tumour metabolism and highlighting a new metabolic network within tumours in which diverse fuel sources are used to promote growth and aggressiveness [195].

Furthermore, in cancer, SREBP has an important role in promoting tumour progression by sustaining lipid production, providing essential substrate to boost cancer cells proliferation [1]. However, no mutations in SREBP gene or protein have been discovered so far, thus its activity must be sustained by hyperactivation or inhibition of its key regulators or by oncogenic signals. First, diverse oncogenic proteins, such as YAP/TAZ, mutant p53 and Myc, have been shown to be activated and stabilized upon ECM stiffening and, in turn, to directly engage key metabolic transducers, such as SREBP, to boost cancer cell proliferation and lipid production [118,133,166,196–199]. Second, SREBP is found dysregulated in many types of cancer [200,201] due to mutation in its upstream regulators. Indeed, it has been shown that mutation in KRAS and PI3K converge to the hyperactivation of the PI3K-Akt-mTORC1 axis that, in turn, stimulate SREBP activity [202]. In addition, mutations on SREBP ubiquitin ligase Fbxw7 has been shown to cause cancer progression, and this might be another mechanism of sustained SREBP activity, by impairment of SREBP degradation [203]. Third, mutations on LKB1, a known activator of AMPK, have been demonstrated to promote cancer growth [204]. In these conditions, AMPK-related targets, such as mTOR and SREBP, are active and could promote cancer cell proliferation [205].

At the same time, also cancer cell metabolism can affect mechanotransduction. Indeed, recent works demonstrated that glutamine regulation controls in part the activity of RhoA. Hyperactive RhoA signalling typically causes tumour formation, but this effect could be

reversed using an inhibitor of glutaminase (GLS1), an enzyme that converts glutamine to glutamate [206]. Another study supported this observation by highlighting that stiffness-induced changes in glutamine flux were mediated in part by the transcriptional regulation of GLS1, suggesting reciprocal feedback between mechanosignaling and glutamine metabolism [207].

In this thesis, we have shown that another pathological condition, the Idiopathic Pulmonary Fibrosis (IPF), which is characterized by chronic deposition of ECM in lung tissue, presents an altered SREBP activity. Indeed, by the analysis of human datasets of lung tissue from patients affected by IPF vs healthy controls we found that SREBP1 activation inversely correlates with the presence of fibrosis, suggesting that in these pathological conditions SREBP1 might respond to alteration of mechanical stimuli. Moreover, it has been recently discovered by Shichino and colleagues that with the progression of IPF, *Srebf1* expression decreased, suggesting its suppressive role in fibroblast activation. Specifically, they found that the overexpression of *Srebf1c* in mice lung fibroblast not only suppressed pro-fibrotic genes, but also enhanced lipid-related genes, as *Scd1, Elovl6, Ptgs1* and *Ptges*, linked to fatty acid and prostaglandin E_2 (PGE2) synthesis respectively [208]. PGE2 and its metabolite resolvin D1 have been reported to play protective role in bleomycin-induced lung fibrosis, thus suggesting that SREBP1c exerts a protective role as well in IPF, possibly mediating the synthesis of anti-fibrotic molecules [209,210].

Given the critical importance of ECM in development and for maintenance of tissue homeostasis, is not surprising that dysregulation of its properties and component leads to diseases, by altering diverse cellular processes. Indeed, it has also recently shown that in skin with keloid scars, a fibroproliferative disorder characterized by increased tissue stiffness and whose expansion is linked to mechanical stress, presents an alteration in lipid-related genes expression. Strikingly, it has been demonstrated that several SREBP target genes were consistently downregulated in stiffened keloids across all patients, providing a probable explanation of the reduced triglycerides and cholesteryl-ester accumulation observed in keloids [211].

Collagens and other protein that compose the ECM are the most prevalent proteins in our tissues, determining their mechanical properties. Collagens are found at higher levels in stiff mature tissues where, their increased concentration is the basis of tissue elasticity. By using

quantitative label-free mass spectrometry for proteomic profiling, it has been shown that collagens and other ECM-associated proteins scale with tissue elasticity and it was also found that the elasticity of bulk tissue is strongly correlated with the composition of the nuclear lamina in terms of its content of A-type and B-type lamins [212]. Moreover, emerging evidence suggest that external mechanical forces impinge on nuclear envelope structure and composition, chromatin organization and gene expression [151]. Furthermore, lamin-A/C-deficient and -mutant cells fail to properly activate mechanoresponsive genes when subjected to mechanical stimulation, suggesting an important role of the nucleus and lamin A/C in cellular mechanotransduction. Although lamin A/C are ubiquitously expressed, many of the LMNA mutations predominantly affect mechanically active tissue, such as skeletal muscle, cardiac muscle and tendons [151]. As such, it is not surprising that mutations within the *LMNA* gene may lead to an inappropriate transduction of mechanical signals and therefore to changes in gene expression profiles. An example is the Dunningan-type familial partial lipodystrophy (FPLD2), which is often accompanied by impairments in the muscle tissue development. FPLD2 is associated with mutations within the *LMNA* gene, specifically characterized by the substitution of the arginine 482 residue in the globular C-terminal domain of lamin A/C. This mutation leads to a reduced lamin A-SREBP1 interaction in the nuclear envelope, therefore leading to SREBP activation [213]. Indeed, it has been recently demonstrated that mouse myoblasts harbouring R482W mutation in lamin A/C have an increased fat accumulation, in terms of formation of intramuscular lipid droplets [214,215].

The above-mentioned diseases are just few examples in which an altered mechanotransduction is affecting biological processes, such as cell metabolism. The link highlighted by our work and by other studies underlies an unexpected crosstalk that need to be further investigated[175,211]. We plan to better define the role of the cytoskeleton-SREBP1 axis in pathological conditions.

This mechano-dependent regulation of lipid metabolism might represent a target for a new therapeutic approach in different diseases, by restoring the correct properties of the ECM and thus the proper metabolic homeostasis of the cell.

Finally, metabolism is experiencing a renaissance because disturbances in metabolic regulation are recognized as a cause of disease. Hence, it will be important to investigate the links between cell metabolism and mechanotransduction in diseases such as cancer, diabetes and obesity which are accompanied by losses or alterations in cell adhesion and metabolic reprogramming.

Material and methods

Cell lines

MCF-10A cells are a human immortalized normal epithelial breast cell line and were cultured in Dulbecco's Modified Eagle's Medium (DMEM)/F12 (LONZA) (1:1) supplemented with 5% Horse Serum (HS), 100U/mL penicillin and 10µg/mL streptomycin, 20 ng/ml recombinant human epidermal growth factor (EGF), 10 µg/ml recombinant human insulin, 500 ng/ml hydrocortisone. MDA-MB-231 are a human breast cancer cell line. IHH are immortalized human hepatocytes. Mahlavu are human hepatocellular carcinoma cells. HT29 are human colorectal adenocarcinoma cells. U87MG and U251 are human glioblastoma cells. U2OS are a human osteosarcoma cells line. H1299 are a human non-small cell lung cancer cell line. PANC-1 are a human pancreatic adenocarcinoma cell line. U87MG and U251 are glioblastoma cell lines. HT29, MDA-MB-231, PANC-1, U2OS, U87MG and U251 cells were cultured in Dulbecco's Modified Eagle's Medium (DMEM, LONZA) supplemented with 10% Foetal Bovine Serum (FBS) 100U/mL penicillin and 10µg/mL streptomycin. Mahlavu cells were cultured in Eagle's Minimum Essential Medium (EMEM, Sigma) supplemented with Foetal Bovine Serum (FBS), 100U/mL penicillin, 10µg/mL streptomycin, 1% Minimum essential medium non-essential amino acids (MEM NEAA), and 1% Glutamax. IHH cells were cultured in Dulbecco's Modified Eagle's Medium (DMEM)/F12 (LONZA) (1:1) supplemented with 10% Foetal Bovine Serum (FBS), 100U/mL penicillin and 10µg/mL streptomycin, 5 µg/ml recombinant human insulin, 1 µg/ml hydrocortisone and 1% Glutamax. H1299 cells were cultured in RPMI 1640 supplemented with 10% Foetal Bovine Serum (FBS), 100U/mL penicillin and 10µg/mL streptomycin.

Primary mouse mammary epithelial cells were cultured in Dulbecco's Modified Eagle's Medium (DMEM) supplemented with 10% Foetal Bovine Serum (FBS), 100U/mL penicillin and 10µg/mL streptomycin, 20 ng/ml recombinant human epidermal growth factor (EGF), 10 µg/ml recombinant human insulin, 500 ng/ml hydrocortisone. Primary hepatocytes were cultured in Dulbecco's Modified Eagle's Medium (DMEM) supplemented with 10% Foetal Bovine Serum (FBS), 100U/mL penicillin, 10µg/mL streptomycin, 1% glutamine, 6 µg/ml insulin and 1µM dexamethasone.

Human cell lines are from ATCC or other laboratories cooperating on the project. *Drosophila melanogaster* Schneider's 2 (S2) cell line was a kind gift from F. Feiguin, International Centre for Genetic Engineering and Biotechnology (ICGEB), Trieste.
Cells were subjected to STR genotyping with PowerPlex 18D System and confirmed in their identity comparing the results to reference cell databases (DMSZ, ATCC and JCRB databases). Cells were tested for mycoplasma contamination with negative results.

Preparation of fibronectin-coated hydrogel matrix

50, 4 or 0.5 kPa Easy Coat hydrogels (Cell guidance system) were coated with 10 μg/ml fibronectin.

Reagents and plasmids

The following compounds and working concentration were used: AICAR (1 mM, Sigma Aldrich A9978), Blebbistatin (50 μM Sigma Aldrich B0560), Cerivastatin (1 μM Sigma Aldrich SML0005), Cholesterol (0.5 mM, Sigma Aldrich C8667), Farnesyl Pyrophosphate (20 μM, Sigma Aldrich F6892), Fatostatin hydrocloryde (20μM, Sigma Aldrich F8932), Fibronectin (10 μg/ml, Sigma Aldrich F0895), GGTI-298 (5 μM, Sigma Aldrich G5169), Geranylgeranyl Pyrophosphate (20 μM, Sigma Aldrich G6025), Y-27632 (20 μM, Sigma Aldrich Y0503). Latrunculin-A (0.5 μM, Santa Cruz Biotechnologies sc-202691), C3 (100 ng/ml, Cytoskeleton CT04). DMSO was purchased from Sigma Aldrich (D4540). Lipoprotein Depleted Serum was purchased from Biowest (S181L). Treatments lasted 24 hours unless otherwise stated.
pEGFP–RhoA-G14V was a gift from C. Schneider (Laboratorio Nazionale CIB, Italy). pcDNA3-EGFP-RhoA-T19N (Addgene plasmid #12967) was a gift from Gary Bokoch. The pLDLR-Luc construct (also known as pES7, Addgene plasmids #14940), harboring the SREBP-responsive Sterol Responsive Element (SRE) sequence (ATCACCCCAC), and the pLDLR-Luc mutSRE construct (LDLR-Luc MUT, Addgene plasmid #14945), harboring a SREBP-unresponsive mutant SRE (ATAACCCCAC)[154] were gifts from Axel Nohturfft. The pGL3-SCD1-Luc construct was generated by cloning a PCR amplified DNA fragment corresponding to nucleotides -405 to -229 of the human SCD1 gene into the pGL3 vector with *KpnI* and *BglII* restriction enzymes.

Transfections

siRNA transfections were performed with Lipofectamine RNAi-MAX (Life technologies) in antibiotic-free medium according to manufacturer instructions. Sequences of siRNAs are reported in Table 1. Control siRNA was AllStars negative control Qiagen 1027281. Plasmid DNA transfections of MDA-MB-231 and MCF-10A cells were performed with LTX (Invitrogen) in antibiotic-free medium according to the manufacturer instructions.

Luciferase assay

pLDLR-Luc (300 ng/cm^2), pLDLR-Luc mutSRE (300 ng/cm^2)[154] , and pGL3-SCD1-Luc reporters (300 ng/cm^2) were co-transfected with the CMV–Renilla construct (30 ng/cm^2), 12 hours after transfection with either siRNAs, pcDNA3 (100 ng/cm^2), pcDNA3–GFP-RhoA-G14V (100 ng/cm^2), or pcDNA3-GFP-RhoA-T19N plasmids (100 ng/cm^2). Luciferase/Renilla signal was analysed in cell lysates, 24 hours after transfection of luciferase reporters, using the Dual-Luciferase Reporter Assay System (Promega E1910).

Quantitative RT-PCR

Cells were harvested in Qiazol lyses reagent (Qiagen) for total RNA extraction, and contaminant DNA was removed by DNase treatment. Quantitative real time PCR analyses were carried out on cDNAs retrotranscribed with iScript™ Advanced cDNA Synthesis Kit (Biorad 172-5038) and analysed with BIORAD CFX96 Touch^{TM} detection system and Biorad CFX Manager software. Quantitative analysis was performed by the $2^{-\Delta\Delta Ct}$ method. *Histone 3* was used as reference gene. PCR primer sequences are reported in Table 2.

Antibodies

The following antibodies and working concentrations were used: anti-Actin C11 (1:5000, Sigma Aldrich A2066, for western blot), anti-SREBP1 2A4 (1:500, Santa Cruz Biotechnology sc13551, for western blot), anti-SREBP1 H160 (1:100, Santa Cruz Biotechnology sc8984, for immunofluorescence), anti-SREBP2 (1:500, BD Bioscience 557037, for western blot), anti-SCD1 (1:1000, Abcam ab19862, for western blot), anti-GAPDH (6C5) (1:5000, Santa Cruz Biotechnology sc32233, for western blot), anti-AMPK (1:1000, Cell Signalling 2532S,

for western blot), anti-AMPK phospho Thr172 (1:1000, Cell Signalling 2531S, for western blot), anti-ACC1 (1:1000, Cell Signalling 3676S, for western blot), anti-ACC1 phospho Ser79 (1:1000, (Cell Signalling 11818S, for western blot), anti-Farnesyl (1:1000, AB4073 Merck Millipore), anti-Hsp90 (1:2000, Santa Cruz Biotechnology sc13119, for western blot), anti-MLC2 (1:1000, Cell Signaling 3675S, for western blot), anti-MLC2 phospho Ser19 (1:500, Cell Signaling 3671S, for western blot and immunofluorescence) anti-FAK C-20 (1:1000, Santa Cruz Biotechnology sc-558, for western blot), anti-FAK phospho Y397 (1:1000, Abcam ab81298, for western blot).

Targeted RNAi screening

74 siRNAs targeting all mRNAs coding for human proteins predicted to be GGTI targets (Table 3) were cherry-picked robotically from a human genome-wide siRNA library (siGENOME SMARTPool; pools of four siRNAs per gene, Dharmacon) and arrayed in 384-well white plates (PerkinElmer). For the screening experiments, MDA-MB-231 cells were transfected with the targeted siRNA library, using a standard reverse transfection protocol[216]. Briefly, the transfection reagent (Lipofectamine RNAiMAX; Life Technologies) was diluted in OPTI-MEM (Life Technologies) and added to the siRNAs arrayed on the 384-well plates; 30 min later, the cells were suspended in culture medium without antibiotics and seeded (2.0×10^3 per well). Twenty-four hours after siRNA transfection, cells were transfected with the LDLR-Luc reporter (Firefly), together with a plasmid expressing Renilla luciferase for normalization, using FuGENE HD Transfection Reagent (Promega) diluted in OPTI-MEM; the transfection mix (10 µl per well) was added to cells using a Multidrop Combi Reagent Dispenser (Thermo Fisher Scientific). Forty-eight hours after transfection of the reporter (i.e. 72 h after siRNA transfection), the cells were lysed in 1 × Glo Lysis Buffer (Promega); Firefly and Renilla luciferase activities were measured using the Dual-Glo Luciferase Assay System (Promega), according to the manufacturer's instructions, using an Envision Multimode Plate Reader (PerkinElmer). Normalized LDLR reporter activity was calculated as fold change over a control non-targeting siRNA.

Western Blot analysis of mammalian and Drosophila S2 cells

For immunoblotting analyses protein were lysed in Lysis Buffer (NP40 1%, Tris-HCL pH=8 50mM, NaCl 150mM, EDTA 1mM) solution, supplemented with protease and phosphatase

inhibitors. Lysates were loaded and separated in SDS-PAGE, followed by Western blotting on Nitrocellulose membranes (Amersham). Blocking was performed in Blotto-tween (PBS, 0.2% Tween-20, not fat dry milk 5%) or with TBST (0.2% Tween-20, Tris/HCl 25 mM pH 7.5) plus 5% BSA (PanReac Applichem) depending on the antibody.

Immunoprecipitation

Immunoprecipitation (IP) experiments were performed using IP buffer (NaCl 120mM, Tris-HCl pH8 20mM, EDTA 1mM, NP40 0,5%) with protease inhibitors. Samples were sonicated three times and cleared by centrifugation for 10 min at 13,000g at 4 °C and incubated for 4h at 4 °C with anti-RhoA or IgG antibodies. After 1 h incubation with protein G-Sepharose (GE Healthcare), immunoprecipitates were washed three times in IP buffer, resuspended in sample buffer, and analyzed by immunoblotting.

Immunofluorescence analysis of mammalian cells

Briefly, cells were fixed in 4% paraformaldehyde for 10 minutes, washed in phosphate buffered saline (PBS), permeabilized with 0.1% Triton X-100 for 10 minutes and blocked in 3% Foetal Bovine Serum FBS/PBS for 30 minutes. Antigen recognition was done by incubation with primary antibody at 4°C for 14 hours and with secondary antibodies (goat anti-mouse Alexa Fluor 568 and goat anti-rabbit Alexa Fluor 488, Life Technologies) at 4°C for 2 hours. Nuclei were stained with Hoechst 33342 (Life Technologies) for 15 minutes.

BODIPY Staining of mammalian cells

Cells were fixed in 4% paraformaldehyde for 15 minutes, stained with 0.1 µg/ml BODIPY-493/503 at 37°C for 30 min and DAPI at 25°C for 15 minutes. Cells were imaged using a Nikon Ti-E inverted fluorescence microscope.

Drosophila cell lines

Drosophila melanogaster Schneider's 2 (S2) line cells are macrophage-like cells of embryonic origin (kind gift from F. Feiguin, International Centre for Genetic Engineering and Biotechnology, Trieste) and were cultured in Insect-XPRESS medium (LONZA 12-730)

supplemented with heat-inactivated 10% Foetal Bovine Serum (FBS), 100U/mL penicillin and 10µg/mL streptomycin, at 25°C.

Drosophila lines and housing

The following *Drosophila* lines were used: w^{1118} (as wild type control, kind gift of F. Feiguin, International Centre for Genetic Engineering and Biotechnology, Trieste, Italy), w^{1118}*;UAS-dRhoA*^{RNAi}*/CyO-GFP* (generated from line VDRC#12734, *Vienna Drosophila Resource Center*), w^{1118}*;cg-Gal4* (*Bloomington Drosophila Stock Center* BDSC#7011, kind gift of P. Bellosta, University of Trento, Italy) and w^{1118}*;;UAS-Luciferase*^{RNAi} (*Bloomington Drosophila Stock Center* BDSC#35788, kind gift of B. Mollereau, Ecole Normale Superierure de Lyon, France). The genotype of larvae analysed in Fig. 2h and Fig. 3c, e, f was: w^{1118}*;cg-Gal4;UAS-Luciferase*^{RNAi} (*Luc RNAi*) and w^{1118}*;cg-Gal4/UAS-dRhoA*^{RNAi} (*dRhoA RNAi*). Flies were maintained at 25°C on standard corn/yeast medium.

Dissection and culture of Drosophila larval fat bodies

Fat bodies were dissected from N=6 third instar female larvae in phosphate buffered saline (PBS) and either immediately processed or cultured for 14 hours in Insect-XPRESS medium (LONZA 12-730) supplemented with heat-inactivated 10% Foetal Bovine Serum (FBS), 100U/mL penicillin, 10µg/mL streptomycin and 10 µg/ml Insulin, and drug (Y-27632 or Fatostatin) or drug solvent (according to the manufacturer instructions).

Western Blot analysis of Drosophila fat bodies

Fat bodies freshly dissected in phosphate buffered saline (PBS) and cultured fat bodies washed in phosphate buffered saline (PBS) were transferred in lyses buffer and processed for western blot analysis according to the protocol described for mammalian and *Drosophila* S2 cells.

Whole mount fluorescence staining of Drosophila fat bodies

Drosophila tissues were stained according to a standard whole mount protocol[217,218]. Briefly, fat bodies freshly dissected in phosphate buffered saline (PBS) and cultured fat bodies

washed in phosphate buffered saline (PBS) were fixed in 4% paraformaldehyde for 10 minutes, rinsed three times in phosphate buffered saline (PBS) for 5 minutes, permeabilized with 0.1% Triton X-100/PBS for 10 minutes, and rinsed three times in phosphate buffered saline (PBS) for 5 minutes, at 25°C. Tissues were then incubated with primary antibodies for 14 hours at 4°C, washed three times in phosphate buffered saline (PBS) for 5 minutes, incubated with Alexa Fluor secondary antibodies (488, 568, 594, 647, Thermofisher, 1:400 dilution) at 25°C for 2 hours, and with 0.1 µg/ml BODIPY-493/503 at 25°C for 20 min to stain lipid droplets. After rinsing three times in phosphate buffered saline (PBS) for 5 minutes, tissues were incubated with Hoechst 33342 (Life Technologies) and sealed onto glass slides in Prolong mounting medium. Images were acquired with a Nikon ECLIPSE C1si confocal microscope and processed with Nikon NIS-Elements Imaging Software for quantification of lipid droplets (Confocal microscopy facility, University of Trieste). The mean size of lipid droplets was quantified according to Bi and others work[219] in images from N=6 individuals.

Isolation of mouse mammary epithelial cells

Mammary glands from 8 to 12 week old virgin female mice were enzymatically digested and single cell suspensions of purified mammary epithelial cells (MECs) were obtained following a standard protocol[220]. Briefly, mammary glands were digested at 37°C for 1–2 hours in Epi-Cult-B medium (StemCell Technologies Inc) with 600 U/ml collagenase (Sigma Aldrich) and 200 U/ml hyaluronidase (Sigma Aldrich). After lysis of the red blood cells with NH_4Cl, the remaining cells were washed with PBS/0.02% w/v EDTA. Cells were then dissociated with 0.25% w/v trypsin, 0.2% w/v EDTA for 2 min by gentle pipetting, then incubated in 5 mg/ml Dispase II (Sigma Aldrich) plus 1 µg/ml DNase I (Sigma Aldrich) for 5 minutes, followed by filtration through a 40 µM cell strainer (BD Falcon). MECs were then purified using the EasySep Mouse Mammary Stem Cell Enrichment Kit (StemCell Technologies Inc). MECs were seeded on top of 50 or 0.5 kPa Easy Coat hydrogels (Cell guidance system) coated with 10 µg/ml fibronectin and harvested after 24 hours.

Primary hepatocytes isolation

Briefly, livers were removed quickly from euthanized mice and the tissue was finely minced with scissors and washed several times with HBSS to remove blood clots. After a last wash

with HBSS, the sample was transferred to a falcon with a collagenase solution (0.25 mg/ml Collagenase D in HBSS-Hepes buffer) and was incubated for 45 min at 37°C in a rotating incubator. At the end of the incubation 10 ml of HBSS containing 5% FBS was added. The cell suspension was filtrated through a 70-µm cell strainer (BD Falcon) and centrifuged at 50 g for 5 min at 4°C. The supernatant was discarded, and fresh medium was added. Isolated cells were then seeded on top of 50 kPa or 0.5 kPa Easy Coat hydrogels (Cell guidance system) coated with 10 µg/ml fibronectin and harvested after 24 hours.

Isolation of mouse mesenchymal stem cells

Mouse mesenchymal stem cells (mMSCs) were isolated from 12-week-old. Mice were anaesthetised, sacrificed, and the femurs were harvested. After isolation and cleaning, the marrow was flushed from the bones using 26-gauge needle and 3 mL syringe into complete phosphate buffered saline (PBS) with 2% Foetal Bovine Serum (FBS) and 1mM EDTA. Cell were gently resuspended and further purified with the EasySep mouse MSC isolation kit (Stem cell 19771), following manufacturer instructions. Viable cells were subsequently resuspended in a growth medium (non-differentiating medium) consisting of Dulbecco's Modified Eagle's Medium (DMEM, LONZA), 15% Foetal Bovine Serum (FBS, Euroclone), 2mM Glutamine, 100U/mL penicillin and 10µg/mL streptomycin. Cells were then seeded on cell culture dishes and placed at 37°C 20% O_2. The culture medium was replaced every 2 days until reaching 80% confluence (2 days).

Differentiation of mouse mesenchymal stem cells in culture

For spontaneous differentiation on soft matrix, mMSCs were seeded in non-differentiating medium on 50 or 0.5 kPa Easy Coat hydrogels (Cell guidance system) fibronectin-coated hydrogels until reaching 80% confluence (2 days). Then they were cultured in fresh non-differentiating medium or fresh non-differentiating medium supplemented with fatostatin, for 5 days. Cells were then fixed in 4% paraformaldehyde, stained with Oil-Red-O (Sigma Aldrich), rinsed three times with deionised H_2O and imaged. For pharmacological induction of adipogenic differentiation on stiff matrix, mMSCs were seeded in non-differentiating medium on plastic culture dishes (Euroclone) until reaching 80% confluence (2 days). Then they were cultured in either non-differentiating medium, or differentiating medium, consisting of Dulbecco's Modified Eagle's Medium (DMEM, LONZA) supplemented with 15% Foetal

Bovine Serum (FBS, Euroclone), penicillin 100U/mL, streptomycin 10µg/mL, 500 µM 3-isobutyl-1-methylxanthine (Sigma-Aldrich), 1 µM dexamethasone (Sigma-Aldrich) and 10 µg/ml insulin (Sigma-Aldrich), for 3 days. During this period, DMSO, Y-27632 and fatostatin were added daily to differentiating medium. Then, cells were maintained with DMEM, 15% FBS, penicillin 100U/mL, streptomycin 10µg/mL, 1mM glutamine and 10 µg/ml insulin. After 7 days, cells were then fixed in 4% paraformaldehyde, stained with Oil-Red-O (Sigma-Aldrich), rinsed three times with deionised H_2O and imaged.

Animal care

The mice were housed and used in a specific pathogen-free (SPF) animal facility. Procedures involving animals and their care were performed in conformity with institutional guidelines (D.L. 116/92 and subsequent complementing circulars).

Analysis of microarray data

To investigate gene set differentially enriched upon plating on matrixes with different stiffness, we compared the expression profiles of MDA-MB-231 breast cancer cells plated on a stiff substrate (plastic) with the same cells plated on a soft substrate (hydrogels 0.5 kPa). Raw gene expression data were downloaded from Gene Expression Omnibus GSE93529 [166]. All data analyses were performed in R (version 3.2.4) using Bioconductor libraries (BioC 3.2) and R statistical packages. Probe level signals were converted to expression values using the robust multi-array average procedure RMA of the Bioconductor affy package. Functional enrichment was performed using Gene Set Enrichment Analysis (http://www.broadinstitute.org/gsea/index.jsp) and gene sets of the Molecular Signature Database (http://software.broadinstitute.org/gsea/msigdb/index.jsp). In particular, we investigated whether the expression levels of MDA-MB-231 cells grown on a soft substrate were associated with elevated expression of the 674 Reactome gene sets. GSEA software was applied on log2 expression data of MDA-MB-231 cells cultured on stiff and soft substrates. Gene sets were considered significantly enriched at FDR < 5% when using Signal2Noise as metric and 1,000 permutations of gene sets. The dot plot in Fig. 16 was generated using the ggplot2 R package (v.2.2.1, https://cran.r-project.org/web/packages/ggplot2/index.html).

Analysis of human sample datasets

To generate a specific SREBP1 transcriptional signature, we selected genes altered in SREBP1 knock-in and SCAP knock-out, but not SREBP2 knock-in mice[167]. We then compiled a list of the 16 human orthologues of those genes using the DIOPT-DRSC Integrative Ortholog Prediction Tool[221]. We fetched the following datasets from the NCBI GEO database: GSE99621 (from Luzina et al., 2018)[171] and GSE49175 (from Sun et al., 2013)[168]. GSE49175 data were downloaded from the sample table matching each entry, and the log2(mean sample signal/mean signal in reference control) was used as the expression value for each probe. For GSE49175, RNA-seq raw reads were fetched by the NCBI SRA fastq tool[222] and uploaded to the Galaxy web platform, using the public server at usegalaxy.org[223] for analysis. The quality of the reads was assessed by the FastQC tool[224]. The reads were de-interlaced with the FastQ de-interlacer tool[225] and subsequently trimmed using the Trimmomatic [226] with an IlluminaClip step to remove the matching adapter sequences and a sliding-window following step, averaging across 4 bases and requiring average quality of 20. We then used HISAT2[227] to align the reads on the GRChg38 reference human genome in an unstranded manner. Aligned reads were subsequently filtered with SAMtools [228], keeping only aligned reads with minimum MAPQ quality score of 20 and mapped in a proper pair. Aligned reads were counted using featureCounts [229]. Raw data counts were subjected to the Variance Stabilizing Transformation from the DeSeq2 R package (R Development core team, 2008) [230] to obtain normally distributed data for further analyses. The obtained expression data for both datasets were processed by a combined score with zero mean transformation, and the average expression of the SREBP1 signature was calculated averaging the z-score of all the genes in the list. The average value was used as a measure of SREBP1 signature expression. Statistical significance was calculated on the single z-score for all the genes in the signature using a two-way ANOVA test (GraphPad Prism v.7).

Statistics and reproducibility

All the experiments are representative of at least three independent repeats. Graph bars represent mean ± s.d. from n=3 biological replicates. All P values were determined using two-tailed Student's t-test, with a 95% confidence threshold as indicated in figure legends.

Figures

Figure 1

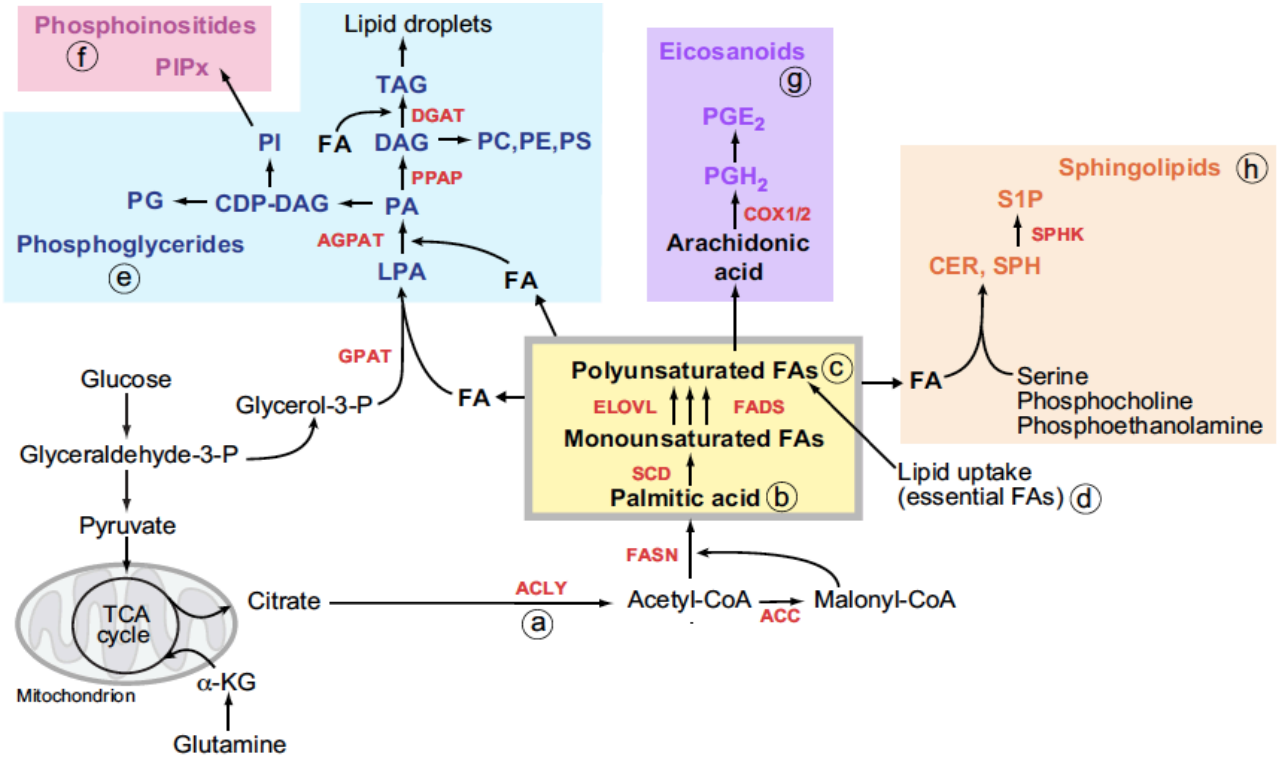

Figure 1 – Schematic overview of lipid biosynthesis pathway. a) Conversion of glucose- or glutamine-derived citrate to acetyl-CoA by ACLY. b) FA biosynthesis, starting from the conversion of acetyl-CoA into malonyl-CoA. Then, repeated condensation of acetyl-CoA and malonyl-CoA by FASN leads to the generation of palmitic acid, a fully saturated 16-carbon FA. The introduction of a double bond in the Δ9 position of the acyl chain by SCD generates MUFAs. c) Elongation and desaturation produce FAs with different saturation levels. d) Essential FAs (ω3 and ω6) cannot be synthesized by human cells and are uptaken from dietary sources. (e,f) Saturated and unsaturated FAs are linked to glycerol-3-phosphate (glycerol-3-P) to give rise to (e) phosphoglycerides and (f) phosphoinositides. (g) Arachidonic acid, a long-chain PUFA, is used for the synthesis of eicosanoids. (h) FAs are utilized for the production of sphingolipids, which contain acyl chains and polar head groups derived from serine, phosphocholine or phosphoethanolamine [19].

Figure 2

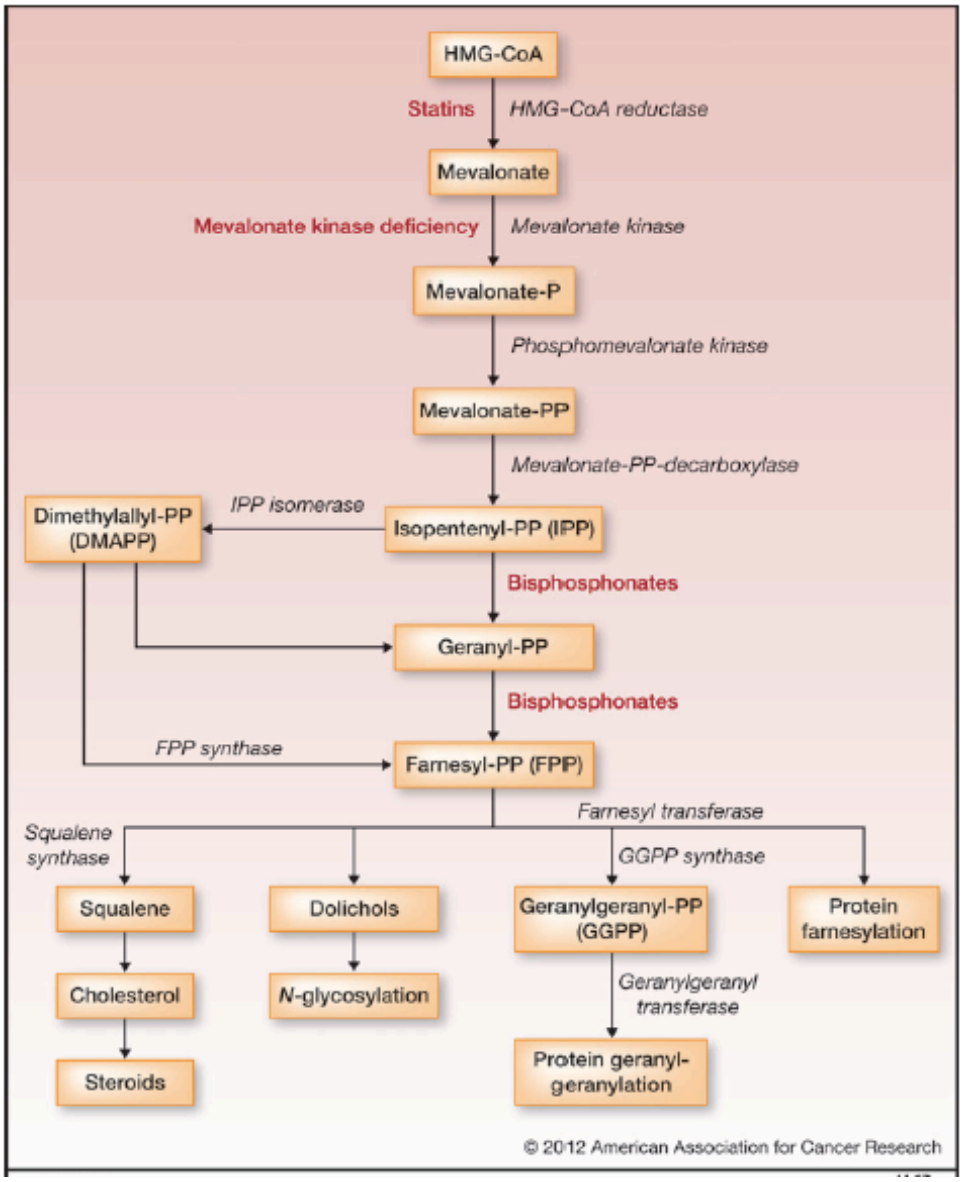

Figure 2 – The mevalonate pathway cascade. Starting from HMG-CoA molecule, the pathway leads to the production of important metabolites for the cell, going from mevalonate to the production of isoprenoid precursor units, required for the biosynthesis of important molecules that contribute to diverse cellular functions, ranging from cholesterol synthesis to N-glycosylation and protein prenylation. Statins and bisphosphonates are classes of drugs that leads to the inhibition of HMG-CoA reductase and Farnesyl-diphosphate synthase (*FDPS*), thereby inhibiting cholesterol production and protein prenylation [231].

Figure 3

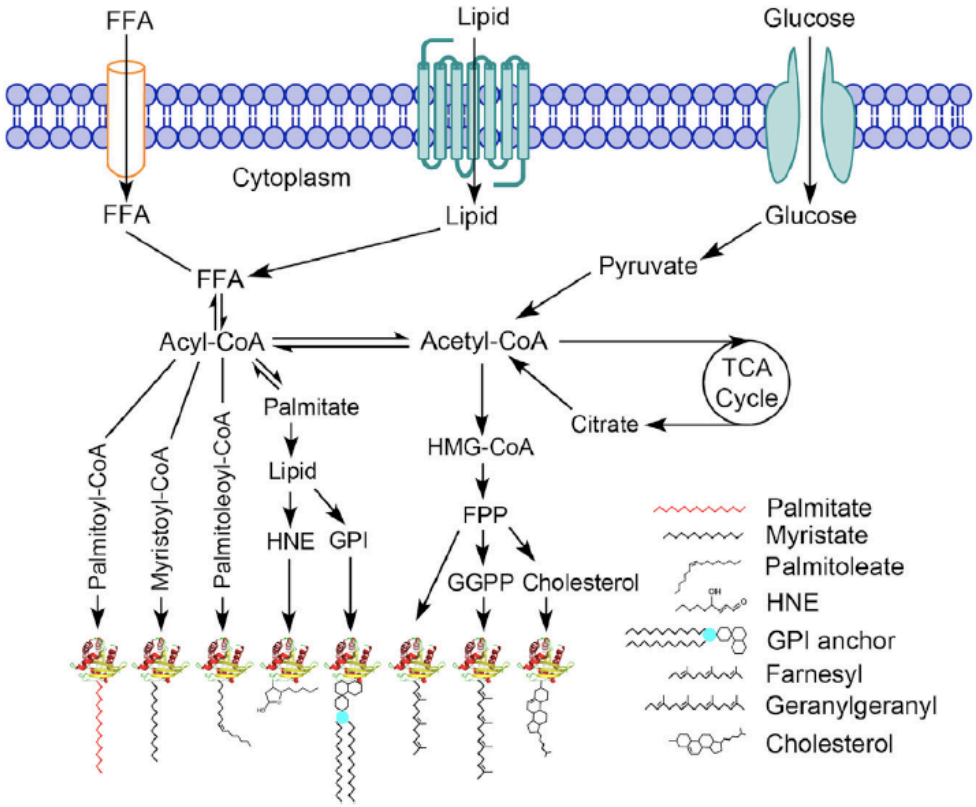

Figure 3 – Protein lipidation processes. Lipids derived from the uptake and from the biosynthesis inside the cell can be utilized as molecules for protein post-translational modifications. Proteins can be modified by at least 6 types of lipid, including saturated and unsaturated fatty acids (palmitate, myristate, and palmitoleate etc.), isoprenoids (farnesyl and geranylgeranyl), GPI anchors, cholesterols) and lipid derived electrophiles (HNE etc.)[48].

Figure 4

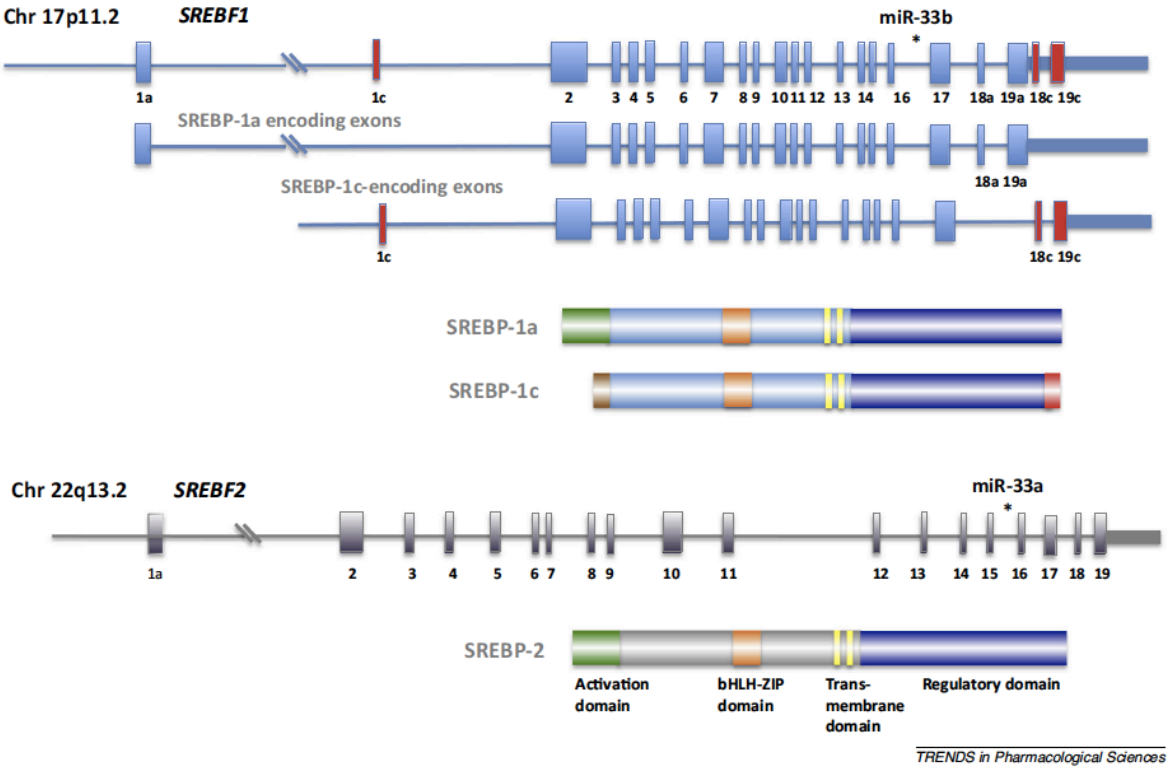

Figure 4 – SREBPs gene and proteins. Schematic representation of gene encoding for *SREBF* and protein structure of SREBP1a, SREBP1c and SREBP2. miR33a and miR33b are also shown [232].

Figure 5

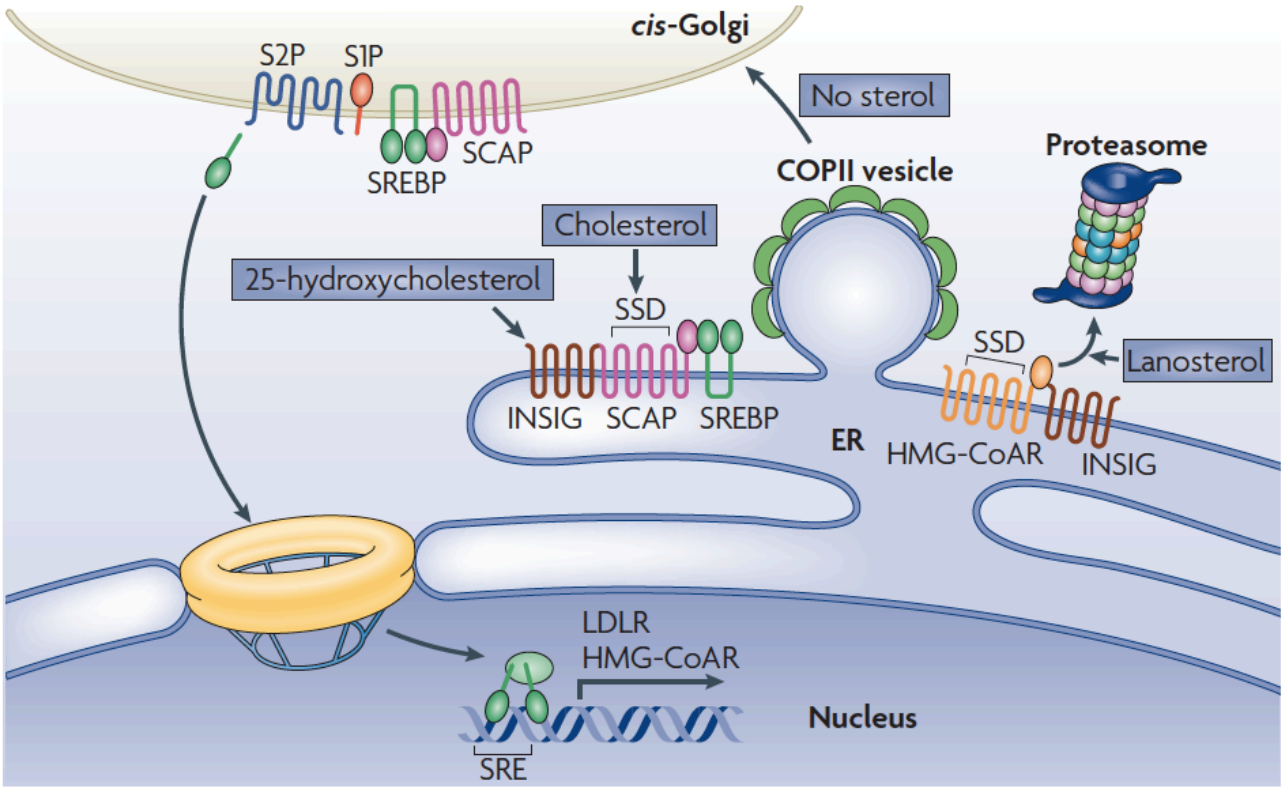

Figure 5 – SREBPs activation pathway. Under conditions of high sterol levels in the endoplasmic reticulum (ER), the ER retention protein INSIG prevents entry of the SREBP–SCAP (SREBP cleavage activating protein) complex to COPII-coated vesicles. Transport of SREBP to the Golgi is necessary for proteolytic release of the N-terminal domain, which is then transported to the nucleus to activate sterol-regulated genes (such as hydroxymethyl-glutaryl CoA reductase (HMG-CoAR)) and the low-density lipoprotein receptor (LDLR)). HMG-CoAR is also post-transcriptionally regulated by sterol, with INSIG binding of the protein leading to its proteasomal degradation. SSD, sterol-sensing domain; SRE, sterol regulatory element [233].

Figure 6

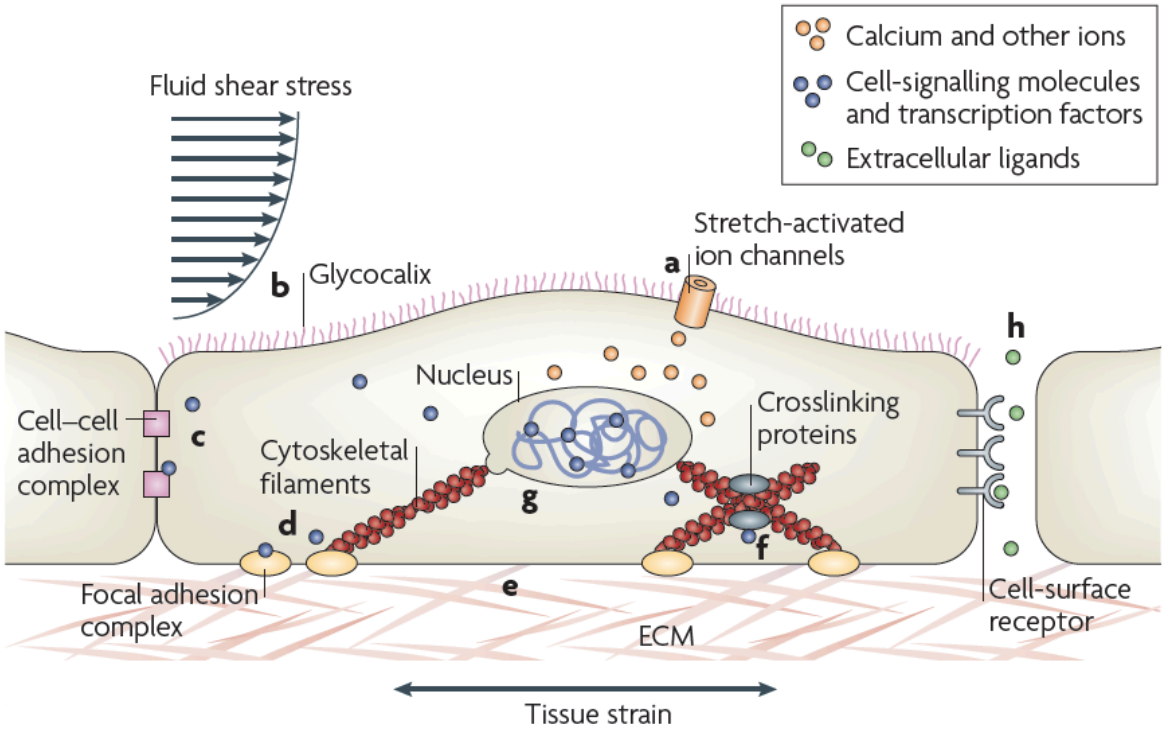

Figure 6 – Cellular components involved in mechanotransduction. a) Stretch-activated ion channels in the plasma membrane open in response to membrane strain and let the influx of ions in the cell, such as calcium. b) In endothelial cells, the glycocalix can mediate mechanotransduction signaling in response to fluid shear stress. c,d) Cell–cell junctional receptors or ECM–cell focal adhesions allow cells to sense the environment. e) modifications of ECM proteins, such as fibronectin, can start mechanotransduction signaling. f) Intracellular forces can induce conformational changes in cytoskeletal elements as filaments, thus activating signaling pathways. g) The nucleus itself acts as a mechanosensor. Intracellular deformations can alter chromatin conformation and modulate access to transcription factors. h) Compression of the intercellular space can alter the concentration of signaling molecules. Additionally, changes in G-protein-coupled receptors, lipid fluidity and mitochondrial activity have been proposed as mechanosensors [125]

Figure 7

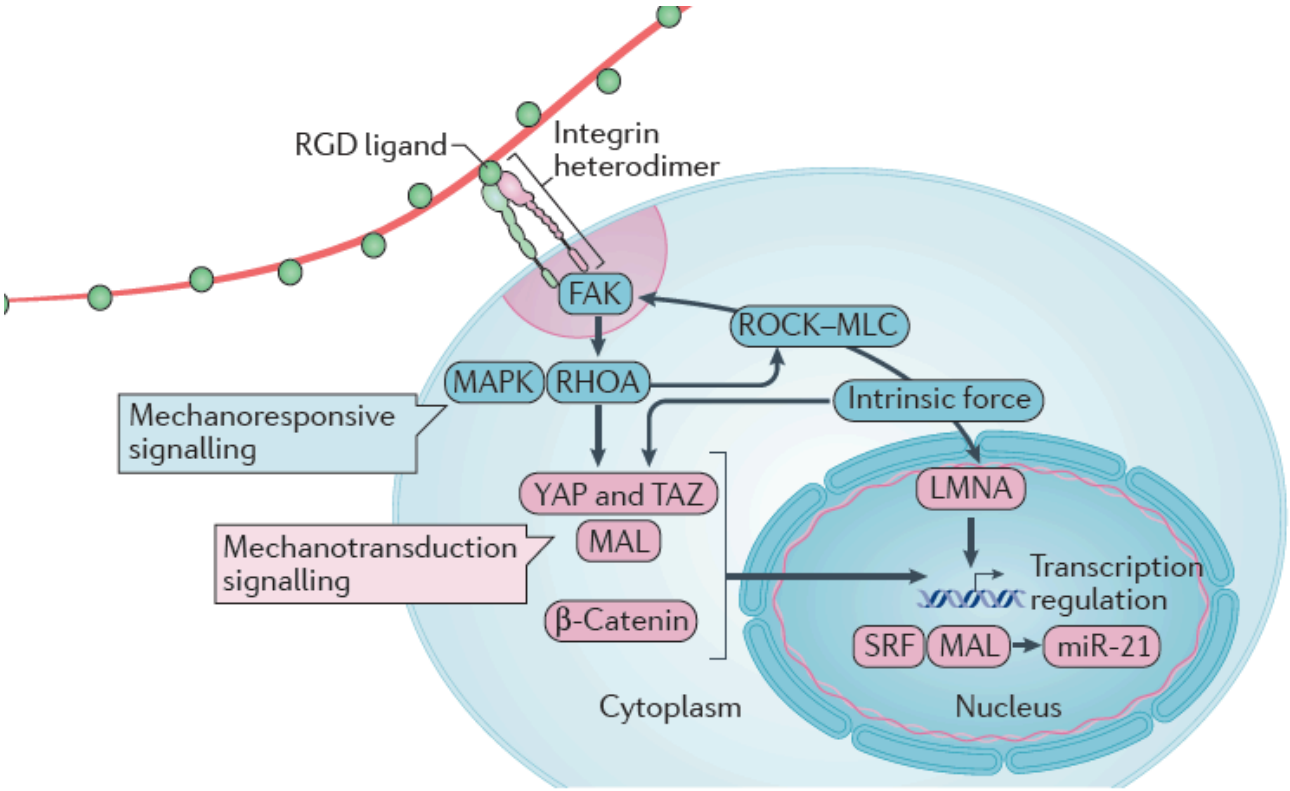

Figure 7 – Interaction between ECM and intracellular pathways. ECM mechanics regulates the stability of focal adhesions that are characterized by the presence of focal adhesion kinase (FAK), which in turn activates mechanoresponsive elements, such as MAPK and RhoA. RhoA transmits the mechanical signal by activating RHO-associated protein kinase 1 (ROCK), which in turn phosphorylates the myosin light chain (MLC) to generate actomyosin forces and contraction. This increased contractility stimulates nuclear translocation of transcription regulators, such as MAL (also known as MRTF-A); a globular (G)-actin-binding co-activator of serum response factor (SRF), YAP/TAZ, as well as β-catenin, thereby turning on mechanoresponses. Mechanical forces are also physically coupled to the nucleus via nuclear lamina proteins, such as lamin A (LMNA), which can affect chromatin structure and epigenetic regulation. RGD, arginine–glycine–aspartate. [234]

Figure 8

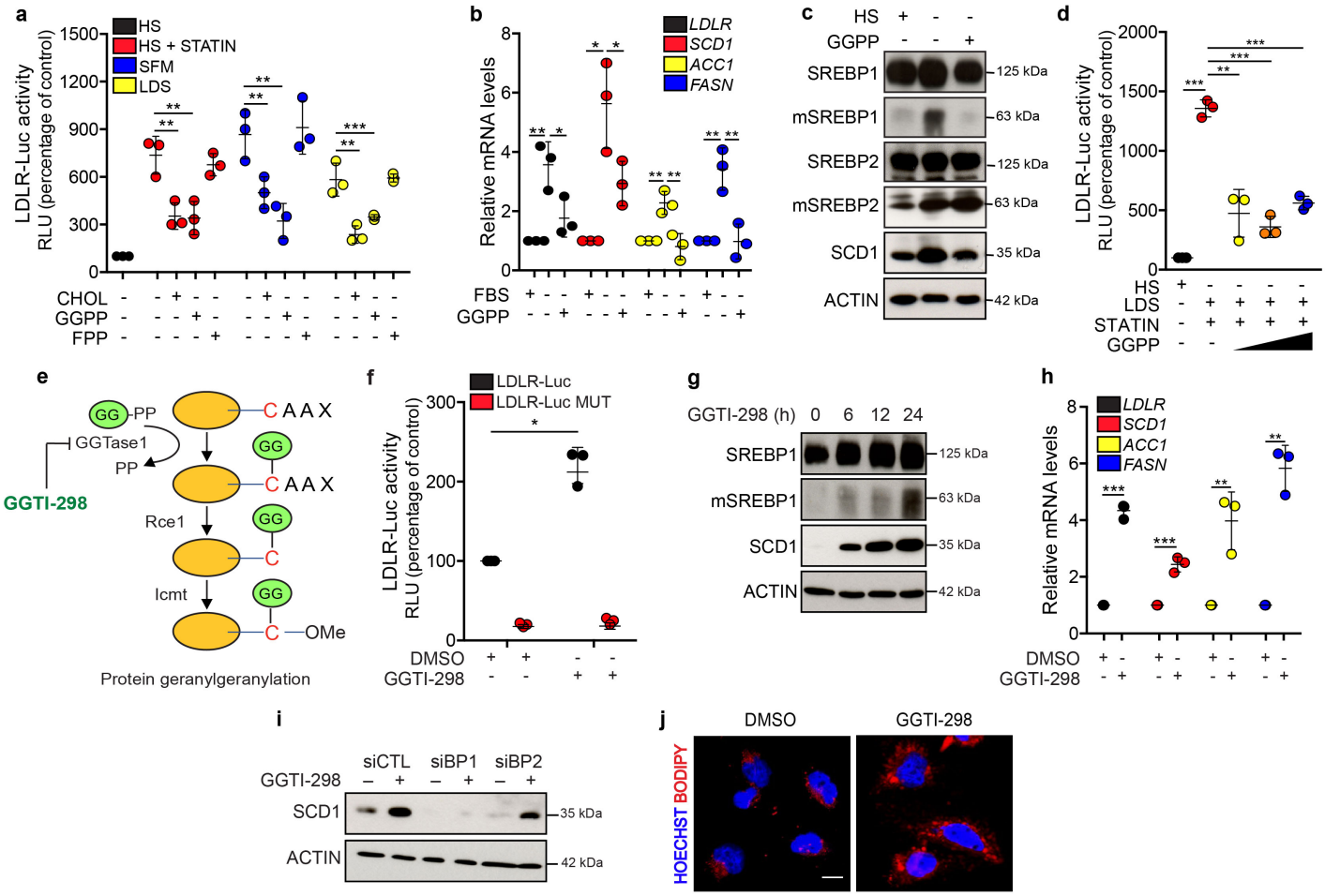

Figure 8 - **Protein geranylgeranylation regulates SREBP1**. **a**, Low density lipoprotein receptor promoter-luciferase (LDLR-Luc) assay in MCF-10A cells. Medium containing 5% horse serum (HS, as control) was replaced with 5% HS medium supplemented with 10 μM cerivastatin (STATIN), serum-free medium (SFM), or 2% lipid serum (lipid-depleted serum, LDS) medium, for 24 hours. Cells were either mock-treated, or treated with cholesterol (CHOL), geranylgeranyl pyrophosphate (GGPP), or farnesyl pyrophosphate (FPP). **b**, RT-qPCR quantification of LDLR, SCD1, ACC1 and FASN gene expression in MCF-10A cells. **c**, Western blot analysis of MCF-10A cells. **d**, LDLR-Luc assay in MCF-10A cells. 5% HS medium (control) was replaced with medium supplemented with 2% LDS and 1 μM cerivastatin (STATIN), and increasing doses of GGPP (20, 40 and 100 μM) for 24 hours. **e**, Scheme of geranylgeranyl (GG) conjugation to cysteine. **f**, LDLR-Luc assay in MCF-10A cells treated with DMSO as control or geranylgeranyl pyrophosphate transferase I inhibitor (GGTI-298). Cells transfected with the mutated construct LDLR-Luc MUT underwent the same treatments. **g**, Western blot analysis of MCF-10A cells treated with GGTI-298 for the indicated time (hours, h). **h**, RT-qPCR quantification of LDLR, SCD1, ACC1 and FASN gene expression in MCF-10A cells treated with DMSO as control or GGTI-298. **i**, Western blot

analysis of MCF-10A cells transfected with control (siCTL) SREBP1 (siBP1) and SREBP2 (siBP2) siRNAs and treated with GGTI-298 for 24 hours. **j**, BODIPY 493/503 staining of lipid droplets (in red) in Mahlavu cells treated with GGTI-298. Nuclei were stained with HOECHST (in blue). Scale bar, 15 μm. Graph bars represent mean and ± s.d. of n=3 biological replicates. Values in a, b and f are expressed as Relative Luminometer Units (RLU). Values in b and h are expressed as mRNA levels relative to control. In b and c, 5% HS medium (control) was replaced with SFM or SFM supplemented with GGPP for 24 hours. For western blots, ACTIN was used as loading control, mSREBP indicates mature protein. Blots and images are representative of n=3 biological replicates. P value: *P < 0.05, **P < 0.01, ***P < 0.001 by two-tailed Student's t-test for all analyses.

Figure 9

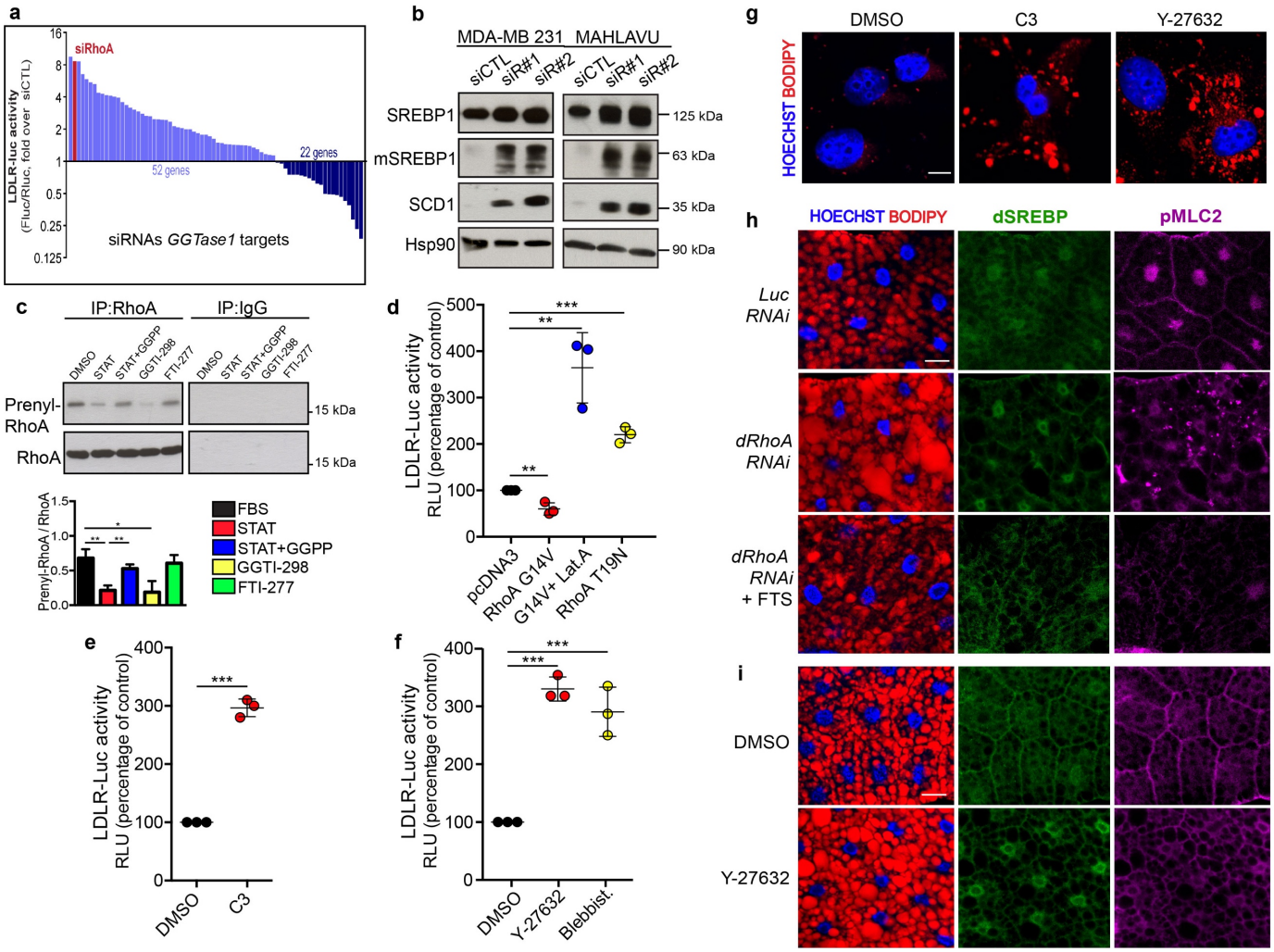

Figure 9 - RhoA and acto-myosin regulate the activity of hSREBP1 and dSREBP. a, Screening of low-density Lipoprotein receptor promoter-luciferase activity in MDA-MB-231 cells transfected with constructs expressing firefly (LDLR-Luc) and renilla (Rluc) luciferase and either control siRNA (siCTL) or siRNAs targeting genes encoding geranylgeranyl pyrophosphate transferase I (GGTase1) protein substrates. **b**, Western blot analysis of MDA-MB-231 and Mahlavu cells 48 hours after transfection with siCTL or RhoA targeting siRNAs (siR#1 and siR#2). Hsp90 was used as loading control. mSREBP indicates mature protein. **c**, Western blot analyses of immunoprecipitated (IP) RhoA in MCF-10A cells treated DMSO (as control), 1 µM cerivastatin (STAT), 1 µM cerivastatin and 20 µM GGPP (STAT+GGPP), 5 µM GGTI-298 or 5 µM FTI-277. IgGs were used as IP control. **d**, LDLR-Luc assay in MCF-10A cells 12 hours after transfection with pcDNA3-GFP control plasmid, pcDNA3-GFP-RhoA G14V construct with a 6 hours DMSO treatment, pcDNA3-GFP-RhoA G14V construct with a 6 hours Latrunculin A (G14V + Lat.A) treatment, or pcDNA3-GFP-RhoA T19N construct. **e**, LDLR-Luc assay in MCF-10A cells treated with either DMSO as control or C3 for 24 hours. **f**, LDLR-Luc assay in MCF-10A cells treated with either DMSO as control, Y-27632, or Blebbistatin (Blebbist.) for 24 hours. **g**, BODIPY 493/503 staining of

lipid droplets (in red) in Mahlavu cells treated with either DMSO, C3 or Y-27632 for 24 hours. Scale bar, 15 μm. **h**, **i** BODIPY 493/503 staining of lipid droplets (in red) and immunofluorescence analysis of dSREBP (in green) and phosphorylated myosin light chain (pMLC2, in magenta) in *Drosophila* larval fat body from (h) flies expressing either Luciferase or dRhoA RNAi, or dRhoA RNAi and treated with fatostatin (FTS) and (i) wild type flies treated with either DMSO or Y-27632. Scale bar, 20 μm.

Graphs bars in c-f represent mean ± s.d. of n=3 biological replicates. Values in d-f are expressed as Relative Luminometer Units (RLU). Nuclei in h-I were stained with HOECHST (in blue). Blots and images are representative of n=3 biological replicates. P value: *P < 0.05, **P < 0.01, ***P < 0.001 by two-tailed Student's t-test for all analyses.

Figure 10

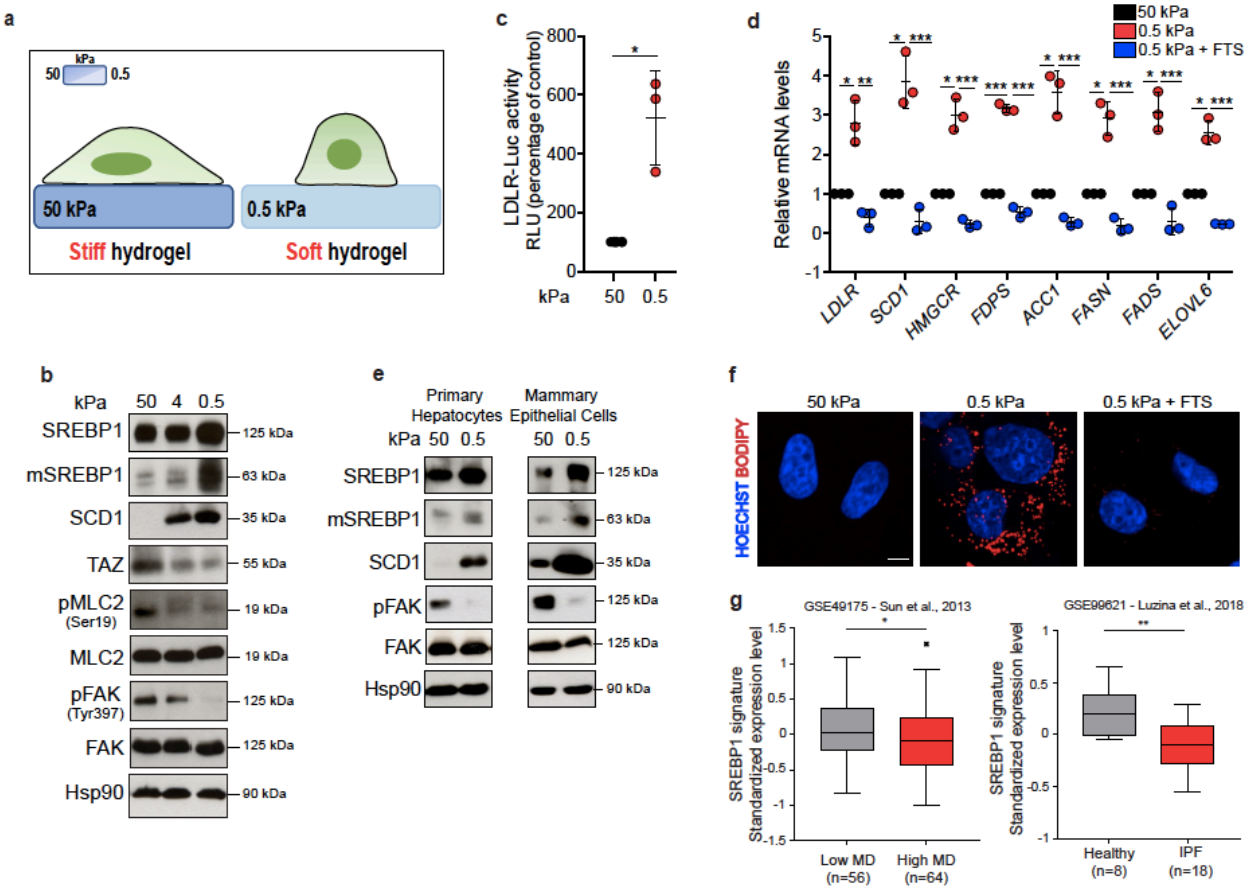

Figure 10 - SREBP1 is under the control of mechanical cues. a, Scheme of cell (in green) adhesion to fibronectin-coated hydrogel matrix (in blue) with 50 and 0.5 kPa elastic modulus. **b**, Western blot analysis of MCF-10A cells cultured on fibronectin-coated hydrogel matrix of high (50 kPa elastic modulus), intermediate (4 kPa elastic modulus) or low (0.5 kPa elastic modulus) stiffness, for 24 hours. **c**, Low density lipoprotein receptor promoter-luciferase (LDLR-Luc) assay in MCF-10A cells cultured on stiff (50 kPa elastic modulus, as control) or soft (0.5 kPa elastic modulus) fibronectin-coated hydrogel matrix for 24 hours. **d**, RT-qPCR quantification of the expression of the indicated genes in MCF-10A cells cultured on stiff (50 kPa elastic modulus, as control) or soft (0.5 kPa elastic modulus) fibronectin-coated hydrogel matrix, or soft (0.5 kPa elastic modulus) fibronectin-coated hydrogel matrix with fatostatin treatment (FTS), for 24 hours. **e**, Western blot analysis of primary cultures of hepatocytes and mammary epithelial cells on stiff (50 kPa elastic modulus) or soft (0.5 kPa elastic modulus) fibronectin-coated hydrogel matrix for 24 hours. **f**, BODIPY 493/503 staining of lipid droplets (in red) in Mahlavu cells cultured on stiff (50 kPa elastic modulus, as control, in black) or soft (0.5 kPa elastic modulus, in red) fibronectin-coated hydrogel matrix, or soft (0.5 kPa elastic modulus) fibronectin-coated hydrogel matrix with fatostatin treatment (FTS, in blue), for 24 hours. Nuclei were stained with HOECHST (in blue). Scale bar, 10 µm. **g**, Average standardized expression levels of SREBP1 signature in human

samples datasets of normal breast tissue with high vs low mammographic density (MD) and Idiopathic Pulmonary Fibrosis (IPF) patients vs healthy controls.
Graphs bars represent mean ± s.d. of n=3 biological replicates. P value: *P < 0.05 by two-tailed Student's t-test (c, d) and two-way ANOVA (g). For western blots, Hsp90 was used as loading control, mSREBP indicates mature protein. Blots and images are representative of n=3 biological replicates.

Figure 11

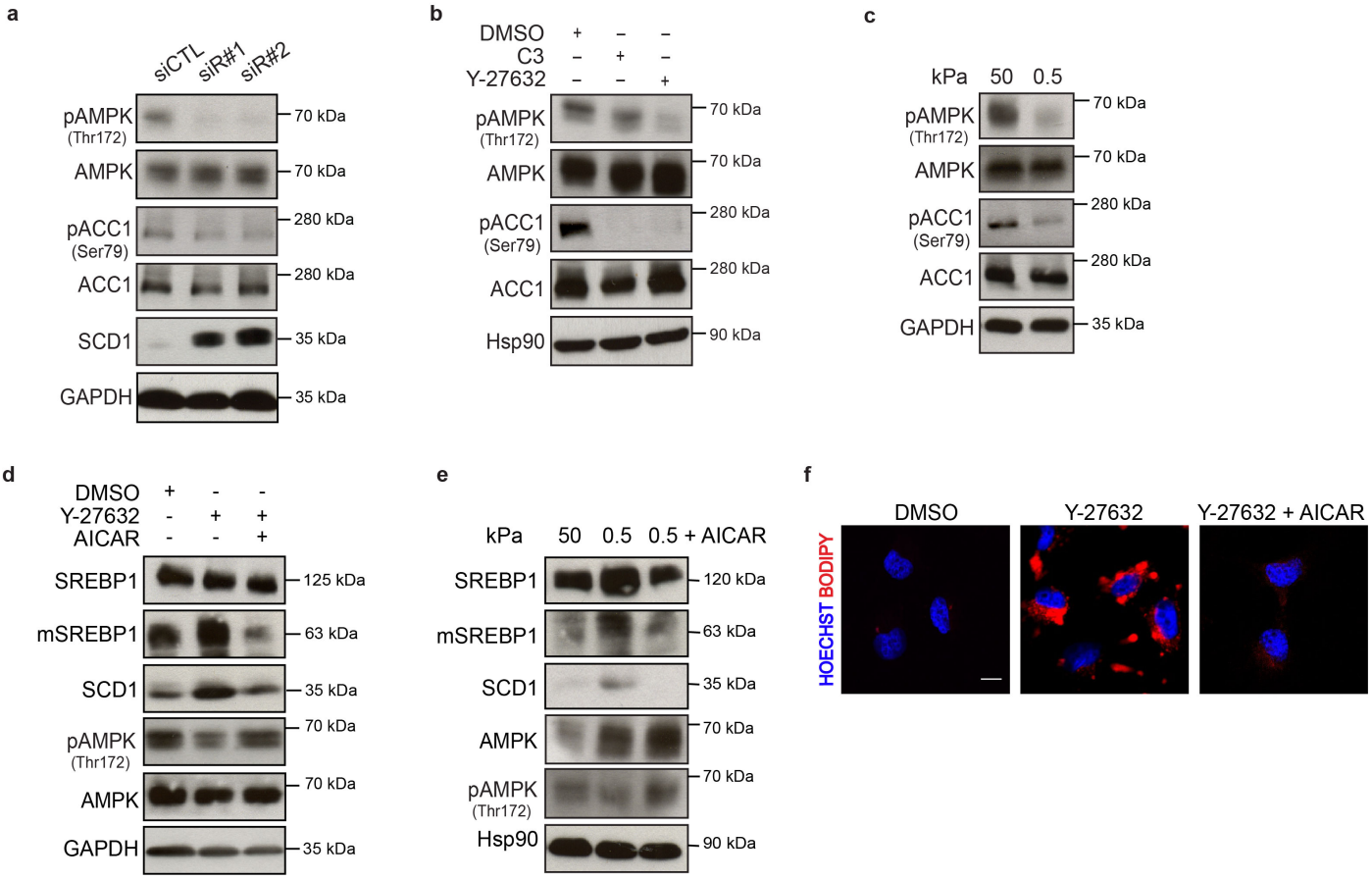

Figure11 - AMPK suppresses SREBP1 activation downstream of mechanical inputs. **a**, Western blot analysis of MCF-10A cells 48 hours after transfection with either control (siCTL) or RhoA targeting siRNA (siR#1 and siR#2). GAPDH was used as loading control. **b**, Western blot analysis of MCF-10A cells treated with either DMSO, C3 or Y-27632, for 24 hours. Hsp90 was used as loading control. **c**, Western blot analysis MCF-10A cells cultured on either stiff (50 kPa elastic modulus) or soft (0.5 kPa elastic modulus) fibronectin-coated hydrogel matrix for 24 hours. GAPDH was used as loading control. **d**, Western blot analysis of MCF-10A cells treated with either DMSO, Y-27632 or AICAR, for 24 hours. GAPDH was used as loading control. **e**, Western blot analysis of MCF-10A cells cultured on either stiff (50 kPa elastic modulus) or soft (0.5 kPa elastic modulus) fibronectin-coated hydrogel matrix, or soft (0.5 kPa elastic modulus) fibronectin-coated hydrogel matrix with AICAR treatment, for 24 hours. Hsp90 was used as loading control. **f**, BODIPY 493/503 staining of lipid droplets (in red) in Mahlavu cells treated with Y-27632 or Y-27632 and AICAR, for 24 hours. Nuclei were stained with HOECHST (in blue). Scale bar, 15 μm.
For western blots, mSREBP indicates mature protein. Blots and images are representative of n=3 biological replicates.

Figure 12

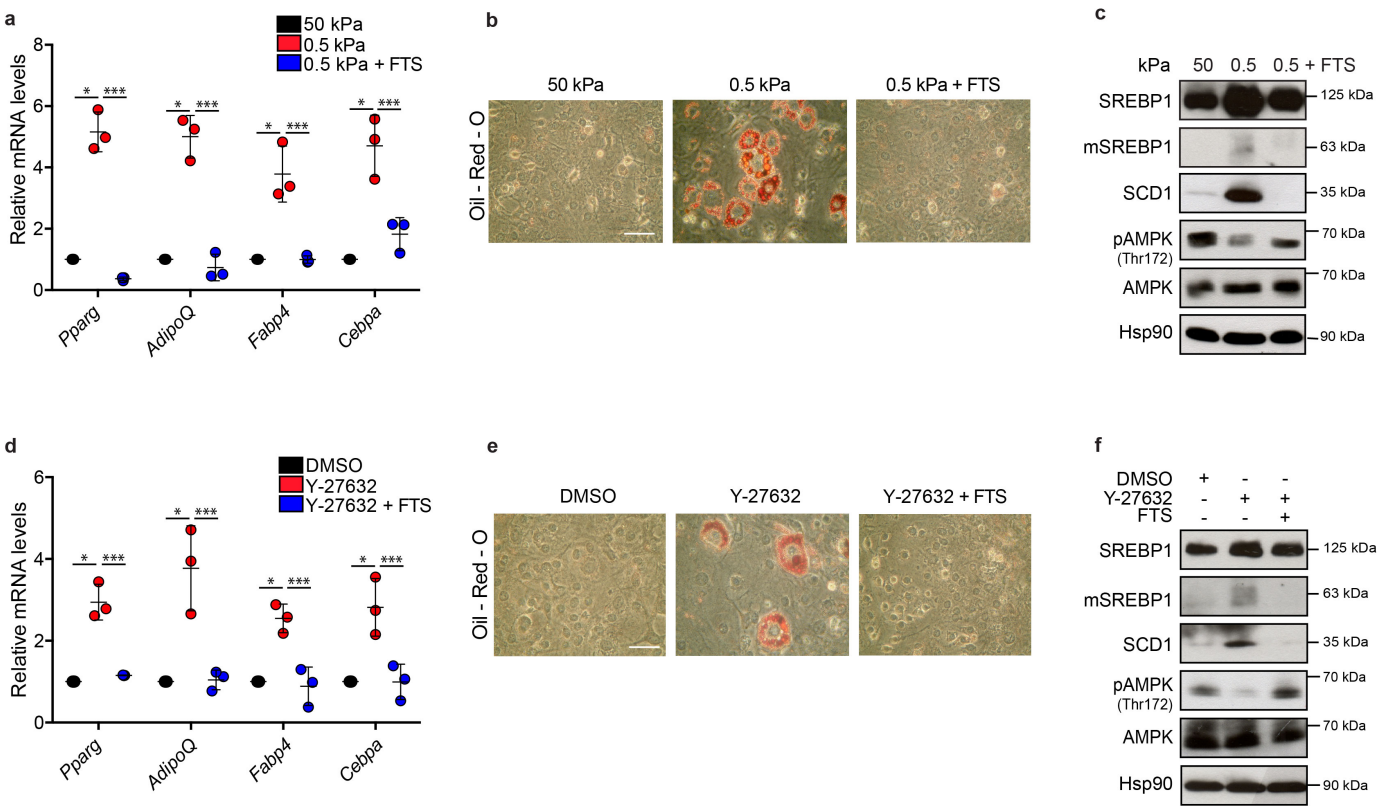

Figure 12 - SREBP1 regulates mesenchymal stem cell commitment upon cytoskeleton remodelling. a, RT-qPCR quantification of the indicated genes in mouse mesenchymal stem cells (mMSCs) cultured on stiff (50 kPa elastic modulus, as control) or soft (0.5 kPa elastic modulus) fibronectin-coated hydrogel matrix, or soft (0.5 kPa elastic modulus) fibronectin-coated hydrogel matrix with fatostatin treatment (FTS). Values are expressed as mRNA levels relative to control. **b**, Oil-Red-O staining of lipid droplets (in red) in mMSCs cultured on either stiff (50 kPa elastic modulus) or soft (0.5 kPa elastic modulus) fibronectin-coated hydrogel matrix, or soft (0.5 kPa elastic modulus) fibronectin-coated hydrogel matrix with fatostatin treatment (FTS). Scale bar, 100 μm. **c**, Western blot analysis of mMSCs cultured on either stiff (50 kPa elastic modulus) or soft (0.5 kPa elastic modulus) fibronectin-coated hydrogel matrix, or soft (0.5 kPa elastic modulus) fibronectin-coated hydrogel matrix with fatostatin treatment (FTS). **d**, RT-qPCR quantification of the indicated genes in mMSCs cultured in differentiating medium and treated with either DMSO as control, or with Y-27632, or Y-27632 and fatostatin (Y-27632 + FTS). Values are expressed as mRNA levels relative to control. **e**, Oil-Red-O staining of lipid droplets (in red) in mMSCs cultured in differentiating medium and treated with DMSO as control, or with Y-27632 or Y-27632 and fatostatin (Y-27632 + FTS). Medium composition is detailed in the Methods section. Scale bar, 100 μm. **f**, Western blot analysis of mMSC cultured in differentiating medium and treated with either DMSO as control or with Y-27632, or Y-27632 and fatostatin (FTS).

Graph bars represent mean ± s.d. of n=3 biological replicates. For western blots, Hsp90 was used as loading control, mSREBP indicates mature protein. P value: *P < 0.05, ***P < 0.001

by two-tailed paired Student’s t-test. Blots and images are representative of n=3 biological replicates.

Figure 13

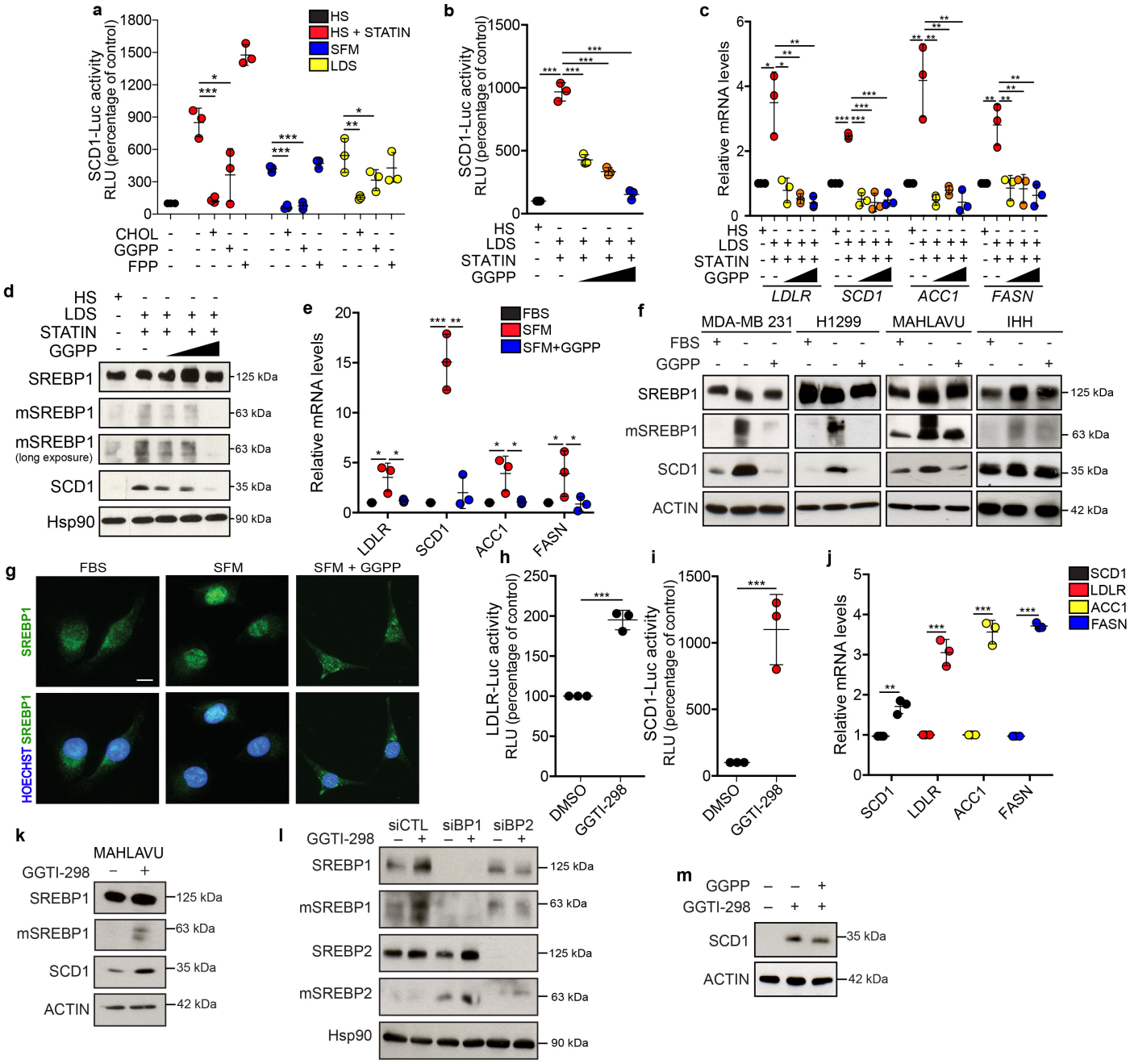

Figure 13 - **a**, SCD1-Luc assay in MCF-10A cells treated with cholesterol (CHOL), geranylgeranyl (GGPP) or farnesyl pyrophosphate (FPP). 5% horse serum (HS) medium (control) was supplemented with 10 µM cerivastatin (STATIN), replaced with serum-free (SFM), or 2% lipid serum (lipid-depleted serum, LDS) medium. **b-d**, SCD1-Luc assay (**b**), LDLR, SCD1, ACC1 and FASN RT-qPCR (**c**) SREBP1 and SCD1 western blot (**d**) in MCF-10A cells. 5% HS medium (control) was replaced with 2% LDS medium supplemented with 1 µM cerivastatin (STATIN) and 20, 40, 100 µM GGPP. **e**, LDLR, SCD1, ACC1 and FASN RT-qPCR in IHH cells. 5% HS medium (control) was replaced with SFM or SFM supplemented with GGPP. **f**, SREBP1 and SCD1 western blot in MDA-MB 231, H1299,

Mahlavu and IHH cells cultured in 10% foetal bovine serum (FBS) medium, SFM, or SFM supplemented with GGPP. **g**, SREBP1 Immunofluorescence (green) in MDA-MB 231 cells cultured in 10% FBS medium, SFM, or SFM supplemented with GGPP. Nuclei were stained with HOECHST (in blue). Scale bar 15 μm. **h**, LDLR-Luc assay in IHH cells treated with DMSO (control) or geranylgeranyl transferase I inhibitor (GGTI-298). **i**, SCD1-Luc assay in MCF-10A cells treated with DMSO (control) or 5μM GGTI-298. **j**, LDLR, SCD1, ACC1 and FASN RT-qPCR in IHH cells treated with DMSO (control) or 5μM GGTI-298. **k**, Western blot analysis of Mahlavu cells treated with DMSO (control) or 5μM GGTI-298. **l**, Western blot analysis of MCF-10A cells transfected with control (siCTL), SREBP1 (siBP1) or SREBP2 (siBP2) siRNA and treated with GGTI-298. **m**, Western blot analysis of MCF-10A cells treated with DMSO, GGTI-298 or GGTI-298 and GGPP.
Graph bars represent mean ± s.d. of n=3 biological replicates. Treatments lasted 24 hours Values in a, b, h are expressed as Relative Luminometer Units (RLU). RT-qPCR values are expressed as mRNA levels relative to control. P value: *P < 0.05, **P < 0.01, ***P < 0.001 by two-tailed Student's t –test for all the analyses. Blots are representative of n=3 biological replicates. For western blots, mSREBP indicates mature protein, Actin and Hsp90 were loading controls.

Figure 14

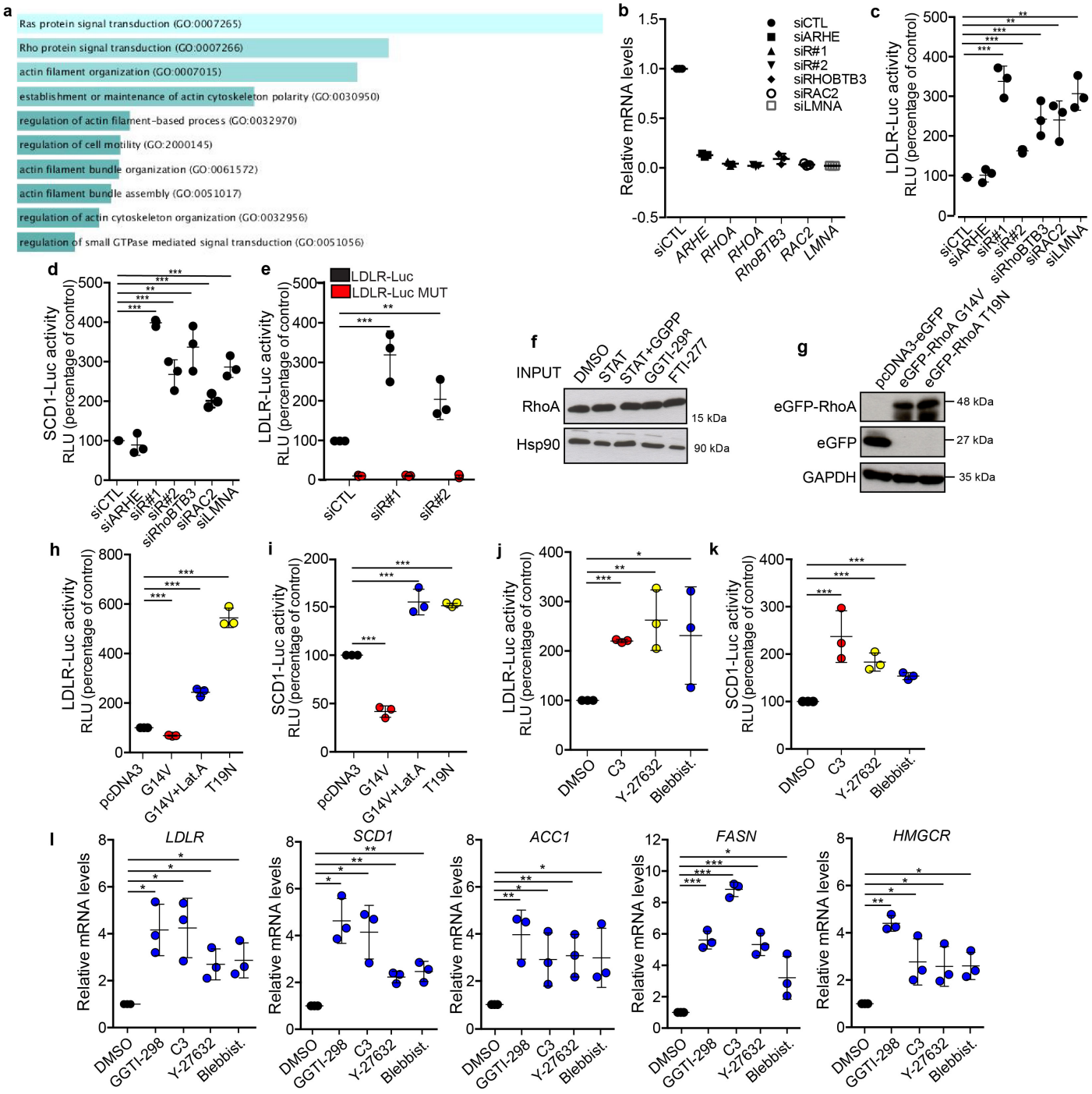

Figure 14 - **a**, Gene ontology Biological Process categories that are significantly enriched in geranylgeranylated proteins that negatively regulate SREBP. **b**, RhoE/AHRE, RhoA, RhoBTB3, Rac2 and Lamin A RT-qPCR in MDA-MB-231, 48h after transfection with control siRNA (siCTL) or siRNAs targeting RhoE (siARHE), RhoA (siR#1 and siR#2), RhoBTB3 (siRHOBTB3), Rac2 (siRAC2) and Lamin A (siLMNA). **c**, LDLR-Luc assay in MDA-MB 231 cells transfected with siCTL siARHE, siRhoA#1, siRhoA#2, siRHOBTB3, siRAC2 or siLMNA. **d**, SCD1-Luc assay in MDA-MB 231 cells transfected with either siCTL siARHE, siRhoA#1, siRhoA#2, siRHOBTB3, siRAC2 or siLMNA. **e**, LDLR-Luc assay in IHH cells

transfected with siCTL, siRhoA#1, or siRhoA#2, Cells transfected with the mutated construct LDLR-Luc MUT underwent the same treatments. **f**, Western blot analysis of MCF-10A cells treated DMSO (as control), 1 μM cerivastatin (STAT), 1 μM cerivastatin and 20 μM GGPP (STAT+GGPP), 5 μM GGTI-298 or 5 μM FTI-277. **g**, Western blot analysis of MCF-10A cells transfected with pcDNA3-eGFP, pcDNA3-eGFP-RhoA G14V and pcDNA3-eGFP-RhoA T19N. **h**, LDLR-Luc assay in IHH cells (**h**), SCD1-Luc assay in MCF-10A cells (**i**) 12 hours after transfection with pcDNA3-GFP control plasmid, pcDNA3-GFP-RhoA G14V construct with a 6 hours DMSO treatment, pcDNA3-GFP-RhoA G14V construct with a 6 hours Latrunculin A (G14V + Lat.A) treatment, or pcDNA3-GFP-RhoA T19N construct. **j**, **k**, **l**, LDLR-Luc assay in IHH cells (**j**), SCD1-Luc assay (**k**), LDLR, SCD1, ACC1, FASN and HMGCR RT-qPCR (**l**) in MCF-10A cells treated with DMSO (control), GGTI-298, C3, Y-27632 or Blebbistatin (Blebbist.) for 24 hours.

Graph bars represent mean ± s.d. of n=3 biological replicates. Values in c-e, h-k are expressed as Relative Luminometer Units (RLU). RT-qPCR values are expressed as mRNA levels relative to control. Blots are representative of n=3 biological replicates. P value: *P < 0.05, **P < 0.01, ***P < 0.001 by two-tailed Student's t-test for all analyses. For western blots, GAPDH and Hsp90 were loading controls.

Figure 15

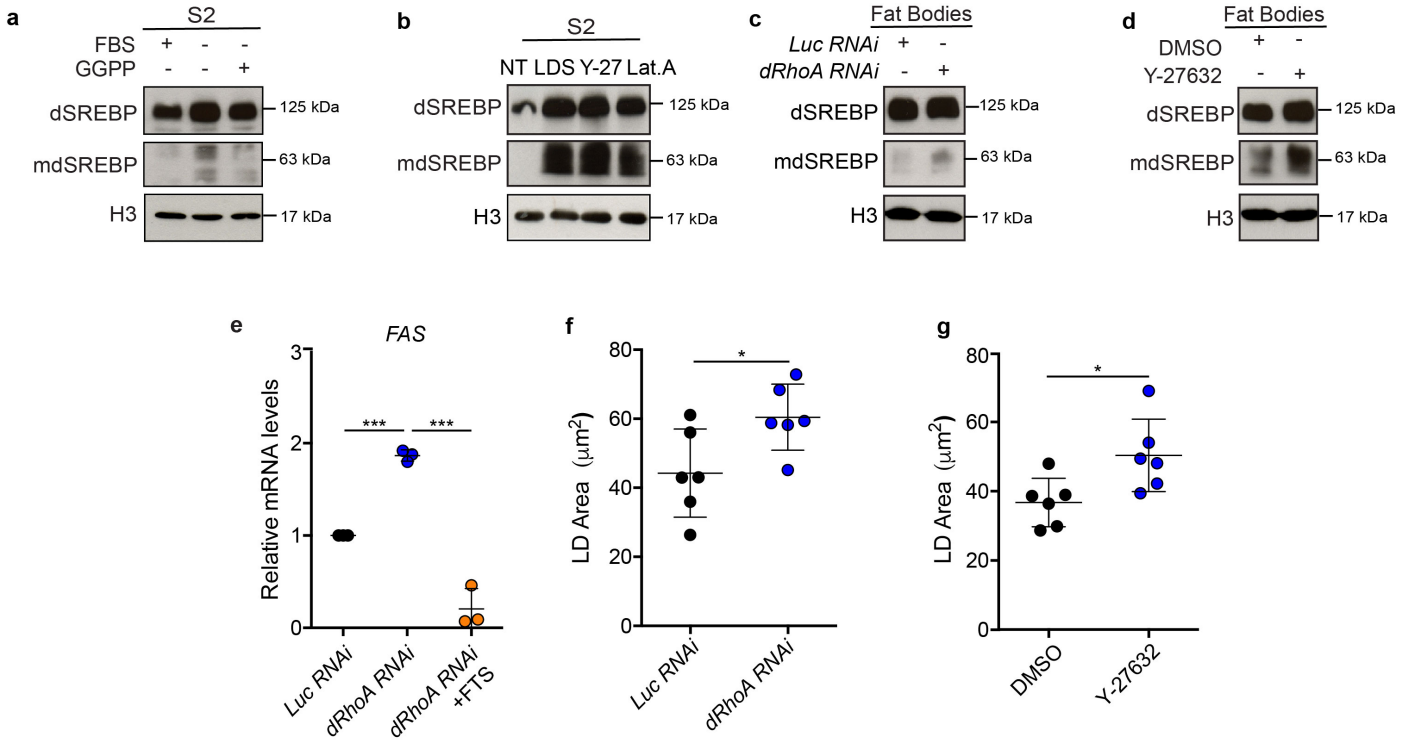

Figure 15 - **a**, Western blot analysis of S2 *Drosophila* cells treated as follows: cell culture medium containing 10% foetal bovine serum (FBS) was replaced with serum-free medium or serum-free medium supplemented with GGPP. **b**, Western blot analysis of S2 *Drosophila* cells treated as follows: cell culture medium containing 10% FBS (non-treated, NT) was either replaced with medium containing 2% lipid serum (lipid-depleted serum, LDS), or supplemented with Y-27632 (Y27) or Latrunculin A (Lat.A). **c**, Western blot analysis of *Drosophila* larval fat bodies expressing Luciferase RNAi (Luc) or dRhoA RNAi. **d**, Western blot analysis of wild type *Drosophila* larval fat bodies treated with either DMSO or Y-27632 for 16 hours. **e**, RT-qPCR quantification of the expression of the Fatty Acid Synthase (FAS) dSREBP target gene in *Drosophila* larval fat bodies expressing Luc RNAi (as control, in black), dRhoA RNAi (in blue), or dRhoA RNAi and treated with fatostatin for 16 hours (FTS, in orange). Values are expressed as mRNA levels relative to control. Bars represent mean value ± s.d. of n=3 biological replicates. Rp49 was used as reference gene. **f**, Quantification of lipid droplet size in *Drosophila* larval fat bodies expressing Luc RNAi (as control, in black), dRhoA RNAi (in blue), or dRhoA RNAi and treated with fatostatin for 16 hours (FTS, in orange). Representative images are shown in Figure 2h. **g**, Quantification of lipid droplet size in wild type *Drosophila* larval fat bodies treated with either DMSO (in black) or Y-27632 (in blue). Representative images are shown in Fig. 2h.

Graph bars represent mean value ± s.d. of n=3 biological replicates (e) or n=6 individuals (f and g). For all western blots, H3 was used as loading control. Blots are representative of n=3 biological replicates. For western blots, mSREBP indicates mature protein. P value: *P < 0.05, ***P < 0.001 by two-tailed Student's t-test for all analyses.

Figure 16

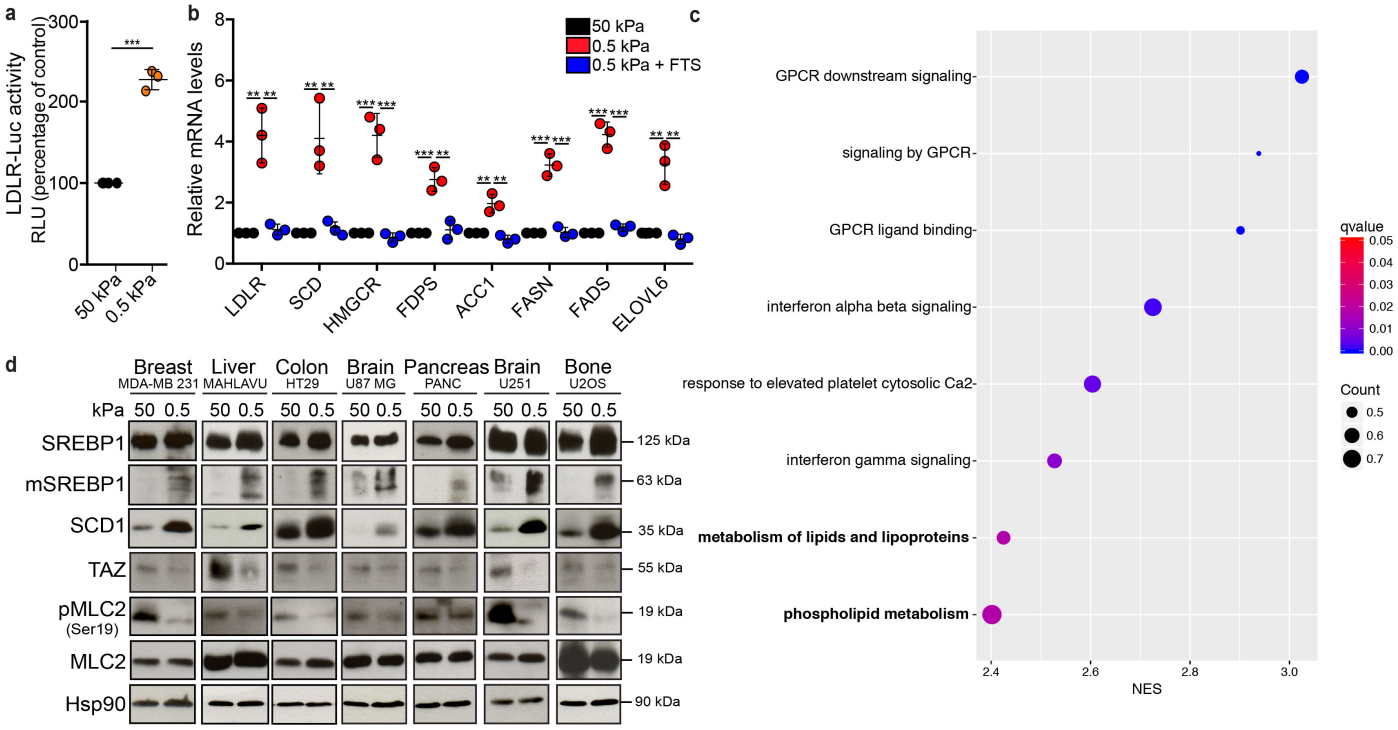

Figure 16 - a, Low density lipoprotein promoter-luciferase (LDLR-Luc) reporter assay in IHH cells cultured on either stiff (50 kPa elastic modulus, as control) or soft (0.5 kPa elastic modulus) fibronectin-coated hydrogel matrix for 24 hours. Graphs bars represent mean value ± s.d. of n=3 biological replicates. P value: *P < 0.001 by two-tailed Student's t-test for all analyses. **b**, RT-qPCR quantification of the expression of the indicated genes in IHH cells cultured on either stiff (50 kPa elastic modulus, as control) or soft (0.5 kPa elastic modulus) fibronectin-coated hydrogel matrix, or soft fibronectin-coated hydrogel matrix with fatostatin treatment (FTS), for 24 hours. Graphs bars represent mean value ± s.d. of n=3 biological replicates. P value: **P < 0.01, ***P < 0.001 by two-tailed Student's t-test for all analyses. **c**, Reactome gene sets that are significantly enriched (FDR q value < 0.05) in MDA-MB-231 cells cultured on a soft substrate. Dot size represents the fraction of genes contributing to the enrichment score in each gene set (count); the positive normalized enrichment score (NES) indicates the degree to which Reactome gene sets are overrepresented in cells grown on the soft (as compared to cells grown on the stiff) substrate. Gene expression data were obtained from n=4 biological replicates for each condition (GSE93529). **d**, Western blot analysis of cell lines originated from the indicated tissues, cultured on either stiff (50 kPa elastic modulus) or soft (0.5 kPa elastic modulus) fibronectin-coated hydrogel matrix for 24 hours. Hsp90 was used as loading control. Blots are representative of n=3 biological replicates. mSREBP indicates mature protein.

Tables

Table 1 | List of siRNAs sequences

Human SREBP1	siSREBP-1	AUCUCUGAAGGAUCUGGUG
Human SREBP2	siSREBP-2	GCCCUCUAUUGGAUGAUGC
Human RhoA	siRhoA#1	AUGGAAAGCAGGUAGAGUU
Human RhoA	siRhoA#2	GAAAGACAUGCUUGCUCAU
Human ARHE	siARHE	UAGUAGAGCUCUCCAAUCACA
Human RhoBTB3	siRhoBTB3	AGGAAGAAGUUGAAAGAUUUU
Human RAC2	siRAC2	CCUCUUUUGGAACAACAUA
Human LMNA	siLMNA	GGAUGAGGAUGGAGAUGAC

Table 2 | List of primers used for qRT-PCR

human *LDLR*	Fw	AAGCCATTCACTTCCCCAATC
	Rv	GCCTCACCGTGCATGTTTTA
human *SCD1*	Fw	CACTTGGGAGCCCTGTATGG
	Rv	TGAGCTCCTGCTGTTATGCC
human *HMGCR*	Fw	GGACCCCTTTGCTTAGATGAAA
	Rv	CCACCAAGACCTATTGCTCTG
human *FDPS*	Fw	CTTCCTATAGCTGCAGCCATGTAC
	Rv	GCATTGGCGTGCTCCTTCT
human *ACC1*	Fw	CATATTGAGGATGACAGGCTGG
	Rv	CTCATAGTTGACCTGCTTTCTG
human *FASN*	Fw	CATCCAGATAGGCCTCATAGA
	Rv	CTCCATGAAGTAGGAGTGGAA
human *FADS1*	Fw	GCTACTTCACCTGGGACGAG
	Rv	GTGGAAGGCCACAAAGGGAT
human *ELOVL6*	Fw	CTCGAAATCAAGCGCTTTACAGA
	Rv	AGGCAGCATACAGAGCAGAAA
human *RhoA*	Fw	ATTCGTTGCCTGAGCAATGG
	Rv	TGTGTCCCACAAAGCCAACT
human ARHE	Fw	GCCAGCCAGAAATTATCCAGC
	Rv	CTTGGCGAAGACATGGAGC
human RHOBTB3	Fw	ACTCCACAGCCTTGATGACTT
	Rv	AAGCACCTGGTTGTTCAAGTT
human RAC2	Fw	CGCCAAGTGGTTCCCAGAAG
	Rv	AGCTGAGCACTCCAGGTATTT
human *H3*	Fw	GTGAAGAAACCTCATCGTTACAGGCCTGGT
	Rv	CTGCAAAGCACCAATAGCTGCACTCTGGAA
mouse *Pparg*	Fw	AAGAGCTGACCCAATGGTTG
	Rv	ACCCTTGCATCCTTCACAAG
mouse *AdipoQ*	Fw	GACAAGGCCGTTCTCTTCAC
	Rv	CAGACTTGGTCTCCCACCTC
mouse *Cebpa*	Fw	GAACAGCAACGAGTACCGGGTA
	Rv	GCCATGGCCTTGACCAAGGAG
mouse *Fabp4*	Fw	AAGTGGGAGTGGGCTTTGC
	Rv	CCGGATGGTGACCAAATCC
mouse *Gapdh*	Fw	ATCCTGCACCACCAACTGCT
	Rv	GGGCCATCCACAGTCTTCTG
Drosophila FAS	Fw	CCCCAGGAGGTGAACTCTATCA
	Rv	GACTTGACCGATCCGATCAAC

Drosophila Rp49	Fw	ATCGGTTACGGATCGAACAA
	Rv	GACAATCACCTTGCGCTTCT
Drosophila RhoA	Fw	GTGGATGGCAAACAGGTGGAGC
	Rv	GCGAATCGGGTGAATCCACTGAG

Table 3 | List of proteins that negatively regulate LDLR-Luc upon siRNA silencing

Protein Name	Gene ID	Fluc/Rluc, fold over siCTL
ARHE	390	9,446
RHOA	387	8,590
RHOBTB3	22836	8,568
RAC2	5880	6,500
LMNA	4000	5,802
KIAA1164	54629	5,448
RHOB	388	5,253
FLJ23878	200172	4,339
GNG13	51764	4,264
RAP1A	5906	4,136
UBL3	5412	4,083
FLJ11280	55793	4,013
LMNB2	84823	3,898
RHOJ	57381	3,551
GBP5	115362	3,345
MRAS	22808	3,126
RHOG	391	3,003
PALM2	114299	2,898
ARHN	8153	2,757
MPI	4351	2,637
MGC42105	167359	2,620
GNG2	54331	2,448
YKT6	10652	2,437
BC008967	89927	2,413
RAC3	5881	2,404
GBP2	2634	2,324
OAS1	4938	2,113
GNG7	2788	2,063
GNG10	2790	2,034
LMNB1	4001	1,986
PEX19	5824	1,984
DIRAS1	148252	1,875
RASL10B	91608	1,815
FBXL20	84961	1,755
RHOF	54509	1,752
GNG12	55970	1,700

PPP1R16A	84988	1,615
RAB8A	4218	1,477
GNG3	2785	1,464
C10ORF25	220979	1,429
RHOC	389	1,425
RRAS	6237	1,410
RPGR	6103	1,405
GNG4	2786	1,398
RAB18	22931	1,392
PDE6B	5158	1,375
RAP1B	5908	1,332
CPLX4	339302	1,286
RAC1	5879	1,202
RAB8B	51762	1,152
PTP4A3	11156	1,132
FBXO10	26267	1,119
CAMK1G	57172	0,976
KRAS2	3845	0,957
C17ORF37	84299	0,865
RRAS2	22800	0,755
RALB	5899	0,755
RNF208	727800	0,754
NRAS	4893	0,743
DIRAS2	54769	0,726
GRK7	131890	0,702
ARHI	9077	0,667
RRP22	10633	0,627
GNG8	94235	0,606
CPLX3	594855	0,501
RND1	27289	0,498
FBXL2	25827	0,495
RHEB	6009	0,486
CNP	1267	0,469
RAP2B	5912	0,430
CDC42	998	0,394
DNAJB2	3300	0,287
RALA	5898	0,234
PALM	5064	0,189

Table 4 | SREBP1 gene signature generated for human samples validation.

ACACB	ACSL4	ACSL5	CSAD
ECHDC1	EHHADH	FADS1	FADS2
GPAM	GSTM1	GSTT1	IGHM
PDK1	RARRES1	SCD	THSRP

References

1. Santos, C. R. & Schulze, A. Lipid metabolism in cancer. *FEBS J.* **279**, 2610–2623 (2012).
2. Klose, C., Surma, M. A. & Simons, K. Organellar lipidomics-background and perspectives. *Current Opinion in Cell Biology* **25**, 406–413 (2013).
3. Muro, E., Ekin Atilla-Gokcumen, G. & Eggert, U. S. Lipids in cell biology: how can we understand them better? *Mol. Biol. Cell* **25**, 1819–1823 (2014).
4. Röhrig, F. & Schulze, A. The multifaceted roles of fatty acid synthesis in cancer. *Nat. Rev. Cancer* (2016). doi:10.1038/nrc.2016.89
5. Santos, A. L. & Preta, G. Lipids in the cell: organisation regulates function. *Cell. Mol. Life Sci.* **75**, 1909–1927 (2018).
6. Karantonis, H., Nomikos, T. & Demopoulos, C. Triacylglycerol Metabolism. *Curr. Drug Targets* **10**, 302–319 (2009).
7. Kazantzis, M. & Stahl, A. Fatty acid transport proteins, implications in physiology and disease. *Biochimica et Biophysica Acta - Molecular and Cell Biology of Lipids* **1821**, 852–857 (2012).
8. Goldberg, I. J., Eckel, R. H. & Abumrad, N. A. Regulation of fatty acid uptake into tissues: Lipoprotein lipase- And CD36-mediated pathways. *J. Lipid Res.* **50**, (2009).
9. Furuhashi, M. & Hotamisligil, G. S. Fatty acid-binding proteins: Role in metabolic diseases and potential as drug targets. *Nature Reviews Drug Discovery* **7**, 489–503 (2008).
10. Nelson, D. L. & Cox, M. M. *Lehninger Principles of Biochemistry*. *Bmj* **4**, (1970).
11. Schreurs, M., Kuipers, F. & Van Der Leij, F. R. Regulatory enzymes of mitochondrial β-oxidation as targets for treatment of the metabolic syndrome. *Obesity Reviews* **11**, 380–388 (2010).
12. Yu, X., Ma, R., Wu, Y., Zhai, Y. & Li, S. Reciprocal Regulation of Metabolic Reprogramming and Epigenetic Modifications in Cancer. *Front. Genet.* **9**, 394 (2018).
13. McDonnell, E. *et al.* Lipids Reprogram Metabolism to Become a Major Carbon Source for Histone Acetylation. *Cell Rep.* **17**, 1463–1472 (2016).
14. Wellen, K. E. *et al.* ATP-citrate lyase links cellular metabolism to histone acetylation. *Science (80-.).* **324**, 1076–1080 (2009).
15. Shimazu, T. *et al.* Suppression of oxidative stress by β-hydroxybutyrate, an

endogenous histone deacetylase inhibitor. *Science (80-.).* **339**, 211–214 (2013).

16. Feldman, J. L., Baeza, J. & Denu, J. M. Activation of the protein deacetylase SIRT6 by long-chain fatty acids and widespread deacylation by Mammalian Sirtuins. *J. Biol. Chem.* **288**, 31350–31356 (2013).
17. Ye, C., Sutter, B. M., Wang, Y., Kuang, Z. & Tu, B. P. A Metabolic Function for Phospholipid and Histone Methylation. *Mol. Cell* **66**, 180-193.e8 (2017).
18. Pietrocola, F., Galluzzi, L., Bravo-San Pedro, J. M., Madeo, F. & Kroemer, G. Acetyl coenzyme A: A central metabolite and second messenger. *Cell Metabolism* (2015). doi:10.1016/j.cmet.2015.05.014
19. Baenke, F., Peck, B., Miess, H. & Schulze, A. Hooked on fat: the role of lipid synthesis in cancer metabolism and tumour development. *Dis. Model. Mech.* **6**, 1353–1363 (2013).
20. Harayama, T. & Riezman, H. Understanding the diversity of membrane lipid composition. *Nat. Rev. Mol. Cell Biol.* (2018). doi:10.1038/nrm.2017.138
21. Olzmann, J. A. & Carvalho, P. Dynamics and functions of lipid droplets. *Nature Reviews Molecular Cell Biology* **20**, 137–155 (2019).
22. Welte, M. A. & Gould, A. P. Lipid droplet functions beyond energy storage. *Biochim Biophys Acta* **October**, 1260–1272 (2017).
23. Jacquemyn, J., Cascalho, A. & Goodchild, R. E. The ins and outs of endoplasmic reticulum-controlled lipid biosynthesis. *EMBO Rep.* **18**, 1905–1921 (2017).
24. Bartke, N. & Hannun, Y. A. Bioactive sphingolipids: metabolism and function. *J. Lipid Res.* **April**, S91–S96 (2009).
25. Hannun, Y. A. & Obeid, L. M. Principles of bioactive lipid signalling: Lessons from sphingolipids. *Nature Reviews Molecular Cell Biology* **9**, 139–150 (2008).
26. Hannun, Y. A. & Obeid, L. M. Sphingolipids and their metabolism in physiology and disease. *Nature Reviews Molecular Cell Biology* **19**, 175–191 (2018).
27. Wymann, M. P. & Schneiter, R. Lipid signalling in disease. *Nature Reviews Molecular Cell Biology* **9**, 162–176 (2008).
28. Serhan, C. N. & Savill, J. Resolution of inflammation: The beginning programs the end. *Nature Immunology* **6**, 1191–1197 (2005).
29. Funk, C. D. Prostaglandins and Leukotrienes: Advances in Eicosanoid Biology. *Science (80-.).* **294**, 1871–1875 (2001).
30. Vanhaesebroeck, B. *et al.* Synthesis and Function of 3-Phosphorylated Inositol Lipids. *Annu. Rev. Biochem.* **70**, 535–602 (2001).

31. Falkenburger, B. H., Jensen, J. B., Dickson, E. J., Suh, B. C. & Hille, B. Phosphoinositides: Lipid regulators of membrane proteins. in *Journal of Physiology* **588**, 3179–3185 (2010).
32. Morad, S. A. F. & Cabot, M. C. Ceramide-orchestrated signalling in cancer cells. *Nature Reviews Cancer* **13**, 51–65 (2013).
33. Mullen, P. J., Yu, R., Longo, J., Archer, M. C. & Penn, L. Z. The interplay between cell signalling and the mevalonate pathway in cancer. *Nat. Rev. Cancer* (2016). doi:10.1038/nrc.2016.76
34. Thurnher, M., Nussbaumer, O. & Gruenbacher, G. Novel Aspects of Mevalonate Pathway Inhibitors as Antitumor Agents Novel Aspects of Mevalonate Pathway Inhibitors as Antitumor Agents. **18**, 3524–3531 (2012).
35. Clendening, J. W. & Penn, L. Z. Targeting tumor cell metabolism with statins. *Oncogene* **31**, 4967–4978 (2012).
36. Goldstein, J. L. & Brown, M. S. Regulation of the mevalonate pathway. *Nature* **343**, 425–430 (1990).
37. Porter, J. A., Young, K. E. & Beachy, P. A. Cholesterol modification of hedgehog signaling proteins in animal development. *Science (80-.).* **274**, 255–259 (1996).
38. Jeong, J. & McMahon, A. P. Cholesterol modification of Hedgehog family proteins. *J. Clin. Invest.* **110**, 591–596 (2002).
39. Simons, K. & Ehehalt, R. Cholesterol, lipid rafts, and disease. *J. Clin. Invest.* **110**, 597–603 (2002).
40. Olson$, E. N., Towlers, D. A. & Glaser, L. *Specificity of Fatty Acid Acylation of Cellular Proteins*. *The American Society of Biological Chemists, h e* **260**, (1985).
41. Resh, M. D. Fatty Acylation of Proteins: The Long and the Short of it. *Prog Lipid Res* **July**, 120–131 (2016).
42. Martin, D. D. O., Beauchamp, E. & Berthiaume, L. G. Post-translational myristoylation: Fat matters in cellular life and death. *Biochimie* **93**, 18–31 (2011).
43. Chan, P. *et al.* Autopalmitoylation of TEAD proteins regulates transcriptional output of the Hippo pathway. *Nat. Chem. Biol.* **12**, 282–289 (2016).
44. Rocks, O. *et al.* The palmitoylation machinery is a spatially organizing system for peripheral membrane proteins. *Cell* (2010). doi:10.1016/j.cell.2010.04.007
45. Noland, C. L. *et al.* Palmitoylation of TEAD Transcription Factors Is Required for Their Stability and Function in Hippo Pathway Signaling. *Structure* **24**, 179–186 (2016).

46. Kurayoshi, M., Yamamoto, H., Izumi, S. & Kikuchi, A. Post-translational palmitoylation and glycosylation of Wnt-5a are necessary for its signalling. *Biochem. J* **402**, 515–523 (2007).
47. Zurzolo, C. & Simons, K. Glycosylphosphatidylinositol-anchored proteins: Membrane organization and transport. *Biochim. Biophys. Acta - Biomembr.* **1858**, 632–639 (2016).
48. Chen, B., Sun, Y., Niu, J., Jarugumilli, G. K. & Wu, X. Protein Lipidation in Cell Signaling and Diseases: Function, Regulation, and Therapeutic Opportunities. *Cell Chem. Biol.* **25**, 817–831 (2018).
49. Lebreton, S., Zurzolo, C. & Paladino, S. Organization of GPI-anchored proteins at the cell surface and its physiopathological relevance. *Crit. Rev. Biochem. Mol. Biol.* **53**, 403–419 (2018).
50. Briscoe, J. & Thérond, P. P. The mechanisms of Hedgehog signalling and its roles in development and disease. *Nature Reviews Molecular Cell Biology* **14**, 418–431 (2013).
51. Jacob, L. & Lum, L. Deconstructing the Hedgehog Pathway in Development and Disease. (2007). doi:10.1126/science.1147314
52. Wang, M. & Casey, P. J. Protein prenylation: Unique fats make their mark on biology. *Nat. Rev. Mol. Cell Biol.* **17**, 110–122 (2016).
53. Horton, J. D., Goldstein, J. L. & Brown, M. S. Critical review SREBPs : activators of the complete program of cholesterol and fatty acid synthesis in the liver. *J. Clin. Invest.* **109**, 1125–1131 (2002).
54. Bengoechea-Alonso, M. T. & Ericsson, J. SREBP in signal transduction: cholesterol metabolism and beyond. *Curr. Opin. Cell Biol.* **19**, 215–222 (2007).
55. Briggs, M. R., Yokoyama, C., Wang, X., Brown, M. S. & Goldstein, J. L. Nuclear protein that binds sterol regulatory element of low density lipoprotein receptor promoter. I. Identification of the protein and delineation of its target nucleotide sequence. *J. Biol. Chem.* **268**, 14490–14496 (1993).
56. Shimano, H. & Sato, R. SREBP-regulated lipid metabolism: convergent physiology — divergent pathophysiology. *Nat. Rev. Endocrinol.* (2017). doi:10.1038/nrendo.2017.91
57. Yang, F. *et al.* An ARC/Mediator subunit required for SREBP control of cholesterol and lipid homeostasis. *Nature* **442**, 700–704 (2006).
58. Inoue, N. *et al.* Lipid synthetic transcription factor SREBP-1a activates

p21WAF1/CIP1, a universal cyclin-dependent kinase inhibitor. *Mol. Cell. Biol.* **25**, 8938–47 (2005).

59. Reed, B. D., Charos, A. E., Szekely, A. M., Weissman, S. M. & Snyder, M. Genome-wide occupancy of SREBP1 and its partners NFY and SP1 reveals novel functional roles and combinatorial regulation of distinct classes of genes. *PLoS Genet.* **4**, (2008).
60. Gibot, L. *et al.* Human caspase 7 is positively controlled by SREBP-1 and SREBP-2. *Biochem. J.* **420**, 473–483 (2009).
61. Yang, T. *et al.* Crucial step in cholesterol homeostasis: Sterols promote binding of SCAP to INSIG-1, a membrane protein that facilitates retention of SREBPs in ER. *Cell* **110**, 489–500 (2002).
62. Song, B. L., Javitt, N. B. & DeBose-Boyd, R. A. Insig-mediated degradation of HMG CoA reductase stimulated by lanosterol, an intermediate in the synthesis of cholesterol. *Cell Metab.* **1**, 179–189 (2005).
63. Sun, L. P., Li, L., Goldstein, J. L. & Brown, M. S. Insig required for sterol-mediated inhibition of Scap/SREBP binding to COPII proteins in vitro. *J. Biol. Chem.* **280**, 26483–26490 (2005).
64. Debose-boyd, R. A. *et al.* Transport-Dependent Proteolysis of SREBP : Relocation of Site-1 Protease from Golgi to ER Obviates the Need for SREBP Transport to Golgi. **99**, 703–712 (1999).
65. Sakai, J., Nohturfft, A., Goldstein, J. L. & Brown, M. S. Cleavage of sterol regulatory element-binding proteins (SREBPs) at site- 1 requires interaction with SREBP cleavage-activating protein. Evidence from in vivo competition studies. *J. Biol. Chem.* **273**, 5785–5793 (1998).
66. Párraga, A., Bellsolell, L., Ferré-D'Amaré, A. R. & Burley, S. K. Co-crystal structure of sterol regulatory element binding protein 1a at 2.3 Å resolution. *Structure* **6**, 661–672 (1998).
67. Nagoshi, E., Imamoto, N., Sato, R. & Yoneda, Y. Nuclear import of sterol regulatory element-binding protein-2, a basic helix-loop-helix-leucine zipper (bHLH-Zip)-containing transcription factor, occurs through the direct interaction of importin β with HLH-Zip. *Mol. Biol. Cell* **10**, 2221–2233 (1999).
68. Lee, N. J., Zhang, X., Feramisco, J. D., Gong, Y. & Ye, J. Unsaturated fatty acids inhibit proteasomal degradation of insig-1 at a postubiquitination step. *J. Biol. Chem.* **283**, 33772–33783 (2008).

69. Lee, J. N. *et al.* Identification of Ubxd8 protein as a sensor for unsaturated fatty acids and regulator of triglyceride synthesis. *Proc. Natl. Acad. Sci. U. S. A.* **107**, 21424–21429 (2010).
70. Sai, K. *et al.* TAK1 determines susceptibility to endoplasmic reticulum stress and leptin resistance in the hypothalamus. *J. Cell Sci.* **129**, 1855–1865 (2016).
71. Aylon, Y. *et al.* The LATS2 tumor suppressor inhibits SREBP and suppresses hepatic cholesterol accumulation. *Genes Dev.* 1–12 (2016). doi:10.1101/gad.274167.115.
72. Tall, A. R., Yvan-Charvet, L., Terasaka, N., Pagler, T. & Wang, N. HDL, ABC Transporters, and Cholesterol Efflux: Implications for the Treatment of Atherosclerosis. *Cell Metabolism* **7**, 365–375 (2008).
73. Najafi-Shoushtari, S. H. *et al.* MicroRNA-33 and the SREBP host genes cooperate to control cholesterol homeostasis. *Science (80-.).* **328**, 1566–1569 (2010).
74. Inoue, J., Sato, R. & Maeda, M. Multiple DNA Elements for Sterol Regulatory Element-Binding Protein and NF-Y Are Responsible for Sterol-Regulated Transcription of the Genes for Human 3-Hydroxy-3-Methylglutaryl Coenzyme A Synthase and Squalene Synthase. *J. Biochem.* **123**, 1191–1198 (1998).
75. Xiong, S., Chirala, S. S. & Wakil, S. J. Sterol regulation of human fatty acid synthase promoter I requires nuclear factor-Y- and Sp-1-binding sites. *Proc. Natl. Acad. Sci. U. S. A.* **97**, 3948–3953 (2000).
76. Yamamoto, T. *et al.* SREBP-1 Interacts with Hepatocyte Nuclear Factor-4α and Interferes with PGC-1 Recruitment to Suppress Hepatic Gluconeogenic Genes. *J. Biol. Chem.* **279**, 12027–12035 (2004).
77. Ponugoti, B., Fang, S. & Kemper, J. K. Functional interaction of hepatic nuclear factor-4 and peroxisome proliferator-activated receptor-γ coactivator 1α in CYP7A1 regulation is inhibited by a key lipogenic activator, sterol regulatory element-binding protein-1c. *Mol. Endocrinol.* **21**, 2698–2712 (2007).
78. Misawa, K. *et al.* Sterol regulatory element-binding protein-2 interacts with hepatocyte nuclear factor-4 to enhance sterol isomerase gene expression in hepatocytes. *J. Biol. Chem.* **278**, 36176–36182 (2003).
79. Im, S.-S. *et al.* Linking Lipid Metabolism to the Innate Immune Response in Macrophages through Sterol Regulatory Element Binding Protein-1a. *Cell Metab.* **13**, 540–549 (2011).
80. Goldstein, I. *et al.* P53, a novel regulator of lipid metabolism pathways. *J. Hepatol.*

56, 656–662 (2012).

81. Moon, S. H. *et al.* p53 Represses the Mevalonate Pathway to Mediate Tumor Suppression. *Cell* **176**, 564-580.e19 (2019).
82. Freed-Pastor, W. A. *et al.* Mutant p53 Disrupts Mammary Tissue Architecture via the Mevalonate Pathway. *Cell* **148**, 244–258 (2012).
83. Ye, J. & DeBose-Boyd, R. a. Regulation of cholesterol and fatty acid synthesis. *Cold Spring Harb. Perspect. Biol.* **3**, 1–13 (2011).
84. Schultz, J. R. *et al.* Role of LXRs in control of lipogenesis. *Genes Dev.* **14**, 2831–8 (2000).
85. Repa, J. J. *et al.* Regulation of mouse sterol regulatory by oxysterol receptors , LXR ⎵ and LXR ␋. *Genes Dev.* 2819–2830 (2000). doi:10.1101/gad.844900.four
86. Xiao, X. & Song, B. SREBP: a novel therapeutic target. *Acta Biochim. Biophys. Sin. (Shanghai).* **45**, 2–10 (2013).
87. Sakakura, Y. *et al.* Sterol Regulatory Element-Binding Proteins Induce an Entire Pathway of Cholesterol Synthesis. **183**, 176–183 (2001).
88. Sundqvist, A. *et al.* Control of lipid metabolism by phosphorylation-dependent degradation of the SREBP family of transcription factors by SCFFbw7. *Cell Metab.* **1**, 379–391 (2005).
89. Lewis, C. a, Griffiths, B., Santos, C. R., Pende, M. & Schulze, A. Regulation of the SREBP transcription factors by mTORC1. *Biochem. Soc. Trans.* **39**, 495–499 (2011).
90. Giandomenico, V., Simonsson, M., Gronroos, E. & Ericsson, J. Coactivator-Dependent Acetylation Stabilizes Members of the SREBP Family of Transcription Factors. *Mol. Cell. Biol.* **23**, 2587–2599 (2003).
91. Bengoechea-Alonso, M. T. & Ericsson, J. The phosphorylation-dependent regulation of nuclear SREBP1 during mitosis links lipid metabolism and cell growth. *Cell Cycle* **15**, 2753–65 (2016).
92. Düvel, K. *et al.* Activation of a Metabolic Gene Regulatory Network Downstream of mTOR Complex 1. *Mol. Cell* **39**, 171–183 (2010).
93. Cantor, J. R. & Sabatini, D. M. Cancer cell metabolism: One hallmark, many faces. *Cancer Discov.* **2**, 881–898 (2012).
94. Ricoult, S. J. H., Yecies, J. L., Ben-Sahra, I. & Manning, B. D. Oncogenic PI3K and K-Ras stimulate de novo lipid synthesis through mTORC1 and SREBP. *Oncogene* 1–11 (2015). doi:10.1038/onc.2015.179

95. Peterson, T. R. *et al.* MTOR complex 1 regulates lipin 1 localization to control the srebp pathway. *Cell* **146**, 408–420 (2011).
96. Lin, S. C. & Hardie, D. G. AMPK: Sensing Glucose as well as Cellular Energy Status. *Cell Metab.* (2017). doi:10.1016/j.cmet.2017.10.009
97. Li, Y. *et al.* AMPK phosphorylates and inhibits SREBP activity to attenuate hepatic steatosis and atherosclerosis in diet-induced insulin-resistant mice. *Cell Metab.* **13**, 376–388 (2011).
98. Jeon, T.-I. & Osborne, T. F. SREBPs: metabolic integrators in physiology and metabolism. *Trends Endocrinol. Metab.* **23**, 65–72 (2012).
99. Faubert, B. *et al.* AMPK Is a Negative Regulator of the Warburg Effect and Suppresses Tumor Growth In Vivo. *Cell Metab.* **17**, 113–124 (2013).
100. Lee, A. S. The glucose-regulated proteins: Stress induction and clinical applications. *Trends Biochem. Sci.* **26**, 504–510 (2001).
101. Colgan, S. M., Tang, D., Werstuck, G. H. & Austin, R. C. Endoplasmic reticulum stress causes the activation of sterol regulatory element binding protein-2. *Int. J. Biochem. Cell Biol.* **39**, 1843–1851 (2007).
102. Pai, J., Brown, M. & Goldstein, J. Purification and {cDNA} cloning of a second apoptosis-related cysteine protease that cleaves and activates sterol regulatory element binding proteins. *Proc. Natl. Acad. Sci. U. S. A.* **93**, 5437–5442 (1996).
103. Rawson, R. B. The SREBP pathway--insights from Insigs and insects. *Nat. Rev. Mol. Cell Biol.* **4**, 631–640 (2003).
104. Osborne, T. F. & Espenshade, P. J. Evolutionary conservation and adaptation in the mechanism that regulates SREBP action: What a long, strange tRIP it's been. *Genes Dev.* **23**, 2578–2591 (2009).
105. Seegmiller, A. C. *et al.* The SREBP Pathway in DrosophilaRegulation by Palmitate, Not Sterols. *Dev. Cell* **2**, 229–238 (2002).
106. Dobrosotskaya, I. Y., Seegmiller, a C., Brown, M. S., Goldstein, J. L. & Rawson, R. B. Regulation of SREBP processing and membrane lipid production by phospholipids in Drosophila. *Science* **296**, 879–883 (2002).
107. Kunte, A. S., Matthews, K. A. & Rawson, R. B. Fatty acid auxotrophy in Drosophila larvae lacking SREBP. *Cell Metab.* **3**, 439–448 (2006).
108. McKay, R. M., McKay, J. P., Avery, L. & Graff, J. M. C. elegans: A model for exploring the genetics of fat storage. *Dev. Cell* **4**, 131–142 (2003).
109. Ashrafi, K. Obesity and the regulation of fat metabolism. *WormBook : the online*

review of C. elegans biology 1–20 (2007). doi:10.1895/wormbook.1.130.1

110. Kniazeva, M., Crawford, Q. T., Seiber, M., Wang, C. Y. & Han, M. Monomethyl branched-chain fatty acids play an essential role in Caenorhabditis elegans development. *PLoS Biol.* **2**, (2004).
111. Kniazeva, M., Euler, T. & Han, M. A branched-chain fatty acid is involved in post-embryonic growth control in parallel to the insulin receptor pathway and its biosynthesis is feedback-regulated in C. elegans. *Genes Dev.* **22**, 2102–2110 (2008).
112. McTaggart, S. J. Isoprenylated proteins. *Cell. Mol. Life Sci.* **63**, 255–267 (2006).
113. Zhang, F. L. & Casey, P. J. Protein prenylation: molecular mechanisms and functional consequences. *Annu. Rev. Biochem.* **65**, 241–269 (1996).
114. Wang, M. & Casey, P. J. Protein prenylation: unique fats make their mark on biology. *Nat. Publ. Gr.* (2016). doi:10.1038/nrm.2015.11
115. Edwards, P. & Ericsson, J. Sterols and isoprenoids: signaling molecules derived from the cholesterol biosynthetic pathway. *Annu. Rev. Biochem.* **68**, 157–185 (1999).
116. Eckert, G. P. *et al.* Regulation of the brain isoprenoids farnesyl- and geranylgeranylpyrophosphate is altered in male Alzheimer patients. *Neurobiol. Dis.* **35**, 251–257 (2009).
117. Clendening, J. W. *et al.* Dysregulation of the mevalonate pathway promotes transformation. *Proc. Natl. Acad. Sci. U. S. A.* **107**, 15051–15056 (2010).
118. Sorrentino, G. *et al.* Metabolic control of YAP and TAZ by the mevalonate pathway. *Nat. Cell Biol.* **16**, 357–66 (2014).
119. Downward, J. Targeting RAS signalling pathways in cancer therapy. *Nature Reviews Cancer* **3**, 11–22 (2003).
120. Hall, A. Rho GTpases and the actin cytoskeleton. *Science* **279**, 509–514 (1998).
121. Alcaraz, J. *et al.* Laminin and biomimetic extracellular elasticity enhance functional differentiation in mammary epithelia. *EMBO J.* **27**, 2829–2838 (2008).
122. Mammoto, T. & Ingber, D. E. Mechanical control of tissue and organ development. *Development* **137**, 1407–1420 (2010).
123. DuFort, C. C., Paszek, M. J. & Weaver, V. M. Balancing forces: architectural control of mechanotransduction. *Nat. Rev. Mol. Cell Biol.* **12**, 308–319 (2011).
124. Butcher, D. T., Alliston, T. & Weaver, V. M. A tense situation: forcing tumour progression. *Nat. Rev. Cancer* **9**, 108–122 (2009).

125. Jaalouk, D. E. & Lammerding, J. Mechanotransduction gone awry. *Nat. Rev. Mol. Cell Biol.* **10**, 63–73 (2009).
126. Burridge, K. & Chrzanowska-Wodnicka, M. FOCAL ADHESIONS, CONTRACTILITY, AND SIGNALING. *Annu. Rev. Cell Dev. Biol.* **12**, 463–519 (1996).
127. Alenghat, F. J. & Ingber, D. E. Mechanotransduction: all signals point to cytoskeleton, matrix, and integrins. *Sci. STKE* **2002**, pe6 (2002).
128. Katsumi, A., Orr, A. W., Tzima, E. & Schwartz, M. A. Integrins in Mechanotransduction. *Journal of Biological Chemistry* **279**, 12001–12004 (2004).
129. Humphrey, J. D., Dufresne, E. R. & Schwartz, M. A. Mechanotransduction and extracellular matrix homeostasis. *Nat. Rev. Mol. Cell Biol.* **15**, 802–812 (2014).
130. Geiger, B., Spatz, J. P. & Bershadsky, A. D. Environmental sensing through focal adhesions. *Nat. Rev. Mol. Cell Biol.* **10**, 21–33 (2009).
131. Wolfenson, H., Yang, B. & Sheetz, M. P. Annual Review of Physiology Steps in Mechanotransduction Pathways that Control Cell Morphology. 1–21 (2018). doi:10.1146/annurev-physiol-021317
132. Chen, C. S., Mrksich, M., Huang, S., Whitesides, G. M. & Ingber, D. E. Geometric Control of Cell Life and Death. *Science (80-.).* **276**, 1425–1428 (1997).
133. Dupont, S. *et al.* Role of YAP/TAZ in mechanotransduction. *Nature* **474**, 179–183 (2011).
134. Martino, F., Perestrelo, A. R., Vinarský, V., Pagliari, S. & Forte, G. Cellular mechanotransduction: From tension to function. *Front. Physiol.* **9**, 1–21 (2018).
135. Engler, A. J., Sen, S., Sweeney, H. L. & Discher, D. E. Matrix Elasticity Directs Stem Cell Lineage Specification. *Cell* **126**, 677–689 (2006).
136. Provenzano, P. P., Inman, D. R., Eliceiri, K. W. & Keely, P. J. Matrix density-induced mechanoregulation of breast cell phenotype, signaling and gene expression through a FAK-ERK linkage. *Oncogene* **28**, 4326–4343 (2009).
137. Provenzano, P. P. & Keely, P. J. Mechanical signaling through the cytoskeleton regulates cell proliferation by coordinated focal adhesion and Rho GTPase signaling. *J. Cell Sci.* **124**, 1195–1205 (2011).
138. Connelly, J. T. *et al.* Actin and serum response factor transduce physical cues from the microenvironment to regulate epidermal stem cell fate decisions. *Nat. Cell Biol.* **12**, 711–718 (2010).
139. Sero, J. E. *et al.* Cell shape and the microenvironment regulate nuclear translocation

of NF-κB in breast epithelial and tumor cells. *Mol. Syst. Biol.* **11**, 790 (2015).

140. Samuel, M. S. *et al.* Actomyosin-mediated cellular tension drives increased tissue stiffness and ??-catenin activation to induce epidermal hyperplasia and tumor growth. *Cancer Cell* **19**, 776–791 (2011).
141. Fernández-Sánchez, M. E. *et al.* Mechanical induction of the tumorigenic β-catenin pathway by tumour growth pressure. *Nature* **523**, 92–95 (2015).
142. Wei, S. C. *et al.* Matrix stiffness drives epithelial-mesenchymal transition and tumour metastasis through a TWIST1-G3BP2 mechanotransduction pathway. *Nat. Cell Biol.* **17**, 678–688 (2015).
143. Desprat, N., Supatto, W., Pouille, P. A., Beaurepaire, E. & Farge, E. Tissue Deformation Modulates Twist Expression to Determine Anterior Midgut Differentiation in Drosophila Embryos. *Dev. Cell* **15**, 470–477 (2008).
144. Gordon, W. R. *et al.* Mechanical Allostery: Evidence for a Force Requirement in the Proteolytic Activation of Notch. *Dev. Cell* **33**, 729–736 (2015).
145. Miralles, F., Posern, G., Zaromytidou, A. I. & Treisman, R. Actin dynamics control SRF activity by regulation of its coactivator MAL. *Cell* **113**, 329–342 (2003).
146. Vartiainen, M. K., Guettler, S., Larijani, B. & Treisman, R. Subcellular Localization and Activity. *Science (80-.).* **316**, 1749–1752 (2007).
147. Oka, T., Mazack, V. & Sudol, M. Mst2 and Lats kinases regulate apoptotic function of Yes kinase-associated protein (YAP). *J. Biol. Chem.* **283**, 27534–27546 (2008).
148. Dupont, S. *et al.* Role of YAP/TAZ in mechanotransduction. *Nature* **474**, 179–184 (2011).
149. Kim, N.-G., Koh, E., Chen, X. & Gumbiner, B. M. E-cadherin mediates contact inhibition of proliferation through Hippo signaling-pathway components. *Proc. Natl. Acad. Sci. U. S. A.* **108**, 11930–11935 (2011).
150. Nardone, G. *et al.* YAP regulates cell mechanics by controlling focal adhesion assembly. *Nat. Commun.* **8**, (2017).
151. Kirby, T. J. & Lammerding, J. Emerging views of the nucleus as a cellular mechanosensor. *Nat. Cell Biol.* **20**, 373–381 (2018).
152. Crisp, M. *et al.* Coupling of the nucleus and cytoplasm: Role of the LINC complex. *J. Cell Biol.* **172**, 41–53 (2006).
153. Starr, D. A. & Fridolfsson, H. N. Interactions Between Nuclei and the Cytoskeleton Are Mediated by SUN-KASH Nuclear-Envelope Bridges. *Annu. Rev. Cell Dev. Biol.* **26**, 421–444 (2010).

154. Castoreno, A. B. *et al.* Transcriptional regulation of phagocytosis-induced membrane biogenesis by sterol regulatory element binding proteins. *Proc. Natl. Acad. Sci. U. S. A.* **102**, 13129–34 (2005).
155. Liao, J. K. Isoprenoids as mediators of the biological effects of statins. *Journal of Clinical Investigation* **110**, 285–288 (2002).
156. Maurer-stroh, S. *et al.* Towards Complete Sets of Farnesylated and Geranylgeranylated Proteins. *PLoS Comput Biol* **3**, (2007).
157. Maurer-Stroh, S. & Eisenhaber, F. Refinement and prediction of protein prenylation motifs. *Genome Biol.* **6**, R55 (2005).
158. Allal, C. *et al.* RhoA prenylation is required for promotion of cell growth and transformation and cytoskeleton organization but not for induction of serum response element transcription. *J. Biol. Chem.* **275**, 31001–31008 (2000).
159. Amano, M., Nakayama, M. & Kaibuchi, K. Rho-kinase/ROCK: A key regulator of the cytoskeleton and cell polarity. *Cytoskeleton* **67**, 545–554 (2010).
160. Seegmiller, A. C. *et al.* The SREBP pathway in Drosophila: Regulation by palmitate, not sterols. *Dev. Cell* **2**, 229–238 (2002).
161. Ballard, S. L., Jarolimova, J. & Wharton, K. A. Gbb/BMP signaling is required to maintain energy homeostasis in Drosophila. *Dev. Biol.* **337**, 375–385 (2010).
162. Mizuno, T., Amano, M., Kaibuchi, K. & Nishida, Y. Identification and characterization of Drosophila homolog of Rho-kinase. *Gene* **238**, 437–444 (1999).
163. Winter, C. G. *et al.* Drosophila Rho-associated kinase (Drok) links Frizzled-mediated planar cell polarity signaling to the actin cytoskeleton. *Cell* **105**, 81–91 (2001).
164. Kamisuki, S. *et al.* A Small Molecule That Blocks Fat Synthesis By Inhibiting the Activation of SREBP. *Chem. Biol.* **16**, 882–892 (2009).
165. Seong, J., Wang, N. & Wang, Y. Mechanotransduction at focal adhesions: From physiology to cancer development. *J. Cell. Mol. Med.* **17**, 597–604 (2013).
166. Ingallina, E. *et al.* Mechanical cues control mutant p53 stability through a mevalonate-RhoA axis. *Nat. Cell Biol.* **20**, 28–35 (2018).
167. Horton, J. D. *et al.* Combined analysis of oligonucleotide microarray data from transgenic and knockout mice identifies direct SREBP target genes. *Proc. Natl. Acad. Sci.* **100**, 12027–12032 (2003).
168. Sun, X. *et al.* Relationship of Mammographic Density and Gene Expression: Analysis of Normal Breast Tissue Surrounding Breast Cancer. *Clin. Cancer Res.* **19**, 4972–4982 (2013).

169. Boyd, N. F. *et al.* Mammographic features associated with interval breast cancers in screening programs. *Breast Cancer Res.* **16**, 417 (2014).
170. Liu, F. *et al.* Mechanosignaling through YAP and TAZ drives fibroblast activation and fibrosis. *Am. J. Physiol. Cell. Mol. Physiol.* **308**, L344–L357 (2015).
171. Luzina, I. G. *et al.* Transcriptomic evidence of immune activation in macroscopically normal-appearing and scarred lung tissues in idiopathic pulmonary fibrosis. *Cell. Immunol.* **325**, 1–13 (2018).
172. Li, Y. *et al.* AMPK Phosphorylates and Inhibits SREBP Activity to Attenuate Hepatic Steatosis and Atherosclerosis in Diet-Induced Insulin-Resistant Mice. *Cell Metab.* **13**, 376–388 (2011).
173. Ponugoti, B. *et al.* SIRT1 deacetylates and inhibits SREBP-1C activity in regulation of hepatic lipid metabolism. *J. Biol. Chem.* **285**, 33959–33970 (2010).
174. Hirano, Y., Murata, S., Tanaka, K., Shimizu, M. & Sato, R. Sterol regulatory element-binding proteins are negatively regulated through SUMO-1 modification independent of the ubiquitin/26 S proteasome pathway. *J. Biol. Chem.* **278**, 16809–16819 (2003).
175. Bays, J. L., Campbell, H. K., Heidema, C., Sebbagh, M. & Demali, K. A. Linking E-cadherin mechanotransduction to cell metabolism through force-mediated activation of AMPK. *Nat. Cell Biol.* **19**, 724–731 (2017).
176. Tojkander, S., Ciuba, K. & Lappalainen, P. CaMKK2 Regulates Mechanosensitive Assembly of Contractile Actin Stress Fibers. *Cell Rep.* **24**, 11–19 (2018).
177. Kim, J. B. & Spiegelman, B. M. ADD1/SREBP1 promotes adipocyte differentiation and gene expression linked to fatty acid metabolism. *Genes Dev.* **10**, 1096–1107 (1996).
178. Fajas, L. *et al.* Regulation of Peroxisome Proliferator-Activated Receptor γ Expression by Adipocyte Differentiation and Determination Factor 1/Sterol Regulatory Element Binding Protein 1: Implications for Adipocyte Differentiation and Metabolism. *Mol. Cell. Biol.* **19**, 5495–5503 (1999).
179. McBeath, R., Pirone, D. M., Nelson, C. M., Bhadriraju, K. & Chen, C. S. Cell shape, cytoskeletal tension, and RhoA regulate stem cell lineage commitment. *Dev. Cell* **6**, 483–495 (2004).
180. Liao, J. K. Isoprenoids as mediators of the biological effects of statins. *J. Clin. Invest.* **110**, 285–288 (2002).
181. Clendening, P. *et al.* Dysregulation of the mevalonate pathway promotes transformation. *Proc Natl Acad Sci U S A.* **107**, 15051–6 (2010).

182. Wozniak, M. A. & Chen, C. S. Mechanotransduction in development: a growing role for contractility. *Nat. Rev. Mol. Cell Biol.* **10**, 34–43 (2009).
183. LAMMERDING, J., KAMM, R. D. & LEE, R. T. Mechanotransduction in Cardiac Myocytes. *Ann. N. Y. Acad. Sci.* **1015**, 53–70 (2004).
184. Jaalouk, D. E. & Lammerding, J. Mechanotransduction gone awry. *Nat. Rev. Mol. Cell Biol.* **10**, 63–73 (2009).
185. Burger, E. H. & Klein-Nulend, J. Mechanotransduction in bone--role of the lacuno-canalicular network. *FASEB J.* **13 Suppl**, S101-12 (1999).
186. Wirtz, H. R. & Dobbs, L. G. The effects of mechanical forces on lung functions. *Respiration Physiology* **119**, 1–17 (2000).
187. Serluca, F. C., Drummond, I. A. & Fishman, M. C. Endothelial signaling in kidney morphogenesis: A role for hemodynamic forces. *Curr. Biol.* **12**, 492–497 (2002).
188. Petridou, N. I., Spiró, Z. & Heisenberg, C. P. Multiscale force sensing in development. *Nat. Cell Biol.* **19**, 581–588 (2017).
189. McBeath, R., Pirone, D. M., Nelson, C. M., Bhadriraju, K. & Chen, C. S. Cell shape, cytoskeletal tension, and RhoA regulate stemm cell lineage commitment. *Dev. Cell* **6**, 483–495 (2004).
190. Kim, J. B. & Spiegelman, B. M. ADD 1/SREBP1 promotes adipocyte differentiation and gene expression linked to fatty acid metabolism. *Genes Dev.* **10**, 1096–1107 (1996).
191. Vu, V., Bui, P., Eguchi, M., Xu, A. & Sweeney, G. Globular adiponectin induces LKB1/AMPK-dependent glucose uptake via actin cytoskeleton remodeling. *J. Mol. Endocrinol.* **51**, 155–165 (2013).
192. Hu, H. *et al.* Phosphoinositide 3-Kinase Regulates Glycolysis through Mobilization of Aldolase from the Actin Cytoskeleton. *Cell* **164**, 433–446 (2016).
193. Paszek, M. J. *et al.* Tensional homeostasis and the malignant phenotype. *Cancer Cell* **8**, 241–254 (2005).
194. Vander Heiden, M. G. & DeBerardinis, R. J. Understanding the Intersections between Metabolism and Cancer Biology. *Cell* **168**, 657–669 (2017).
195. Bertero, T. *et al.* Tumor-Stroma Mechanics Coordinate Amino Acid Availability to Sustain Tumor Growth and Malignancy. *Cell Metab.* 1–17 (2018). doi:10.1016/j.cmet.2018.09.012
196. Freed-Pastor, W. A. *et al.* Mutant p53 disrupts mammary tissue architecture via the mevalonate pathway. *Cell* **148**, 244–258 (2012).

197. Enzo, E. *et al.* Aerobic glycolysis tunes YAP/TAZ transcriptional activity. *EMBO J.* **34**, 1349–1370 (2015).
198. Broders-Bondon, F., Ho-Bouldoires, T. H. N., Fernandez-Sanchez, M. E. & Farge, E. Mechanotransduction in tumor progression: The dark side of the force. *J. Cell Biol.* **217**, 1571–1587 (2018).
199. Gouw, A. M. *et al.* The MYC Oncogene Cooperates with Sterol-Regulated Element-Binding Protein to Regulate Lipogenesis Essential for Neoplastic Growth. *Cell Metab.* **30**, 556-572.e5 (2019).
200. Griffiths, B. *et al.* Sterol regulatory element binding protein-dependent regulation of lipid synthesis supports cell survival and tumor growth. *Cancer Metab.* **1**, 3 (2013).
201. Guo, D., Bell, E. H., Mischel, P. & Chakravarti, A. Targeting SREBP-1-driven lipid metabolism to treat cancer. *Curr. Pharm. Des.* **20**, 2619–26 (2014).
202. Porstmann, T. *et al.* SREBP activity is regulated by mTORC1 and contributes to Akt-dependent cell growth. *Cell Metab.* **8**, 224–36 (2008).
203. Bengoechea-Alonso, M. T. & Ericsson, J. A phosphorylation cascade controls the degradation of active SREBP1. *J. Biol. Chem.* **284**, 5885–5895 (2009).
204. Faubert, B. *et al.* Loss of the tumor suppressor LKB1 promotes metabolic reprogramming of cancer cells via HIF-1α. *Proc. Natl. Acad. Sci. U. S. A.* **111**, 2554–2559 (2014).
205. Zhou, G. *et al.* Gain-of-Function Mutant p53 Promotes Cell Growth and Cancer Cell Metabolism via Inhibition of AMPK Activation. *Mol. Cell* **54**, 960–974 (2014).
206. Wang, J. Bin *et al.* Targeting mitochondrial glutaminase activity inhibits oncogenic transformation. *Cancer Cell* **18**, 207–219 (2010).
207. Bertero, T. *et al.* Matrix Remodeling Promotes Pulmonary Hypertension through Feedback Mechanoactivation of the YAP/TAZ-miR-130/301 Circuit. *Cell Rep.* **13**, 1016–1032 (2015).
208. Shichino, S. *et al.* Transcriptome network analysis identifies protective role of the LXR/SREBP-1c axis in murine pulmonary fibrosis. *JCI Insight* **4**, (2019).
209. Zhao, H. *et al.* Pulmonary delivery of docosahexaenoic acid mitigates bleomycin-induced pulmonary fibrosis. *BMC Pulm. Med.* **14**, 64 (2014).
210. Yatomi, M. *et al.* 17(R)-resolvin D1 ameliorates bleomycin-induced pulmonary fibrosis in mice. *Physiol. Rep.* **3**, e12628 (2015).
211. Romani, P. *et al.* Extracellular matrix mechanical cues regulate lipid metabolism through Lipin-1 and SREBP. *Nat. Cell Biol.* **21**, 338–347 (2019).

212. Swift, J. *et al.* Nuclear lamin-A scales with tissue stiffness and enhances matrix-directed differentiation. *Science (80-.).* **341**, (2013).
213. Vadrot, N. *et al.* The p.R482W substitution in A-type lamins deregulates SREBP1 activity in Dunnigan-type familial partial lipodystrophy. *Hum. Mol. Genet.* **24**, 2096–2109 (2015).
214. Wojtanik, K. M. *et al.* The role of LMNA in adipose: A novel mouse model of lipodystrophy based on the Dunnigan-type familial partial lipodystrophy mutation. *J. Lipid Res.* **50**, 1068–1079 (2009).
215. Khromova, N. V. *et al.* R482L Mutation of the LMNA Gene Affects Dynamics of C2C12 Myogenic Differentiation and Stimulates Formation of Intramuscular Lipid Droplets. *Biochem.* **84**, 241–249 (2019).
216. Mano, M., Ippodrino, R., Zentilin, L., Zacchigna, S. & Giacca, M. Genome-wide RNAi screening identifies host restriction factors critical for in vivo AAV transduction. *Proc. Natl. Acad. Sci.* **112**, 11276–11281 (2015).
217. Napoletano, F. *et al.* P53-Dependent Programmed Necrosis Controls Germ Cell Homeostasis During Spermatogenesis. *PLoS Genetics* **13**, (2017).
218. Van Den Brink, D. M. *et al.* Physiological and pathological roles of FATP-mediated lipid droplets in Drosophila and mice retina. *PLOS Genet.* **14**, e1007627 (2018).
219. Bi, J. *et al.* Seipin promotes adipose tissue fat storage through the ER Ca^{2+}-ATPase SERCA. *Cell Metab.* **19**, 861–71 (2014).
220. Rustighi, A. *et al.* Prolyl-isomerase Pin 1 controls normal and cancer stem cells of the breast. *EMBO Mol. Med.* **6**, 99–119 (2014).
221. Hu, Y. *et al.* An integrative approach to ortholog prediction for disease-focused and other functional studies. *BMC Bioinformatics* **12**, 357 (2011).
222. Leinonen, R., Sugawara, H., Shumway, M. & International Nucleotide Sequence Database Collaboration. The sequence read archive. *Nucleic Acids Res.* **39**, D19-21 (2011).
223. Afgan, E. *et al.* The Galaxy platform for accessible, reproducible and collaborative biomedical analyses: 2016 update. *Nucleic Acids Res.* **44**, W3–W10 (2016).
224. Andrews. FastQC A Quality Control tool for High Throughput Sequence Data. *http://www.bioinformatics.babraham.ac.uk/projects/fastqc/*
225. Blankenberg, D. *et al.* Manipulation of FASTQ data with Galaxy. *Bioinformatics* **26**, 1783–1785 (2010).
226. Bolger, A. M., Lohse, M. & Usadel, B. Trimmomatic: a flexible trimmer for Illumina

sequence data. *Bioinformatics* **30**, 2114–2120 (2014).

227. Kim, D., Langmead, B. & Salzberg, S. L. HISAT: a fast spliced aligner with low memory requirements. *Nat. Methods* **12**, 357–360 (2015).
228. Li, H. *et al.* The Sequence Alignment/Map format and SAMtools. *Bioinformatics* **25**, 2078–2079 (2009).
229. Liao, Y., Smyth, G. K. & Shi, W. featureCounts: an efficient general purpose program for assigning sequence reads to genomic features. *Bioinformatics* **30**, 923–930 (2014).
230. Love, M. I., Huber, W. & Anders, S. Moderated estimation of fold change and dispersion for RNA-seq data with DESeq2. *Genome Biol.* **15**, 550 (2014).
231. Thurnher, M., Nussbaumer, O. & Gruenbacher, G. Novel aspects of mevalonate pathway inhibitors as antitumor agents. *Clin. Cancer Res.* **18**, 3524–3531 (2012).
232. Soyal, S. M., Nofziger, C., Dossena, S., Paulmichl, M. & Patsch, W. Targeting SREBPs for treatment of the metabolic syndrome. *Trends Pharmacol. Sci.* **36**, 406–416 (2015).
233. Ikonen, E. V i I p Cellular cholesterol trafficking and compartmentalization. **9**, (2008).
234. Vining, K. H. & Mooney, D. J. Mechanical forces direct stem cell behaviour in development and regeneration. *Nat. Rev. Mol. Cell Biol.* **18**, 728–742 (2017).

Appendix - Publications

During my PhD I have been involved in the following publications:

- Ruggeri N.*, Sorrentino G.*, Zannini A., Ingallina E., **Bertolio R.**, Marotta C., Neri C., Cappuzzello E., Forcato M., Rosato A., Mano M., Bicciato S. and Del Sal G., "**Glucocorticoid receptor signalling activates YAP in breast cancer**", Nature Communications, 2017, 8:14073, doi: 10.1038/ncomms14073.

- Ingallina E.*, Sorrentino G.*, **Bertolio R.,** Lisek K., Zannini A., Azzolin L., Ulloa Severino L., Scaini D., Mano M., Mantovani F., Rosato A., Bicciato S., Piccolo S. and Del Sal G., "**Mechanical cues control mutant p53 stability through a mevalonate – RhoA axis**", Nature Cell Biology, 2018, 20:28–35, doi: 10.1038/s41556-017-0009-8.

- **Bertolio R.,** Napoletano F., Mano M., Maurer-Stroh S., Zannini A., Fantuz M., Bicciato S., Sorrentino G. and Del Sal G., "**Sterol regulatory element binding protein 1 couples mechanical cues to lipid metabolism**", Nature Communications, 2019, 10:1326, doi: 10.1038/s41467-019-09152-7.